Hydrodynamic Studies of the Electrochemical Oxidation of Organic Fuels

by

© *Azam Sayadi*

A thesis submitted to the School of Graduate Studies in partial fulfilment of

the requirements for the degree of

Doctor of Philosophy

Department of Chemistry

Memorial University of Newfoundland

September 2020

St. John's Newfoundland

Abstract

A clear understanding of small organic molecules (SOM) electrochemical oxidation opens a great opportunity for breakthrough in the development of fuel cell technology. SOM such as formic acid, methanol, and ethanol can produce electrical power through their oxidation in the fuel cell's anode. These molecules are also known as organic fuels and theoretically have the potential to produce close to 100% energy efficiency in a fuel cell. However, fast and complete oxidation of some organic fuels, such as ethanol, has not been achieved at this time, and has led to a dramatic decrease in the level of fuel cell efficiency. Therefore, a comprehensive study of the electrocatalytic oxidation mechanisms of organic fuels as well as a determination of the average number of transferred electrons (n_{av}) are crucial for the enhancement of fuel cell efficiency. Hydrodynamic methods are highly effective approaches for these study purposes, and they have the ability to emulate the hydrodynamic conditions of a fuel cell anode.

The main purpose of this project was establishing a simple and novel system for the assessment of various fuel cell catalysts performances in relation to formic acid, methanol and ethanol electrochemical oxidation. For this purpose, we applied two different approaches of hydrodynamic techniques, rotating disk voltammetry (RDV) and flow cell electrolysis. Also, as for fuel cells, thick catalyst layers were applied in our studies in order to obtain meaningful data which are more relevant to an actual fuel cell.

We showed that RDV is a convenient and useful method for the determination of the pure kinetic component of the oxidation current which represents a catalyst

activity. Also, we estimated n_{av} for methanol and ethanol using mathematical treatments related to RDV. Two-electrode and three-electrode flow-through cells were designed to determine the mass transport and kinetic parameters of the formic acid oxidation current, which can be further extended to methanol and ethanol for n_{av} determination. The two-electrode flow-through cell provided for rapid collection of oxidation products and real time measurements of CO_2 for stoichiometric investigations.

Acknowledgements

First and foremost, I would like to express my sincere gratitude to my supervisor Dr. Peter Pickup whose kindness, generosity, continuous support, and knowledge made this journey an invaluable experience while doing the research in his group. Indeed, through this process, I came to realize that he is the best supervisor that I could ever ask for.

This thesis becomes a reality with the support of many individuals. I would like to extend my gratitude to Prof. Christopher M. Kozak, Prof. Cora J. Young, Prof. Peter Warburton, and Dr. Karl J. Jobst for their input and for the time they dedicated as part of the supervisory committee. I would also like to thank the former and current members of Dr. Pickup's research group for their help and support.

My tremendous thanks and appreciation go to every faculty member of the Chemistry Department who attended my comprehensive exam, examined my seminar, and taught me the courses throughout this program. I also highly appreciate the kindness and help from all of the Chemistry Department staff, especially general office staff, and the members of C-CART for providing advice and training on various instruments.

I would like to express my gratitude to NSERC, the School of Graduate Studies, and Dr. Liqin Chen for the financial support throughout my PhD program.

Last but not the least, I am immensely obliged to my dear husband, my little daughter Isla, my mother, father and brothers, whose support, patience, presence and encouragement motivated me throughout this adventurous journey.

Contents

List of Figures

List of Tables

List of Abbreviations

AA	Acetic acid
AL	Acetaldehyde
CA	Chronoamperommetry
CFP	Carbon fiber paper
CV	Cyclic voltammetry
DAFC	Direct alcohol fuel cell
DEFC	Direct ethanol fuel cell
DEMS	Differential electrochemical mass spectroscopy
DFAFC	Direct formic acid fuel cell
DOFC	Direct organic fuel cell
DMFC	Direct methanol fuel cell
DHE	Dynamic hydrogen electrode
EOR	Ethanol oxidation reaction

FA	Formic acid
FAOR	Formic acid oxidation reaction
FTIRS	Fourier transform infrared spectroscopy
GC	Glassy carbon
HER	Hydrogen evolution reaction
K-L	Koutecky-Levich
LSV	Linear sweep voltammetry
MOR	Methanol oxidation reaction
MSE	Mercury sulfide electrode
NDIR	Non-dispersive infrared
NMR	Nuclear magnetic resonance
ORR	Oxygen reduction reaction
PEM	Proton exchange membrane
PEMFC	Proton exchange membrane fuel cell
RDE	Rotating disk electrode
RDV	Rotating disk voltammetry
RHE	Reversible hydrogen electrode

RRDE	Rotating ring disk electrode
RT	Room temperature
SCE	Saturated calomel electrode
SEM	Scanning electron microscopy
SHE	Standard hydrogen electrode
SOM	Small organic molecules
TEM	Transmission electron microscopy

List of Symbols

A	Electrode surface
α	Mass transfer coefficient
C	Concentration
C_0	Concentration at the surface of the electrode
D	Diffusion coefficient
D_{ap}	Apparent diffusion coefficient
E°	Standard potential
E	Potential
F	Faraday constant
λ	Mass transfer parameter
i	Current
i_e	Electron transfer component of kinetic current
i_{lim}	Mass transport limited current

i_k	Kinetic current
i_s	Diffusion related component of kinetic current
k	Rate constant
m	Reaction order
n	Number of electrons involved in a reaction
n_{av}	Number of electrons involved in an oxidation process which includes multiple reactions
n_{ap}	Apparent number of electrons involved in an oxidation process
ω	Angular velocity
u	Flow rate
Q	Charge
R	Gas constant
t	Time
V	Voltage (volts)
V_m	Molar volume of any gas
ν	Kinematic viscosity

Chapter 1

Introduction

1.1 Introduction

Oxidation of small organic molecules (SOM) has been one of the most active targets of investigation in electrochemistry for several decades. SOM oxidation can be employed as a framework to study electrochemical oxidation reactions.[1] Moreover, electrocatalysis studies of SOM provide fundamental information to guide catalyst design.[?] The significance of these investigations is enhanced by the fact that many SOM, such as formic acid, methanol, and ethanol, can be used to produce electrical power through their oxidation.[2] These organic molecules have the potential to produce reasonable energy density and can be applied as fuels in fuel cells. Therefore, SOM are capable of contributing to a wide range of industry sectors.

A fuel cell is an electrochemical cell that can convert chemical energy to electrical energy without a Carnot cycle limitation.[3,4] Therefore, a fuel cell is capable of producing close to 100% energy efficiency in theory. It is like a battery with unlimited capacity in which reactants are supplied continuously into the cell from an external source. On the other hand, products (water and carbon dioxide in theory for an organic fuel) are removed through the cell exhaust. The fuel cell was introduced by a Welsh scientist, Sir William Grove, for the first time in 1839.[5] Due to high demands for a reliable and environmentally friendly sources of power, rapid fuel cell development has occurred during the past few decades. Various generations of fuel cells with different electrolyte materials have been introduced to the industry.

Proton exchange membrane fuel cells (PEMFC) are a type of fuel cell that has a solid thin layer membrane between electrodes for the movement of hydrogen ions generated during fuel oxidation. This type of fuel cell is widely used due to its high

durability and convenience. PEMFC are capable of producing high power densities while having low weight and low operation temperature. These advantages make them an excellent choice for automobile and portable electronics applications.[6–10] Nafion is the most widely used membrane in PEMFC due to its degree of availability. It is a perfluorosulfonic acid membrane consisting of a hydrophobic backbone and hydrophilic side chains. The hydrophobic backbone is tetrafluoroethylene as a continuous phase, and the hydrophilic part is formed by sulfonic acid group ($-SO_3H$) terminals of side chains. Figure 1.1 shows the chemical structure of Nafion.[11–13] The acidic terminals of the side chains provide good proton conductivity in the presence of water, which enhances both hydrogen dissociation from the sulfonic acid and proton transport at the same time.

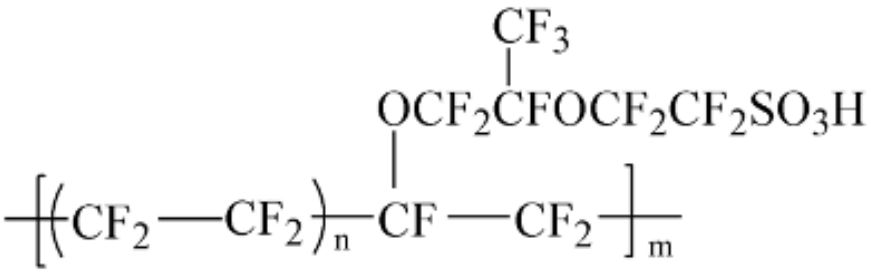

Figure 1.1: The general structure of Nafion.

For many years, hydrogen PEMFC have been on the top of the research ladder. These fuel cells have been applied widely in the transportation industry, for example. However, despite the high energy density of hydrogen (energy produced per mass of fuel = 33.3 $kWh\ kg^{-1}$), it is not an ideal fuel for fuel cells. That is because of complications and dangers associated with its storage and handling as a highly explosive gas, as well as the need for highly purified hydrogen. Therefore, demand

had risen for substitution by liquid fuels and this has led to the introduction of direct organic fuel cells (DOFC).

Organic compounds such as alcohols (e.g. methanol), aldehydes (e.g. furfural) and acids (formic acid) can be supplied to PEMFC either directly (direct organic fuel cell (DOFC)) or indirectly (i.e. used as a source of hydrogen). Ethanol, methanol, and formic acid are renewable through biomass processes. Being liquid is the principal advantage of organic fuels over gas fuels such as hydrogen and ammonia in terms of storage and safe handling.[7,14,15] Also, direct organic PEMFC provide considerable weight and volume advantages over indirect ones due to the elimination of the reforming step. This fact simplifies their application in low-temperature direct PEMFC.[16,17] Nowadays, there are rising demands for high-tech portable electronic devices such as cellular phones and laptop computers with a highly efficient source of power in terms of power output and operation times. DOFC can be used ideally for producing a few hundred watts to around 3 kW power, which for instance is very suitable for military purposes, while their operation doesn't need an electrical power supply.[14,18,19]

1.2 DOFC Reactions

A typical fuel cell consists of two electrodes (anode and cathode) separated by the membrane for ion-transport purposes (i.e., proton), with an external circuit for electron flow between the electrodes.[2,3] DOFC are a type of PEMFC in which oxidation of an organic compound such as formic acid, methanol, and ethanol occurs at the anode, and reduction of oxygen occurs at the cathode, to produce electrical

power. Figure 1.2 represents a simplified schematic of a DOFC. Complete oxidation of the fuel in the presence of water produces protons, carbon dioxide, and electrons (eq. 1.1). Protons and electrons combine with oxygen at the cathode to produce water (eq. 1.2). Oxygen can be either supplied by airflow or pure oxygen gas flow.

$$C_xH_yO_z + (2x - z)\ H_2O \rightarrow x\ CO_2 + (y + 4x - 2z)\ H^+ + n\ e^- \tag{1.1}$$

$$O_2 + 4\ H^+ + 4\ e^- \rightarrow 2\ H_2O \tag{1.2}$$

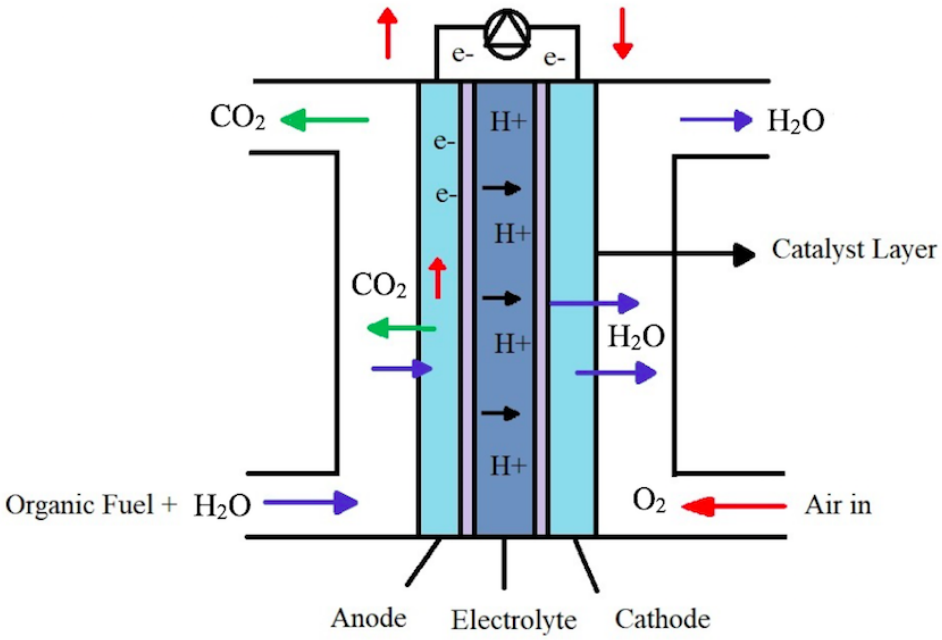

Figure 1.2: Schematic of a DOFC.

DOFC produce maximum charge when the fuel is oxidized completely to water and carbon dioxide. Table 1.1 compares theoretical energy density (per unit of volume or mass) for some organic fuels.[19,20] The energy density of organic fuels increases with the number of produced electrons in the oxidation reaction.[20] On the other hand,

Table 1.1: Energy densities of some organic fuels.[19,20] (E° is standard potential of reaction)

Type of fuel	**Anode reaction**	**Energy density** ($Wh\ L^{-1}$)	**Energy density** ($Wh\ g^{-1}$)
Methanol	$CH_3OH + H_2O \rightarrow CO_2 + 6\ H^+ + 6\ e^- \quad E^\circ = 0.016\ V$	4820	6073
Formic acid	$HCOOH \rightarrow CO_2 + 2\ H^+ + 2e^- \quad E^\circ = -0.17\ V$	1750	1630
Ethanol	$C_2H_5OH + 3\ H_2O \rightarrow 2\ CO_2 + 12\ H^+ + 12\ e^- \quad E^\circ = 0.085\ V$	6280	8028

the energy density is inversely proportional to the molar mass of the fuel molecule. However, complete oxidation of organic fuels is a complicated process and, in most cases, unachievable. In the evaluation of a fuel for DOFC, other factors, such as the toxicity of intermediates, should be considered as well.

1.2.1 Methanol Oxidation

Methanol is inexpensive and can be synthesized either through the direct oxidative conversion of natural gas or from a mixture of CO and H_2 obtained from incomplete combustion of natural gas. It also can be produced using CO_2 from the industrial exhaust through hydrogenative recycling.[19,21–23] Methanol as a liquid fuel with high energy density can be a promising alternative for hydrogen[2,21] in direct methanol fuel cells (DMFC). Methanol reacts at the anode in the presence of water to produce CO_2, 6 protons, and 6 electrons (eq. 1.3).

$$CH_3OH + H_2O \rightarrow 6\ CO_2 + 6\ H^+ + 6\ e^- \tag{1.3}$$

There have been many studies on the methanol oxidation reaction (MOR).[21,24,25] Breiter has suggested a general pattern of parallel pathways for complete oxidation of methanol.[26] After the adsorption of methanol, in one of the pathways, CO is produced and then is oxidized to CO_2. In the other pathway, CO_2 is produced through the oxidation of formic acid and formaldehyde intermediates. Both pathways require a catalyst to break the $C-H$ bonds and facilitate the oxidation of intermediates to CO_2. Various studies have shown that Pt is the most effective catalyst for $C-H$ bond breaking and complete oxidation of methanol.[22,26–28]

MOR in acidic media begins with adsorption of methanol at Pt sites (eq. 1.4) and proceeds through a series of electrochemical dehydrogenation steps (eq. 1.5-1.8).[21,29,30]

$$CH_3OH + Pt \rightarrow Pt - CH_3OH_{ads} \tag{1.4}$$

$$Pt - CH_3OH_{ads} \rightarrow Pt - CH_3O_{ads} + H^+ + e^- \tag{1.5}$$

$$Pt - CH_3O_{ads} \rightarrow Pt - CH_2O_{ads} + H^+ + e^- \tag{1.6}$$

$$Pt - CH_2O_{ads} \rightarrow Pt - CHO_{ads} + H^+ + e^- \tag{1.7}$$

$$Pt - CHO_{ads} + Pt - OH \rightarrow Pt - CO_{ads} + H_2O + Pt \tag{1.8}$$

At sufficiently high potentials, the CO intermediate adsorbed at the Pt surface (Pt–CO_{ads}), can be oxidized to CO_2 as the final step (eq. 1.9 and 1.10).[30,31] This step is also known as oxidative removal of the adsorbed CO.

$$Pt - CO_{ads} + H_2O \rightarrow Pt + CO_2 + 2\ H^+ + 2\ e^- \tag{1.9}$$

$$Pt - CO_{ads} + PtO \rightarrow 2\ Pt + CO_2 \tag{1.10}$$

1.2.2 Formic Acid Oxidation

Formic acid is the simplest small organic fuel that has been applied as a promising fuel for direct fuel cells. $Pt-$ (and $Pd-$) based catalysts are typically used for formic acid oxidation in direct formic acid fuel cells (DFAFC). The oxidation of formic acid occurs through a dual-path mechanism at the surface of platinum.[32] Initially, formic acid is adsorbed on the Pt surface. In the next step, it can be either dehydrogenated (eq. 1.11) to form CO_2[33,34] or dehydrated (eq. 1.12) and blocks (poisons) sites on the Pt surface by CO_{ads}. CO can be further oxidized to produce CO_2 (eq. 1.13).[33,35] The dehydrogenation pathway is known as the direct pathway and dehydration as the indirect pathway.

$$HCOOH_{ads} \rightarrow CO_2 + 2\ H^+ + 2\ e^- \tag{1.11}$$

$$HCOOH_{ads} \rightarrow -CO_{ads} + H_2O \tag{1.12}$$

$$-CO_{ads} + H_2O \rightarrow CO_2 + 2\ H^+ + 2\ e^- \tag{1.13}$$

1.2.3 Ethanol Oxidation

Ethanol is also one of the most studied liquid fuels for fuel cells.[36] Ethanol can be produced from agriculture, forestry, and urban residues. It is less toxic compared to methanol and has a higher energy density (8.03 $kWh\ kg^{-1}$ vs. 6.1 $kWh\ kg^{-1}$). However, the reaction pathways for the ethanol oxidation reaction (EOR) are much more complicated than for the MOR. They involve multi-step mechanisms which provide an obstacle in the development of direct ethanol fuel cells (DEFC). Cleavage of the $C-C$ bond in ethanol is the most challenging step in its mechanisms; therefore,

finding more efficient catalysts becomes a critical issue for DEFC development. The following equations (eq. 1.14-1.19) represent some of the proposed steps for the EOR in the presence of Pt.[37–39]

$$CH_3CH_2OH + Pt \rightarrow Pt\text{–}O - CH_2CH_3 + H^+ + e^- \tag{1.14}$$

$$CH_3CH_2OH + Pt \rightarrow Pt\text{–}CH(OH)CH_3 + H^+ + e^- \tag{1.15}$$

$$Pt\text{–}O - CH_2CH_3 \quad or \quad Pt\text{–}CH(OH)CH_3 \rightarrow Pt\text{–}CHOCH_3 + H^+ + e^- \tag{1.16}$$

$$\begin{aligned} &Pt\text{–}O - CH_2CH_3 \quad or \quad Pt\text{–}CH(OH)CH_3 \\ &\rightarrow Pt - CH_x + Pt\text{–}CH_yO + (7 - x - y)\ H^+ + (7 - x - y)\ e^- \end{aligned} \tag{1.17}$$

$$Pt\text{–}CH_2O \rightarrow Pt - CO + 2\ H^+ + 2\ e^- \tag{1.18}$$

$$Pt - CO + Pt - OH \rightarrow 2\ Pt + CO_2 + H^+ + e^- \tag{1.19}$$

Equation 1.17 shows the $C - C$ bond cleavage. After this step, absorbed species can be further oxidized to CO_{ads} and then CO_2 as the final product. However, the overall efficiency of the complete oxidation of ethanol as a fuel cell reaction is often very low.

1.2.4 Oxygen Reduction

For a continuous flow of current in a fuel cell, there must be an efficient reduction reaction happening in the cathode. This consumes electrons and protons produced through the oxidation of the fuel. Oxygen is the reactant that generally is applied in fuel cell cathodes, and Pt or Pd catalysts are used for the highest reduction efficiency. The oxygen reduction reaction (ORR) occurs through two parallel pathways.[40,41] In the first pathway, which is called dissociative pathway (eq. 1.20-1.22), the oxygen molecule is first absorbed to the surface of the catalyst, and the $O = O$ bond is

weakened by metal-oxygen interaction. Dissociation of oxygen coincides with the addition of a proton to each oxygen to produce water.

$$^1/_2\ O_2 + M_{(reaction\ site)} \rightarrow O - M \tag{1.20}$$

$$O - M + H^+ + e^- \rightarrow HO - M \tag{1.21}$$

$$HO - M + H^+ + e^- \rightarrow H_2O + M \tag{1.22}$$

Complete reduction of oxygen to water through consumption of 4 electrons is the most favorable path, which can also happen through an associative pathway.

The associative pathway starts with protonation of an absorbed oxygen molecule and production of a $HO_2 - M$ intermediate (eq. 1.23-1.24). This intermediate can either reduce to hydrogen peroxide (eq. 1.25) or proceed with complete oxidation to water (eq. 1.26-1.28).

$$O_2 + M_{(reaction\ site)} \rightarrow O_2 - M \tag{1.23}$$

$$O_2 - M + (H^+ + e^-) \rightarrow HO_2 - M \tag{1.24}$$

$$HO_2 - M + (H^+ + e^-) \rightarrow H_2O_2 + M \tag{1.25}$$

$$HO_2 - M + (H^+ + e^-) \rightarrow H_2O + O - M \tag{1.26}$$

$$O - M + (H^+ + e^-) \rightarrow HO - M \tag{1.27}$$

$$HO - M + (H^+ + e^-) \rightarrow H_2O + M \tag{1.28}$$

To achieve high efficiency of ORR, a high loading of Pt is required. Due to the high price of Pt metal, efforts are being made to find alternative non-Pt catalysts. ORR is discussed further in the section 1.4.3.1.

1.3 Typical Voltammetric Observations for DOFC Anodic Reactions

1.3.1 Electrocatalytic Oxidation of Formic Acid at Pt

Formic acid is non-toxic in dilute solutions, and can be produced as a byproduct of levulinic acid synthesis or through reduction of CO_2. Therefore, it has the capacity to become an important renewable fuel.[2,42] Knowing the fact that formic acid can be produced as an intermediate during methanol or ethanol oxidation, adds to the importance of the formic acid oxidation understanding.[16] Moreover, high power density, fast oxidation kinetics, and a high theoretical cell potential are known as the main advantages of DOFC.[34,42,43] However, selecting an appropriate and efficient anode catalyst is the first and foremost challenge to achieve these accomplishments.

As an example, Sanjeske et al. have studied the mechanism of formic acid oxidation reaction (FAOR) on Pt in acidic media by applying an in situ spectroscopy technique for probing oxidation intermediates.[44] Figure 1.3 shows a cyclic voltammogram for the oxidation of a 0.1 M formic acid in 0.5 M sulfuric acid as recorded in Sanjeske et al. studies.[44] During the positive going potential scan, at 0.6 V, an oxidation peak of formic acid was observed, which is stated by authors to be highly influenced by both adsorption/desorption of CO and adsorption of dehydrogenated of formic acid (formate). The second anodic peak was observed at 0.9 V coinciding with the highest concentration of formate with no evidence of CO presence. According to the authors, at this potential all absorbed CO was stripped and the current reduced due to Pt oxide formation at higher potentials. Sanjeske et al.

explained that, during the negative going potential scan at 0.85 V, while the reduction of the oxide layer was still occurring, formate formation commenced and increased in the same pattern as the oxidation peak but with less intensity. They also observed CO formation at 0.5 V, which increased with a potential decrease.[44] Grozovski et

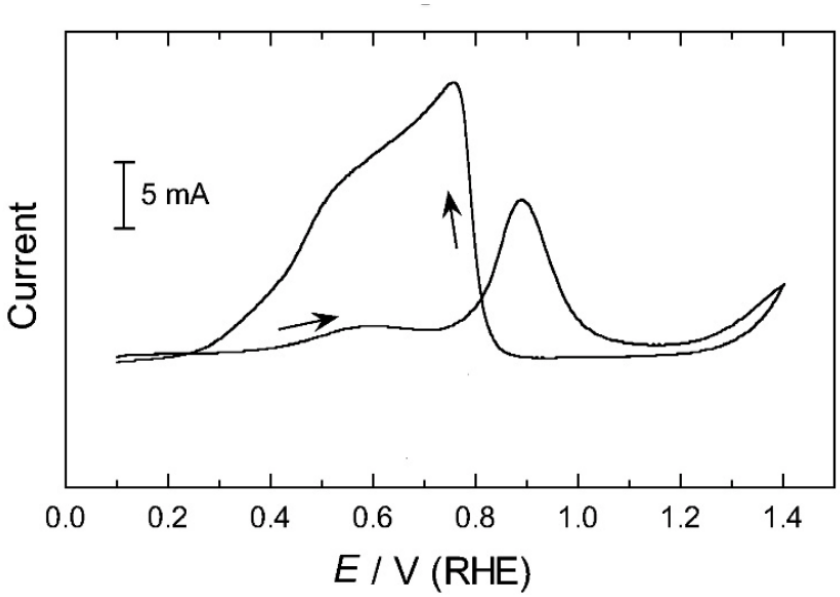

Figure 1.3: Cyclic voltammogram of 0.1 M formic acid in 0.5 M H_2SO_4 at a platinum electrode with scan rate of 50 $mV\ s^{-1}$. Reprinted with permission from Reference,[44] Copyright (2006), American Chemical Society.

al. also studied FAOR on Pt nanoparticles.[45] They stated FAOR occurred mainly through direct oxidation path in negative potential scan until the potential reached to 0.5 V and lower where CO adsorption was initiated. They also observed smaller positive potential scan oxidation currents compared to negative scan and attributed that to the blockage of Pt electrode sites by CO absorption at low potentials.[45]

1.3.2 Electrocatalytic Oxidation of Methanol at Pt

The MOR is the most investigated subject among the oxidation of other small organic molecules and it is the most popular fuel for direct alcohol fuel cells (DAFCs).[19,46] Complete oxidation of methanol to CO_2 requires an efficient catalyst to facilitate $C-H$ bond dissociation. Pt is known to be the most effective catalyst for $C-H$ scission.[22,26–28] Dissociative methanol adsorption on Pt is a multistep process, and it leads to formation of various adsorbed species.

Figure 1.4 shows a typical cyclic voltammogram of 1 M of methanol in 1 M H_2SO_4 at an unsupported platinum electrode as investigated by Prabhuram and Manoharan.[47] They reported that MOR initiated at 0.06 V through dehydrogenation. They also stated that, at this potential, methanol is adsorbed on Pt as well and $Pt-H$ oxidation is commenced. At 0.44 V, the oxidation current was increased sharply to a peak of 0.95 V, which was ascribed to the formation of $PtOH_{ads}$, Pt_2CO, and $PtCO_2H$ species followed by CO_2 production. The distinctive oxidation peak, observed at 0.77 V in the negative potential scan, is attributed to the oxidation of CO_{ads} to CO_2.[47] Zhao et al. investigated oxidation peak of methanol electrooxidation on noble metal electrodes in negative going potential scan. The authors stated the cathodic oxidation peak was originated from oxidation of freshly adsorbed methanol on catalyst surface after metal oxide layer was removed.[48]

1.3.3 Electrocatalytic Oxidation of Ethanol at Pt

Theoretically, ethanol is almost a perfect fuel for fuel cells. It is safe with high energy density and can be simply produced from renewable biomass (i.e. sugar

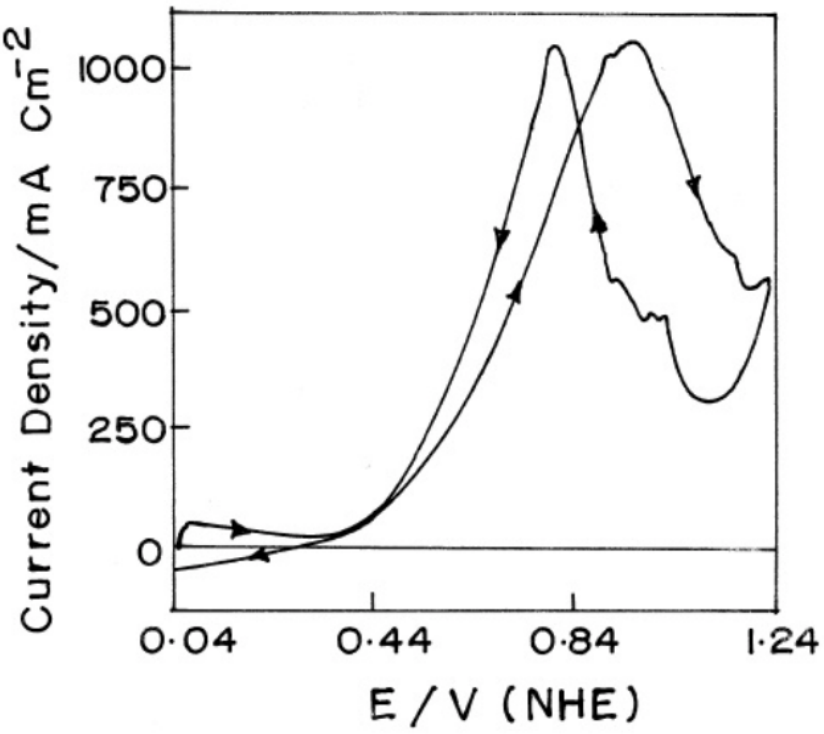

Figure 1.4: Cyclic voltammogram of 1 M methanol in 1 M H_2SO_4 at a unsupported platinum electrode with scan rate of 25 $mV\ s^{-1}$. Reprinted from Reference,[47] Copyright (1998), with permission from Elsevier.

fermentation).[2,21,49] In many studies, Pt is reported to be the most effective catalyst for breaking the $C-C$ bond.[38,50–52] The EOR at Pt occurs in a number of multistep pathways. It is initiated by adsorption of ethanol on the Pt surface while it is decomposed to intermediates such as CH_xCO, C_2HX, CH_xO, CO, and CH_x species. Various spectroscopy techniques have been applied to study EOR mechanisms on Pt and Pt alloys.[1,53,54] Figure 1.5 shows the oxidation of ethanol at Pt, studied by Shao et al. using surface enhanced infrared absorption spectroscopy (SEIRAS) with attenuated total reflection (ATR).[53] Based on their observations, formation of adsorbed CO occurred at almost all scanned potentials but mainly at low potentials

during the positive scan. As the potential was scanned to higher than 0.3 V, acetate formation was initiated and reached a maximum amount at 0.65 V. Also, at this potential the minimum amount of CO_{ads} was observed, which was due to its oxidative removal during the main peak of the first anodic oxidation peak. The second peak appearing in the anodic extreme, overlapping a rising current, was attributed to the desorption of acetate and formation of PtO. In the backward scan, the inhibiting oxide layer on Pt was removed and acetaldehyde/adsorbed acetyl formed from fresh ethanol.

Torrero et al. have investigated the oxidation of ethanol on carbon supported Pt in D_2O using an in situ IR technique.[1] They could detect acetaldehyde and/or acetic acid at potentials higher than 0.4 V (vs. $Ag/AgCl$ reference electrode), which were not possible to distinguish in the presence of the H_2O IR band. They reported acetaldehyde formation at low potentials which is oxidized to acetic acid in presence of hydroxyl groups on Pt at potentials higher than 0.4 V. Also, at potentials higher than 0.6 V both acetaldehyde and acetic acid were observed in this study.

1.4 Electrochemical Techniques

Cyclic voltammetry, chronoamperometry, and rotating disk voltammetry are three powerful electrochemical techniques that we applied in our research. Cyclic voltammetry can provide valuable information regarding kinetics and thermodynamics of oxidation/reduction reactions.[55] Chronoamperometry is also a sensitive and powerful technique for studying diffusion controlled processes occurring at an electrode. Moreover, it can be applied to evaluate the electrochemical activity

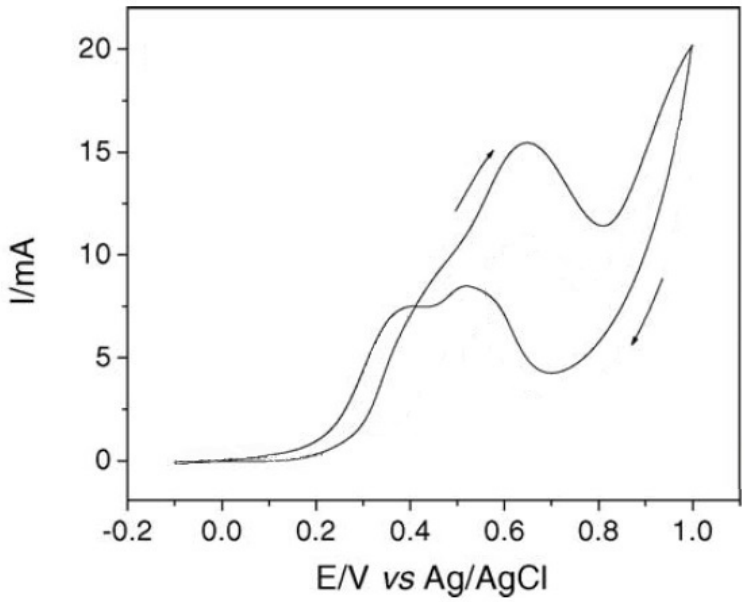

Figure 1.5: Cyclic voltammogram of 0.1 M ethanol oxidation in 0.1 M $HClO_4$ at a Pt thin film electrode. Reprinted from Reference,[53] Copyright (2005), with permission from Elsevier.

and stability of the electrocatalysts.[56] Rotating disk voltammetry is a hydrodynamic method that can be applied as a complementary technique for cyclic voltammetry and chronoamperometry because of its advantages in providing separation of the overall current into its kinetic and mass transport components.[55]

1.4.1 Cyclic Voltammetry

Cyclic voltammetry (CV) consists of cyclic potential scanning of a stationary working electrode between two potential values in a stationary solution and recording the current as a function of potential to produce a cyclic voltammogram (Figure 1.6).[55] The scan rate and number of cycles can be varied, while plotting current versus

potential gives a cyclic voltammogram. A cyclic voltammogram can provide a wide range of information about physical and chemical characteristics of reactants as well as reversibility of a redox reaction. Therefore, in most cases, CV is performed as the first diagnostic experiment in electrochemical studies.[55]

Figure 1.7 shows a typical CV for a reversible redox process with anodic and cathodic current peaks at a similar potential (peak separation $\sim 59/n$ mV).[55] However, for irreversible electrochemical reactions with complicated mechanisms, remarkably different CV are observed, as illustrated in previous sections. Irreversibility can happen chemically (ca. when the product of electrochemical reaction is transferred to a new species before reverse electron transfer reaction ($O + ne^- \rightleftharpoons R \rightarrow P$)) or electrochemically (ca. when the kinetics of the reaction is slow). In these situations the anodic peak shifts to higher potentials and cathodic peak becomes smaller or disappears.

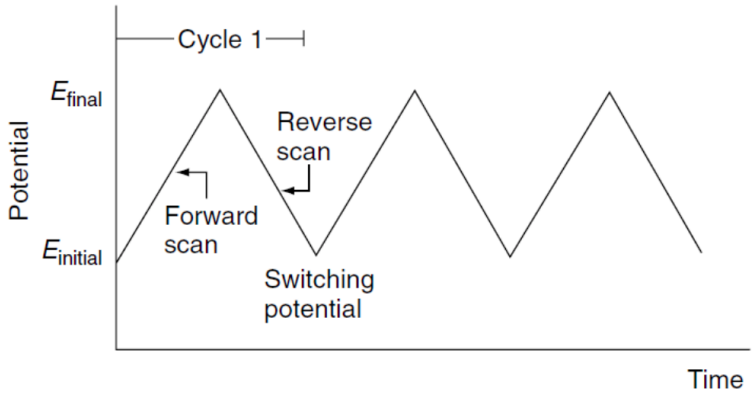

Figure 1.6: Potential changes vs. time in a cyclic voltammetriy experiment.[55]

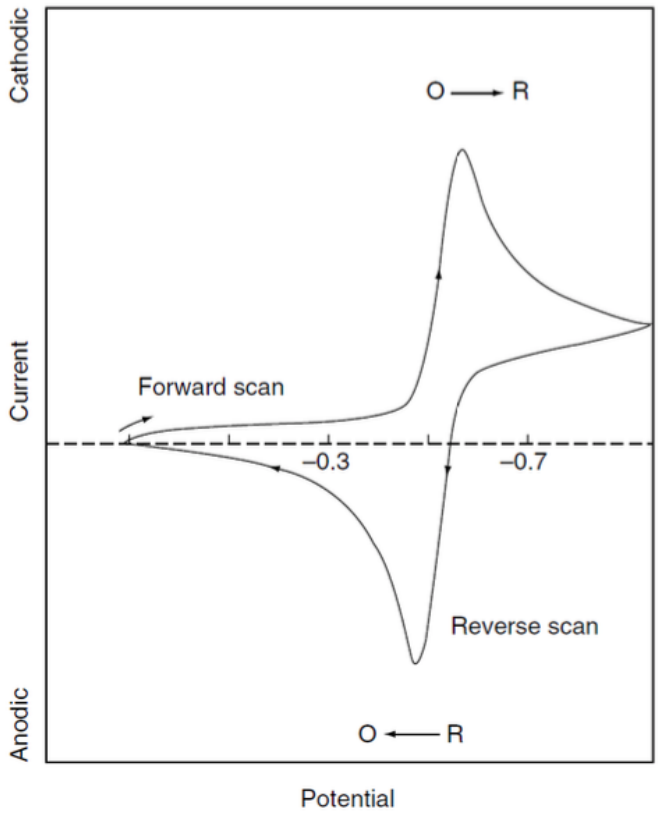

Figure 1.7: Typical cyclic voltammogram for a reversible $O + ne^- \rightleftharpoons R$ redox process.[55]

1.4.1.1 CV of Pt

Many investigations have been reported on the development of anode catalysts to increase the efficiency of DOFC. The literature shows that metal catalysts have different catalytic properties based on their particle size, shape, and chemical composition.[57] Pt is widely used in PEMFC as a major component of both the anode and the cathode catalyst. It has remarkable activity, selectivity, and stability within the SOM framework. Also, it has a high activity for cleavage of the C–C bond of ethanol.[58–61]

Based on the crystallographic orientation of Pt atoms in the electrode structure, the characteristic CV shape of a Pt electrode in an inert electrolyte will be different. Figure 1.8 shows a CV of polycrystalline Pt in an acidic solution.[62] Two important potential regions can be observed in this voltammogram (underpotential adsorption and desorption of hydrogen, and oxide formation and reduction). During anodic scan at low potentials, hydrogen underpotential desorption peaks are observed. Integration of the current in this region can be applied to determine the electrochemically active electrode surface area for normalizing activities. Two merged cathodic peaks observed at low potentials of cathodic scan are related to underpotential adsorption of hydrogen. As the potential decreases to lower than 0.04 V, the hydrogen evolution reaction (HER) occurs.

At potentials between 0.8 V and 1.4 V formation of a Pt oxide layer is observed in a broad, complex anodic wave. At higher potentials (ca. 1.55 V), oxygen evolution occurs. The reverse (cathodic) potential scan strips off the oxide layer and provides a clean, bare Pt surface. A similar voltammetric pattern for hydrogen electrochemistry can be observed for some other metals such as Ir, Rh, Pd and Pt alloys.[31,62,63] The main issue with Pt and Pt-based catalysts is CO adsorption at the Pt surface (due to the poisoning effect of CO). This adsorption blocks the active sites of catalysts and inhibits further oxidization of organic fuels to CO_2. Figure 1.9 Shows CV of CO stripping from the surface of a Pt electrode.[37] In this CV, a sharp peak is observed for CO oxidation at 0.6-8.2 V vs. RHE. In this potential region water is activated towards formation of $Pt-OH$, which facilitates CO oxidation to CO_2. Alloying a more electropositive metal (M) with Pt to provide $M-OH$ groups at lower potentials can reduce the CO poisoning rate.[37,64] Moreover, high loadings of catalyst are needed

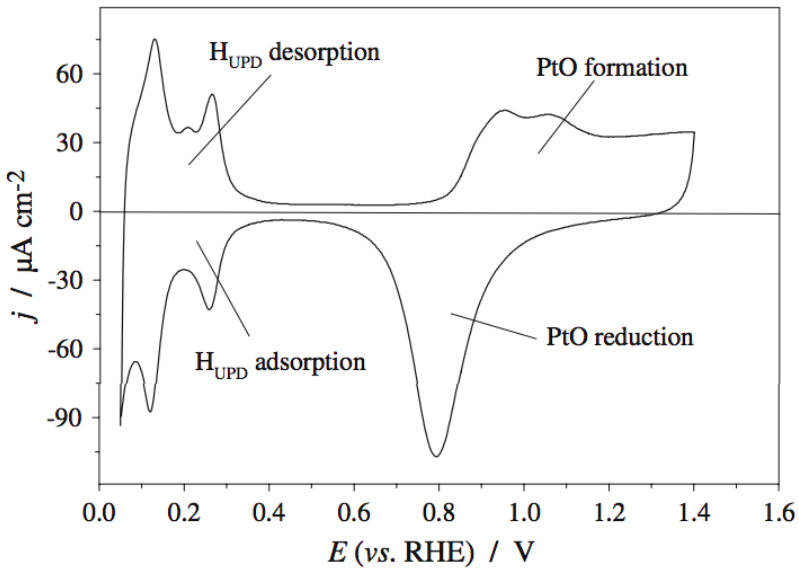

Figure 1.8: Cyclic Voltammogram of a Pt electrode in 1 M H_2SO_4 solution (scan rate = 100 $mV\ s^{-1}$). Reprinted from Reference,[62] Copyright (2010), with permission from Springer.

for a fuel cell; therefore, it becomes very costly to use pure Pt catalysts.[65–67]

1.4.2 Chronoamperometry

Chronoamperometry (CA) is another powerful diagnostic tool in electrochemical analysis. In this technique, the potential of the working electrode is generally stepped from a low enough potential for no reaction to occur to a potential in which the surface layer of the electrode becomes depleted of all electrochemically active reactants (diffusion control).[55,68] In this technique current is recorded as a function of time. Using this method, the charging current is only significant at short times, and therefore the faradaic signal is improved.

The interpretation of current vs. time plots in a step potential is relatively simple

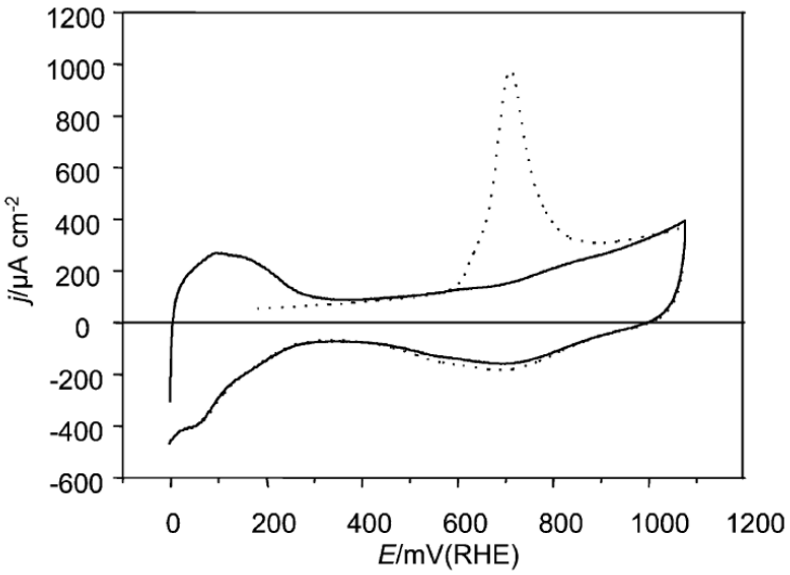

Figure 1.9: CO stripping voltammogram of a Pt catalyst in 0.1 M $HClO_4$ solution. Reprinted from Reference,[37] Copyright (2009), with permission from Elsevier.

for a reversible system; however, for an irreversible or quasi-reversible system, in which electron transfer kinetic is slow, complications arise.[55] Quasi-reversibility occurs when the electron transfer kinetic is slow but not slow enough to be considered an utterly irreversible system. For the systems with slow kinetics, an overpotential is required to facilitate a forward electrochemical reaction. The faradaic current is governed by both the kinetic of the electron transfer and mass transport. To study the kinetics of the electrode process, the kinetics of electron transfer should be the significant factor in directing electrochemical reactions while the effect of mass transport (i.e. diffusion in stationary solution) is negligible. i vs. t plots obtained from CA can provide information for the Tafel plot for mechanistic studies of irreversible reactions.[55] For an irreversible system such as SOM oxidation, the i vs. t plot gives a curve in which the current decays sharply and after a certain amount of time it reaches a steady-

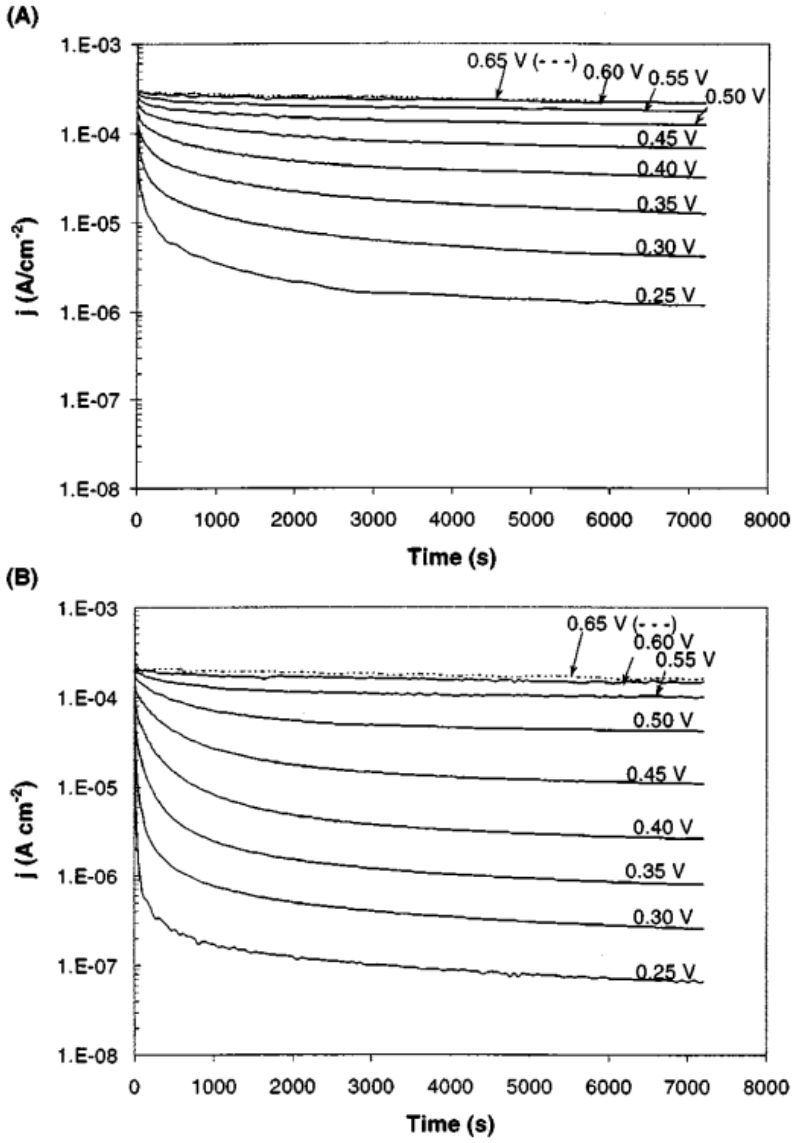

Figure 1.10: Current vs. time plots for step potential experiments in 0.1 M formic acid in 0.1 M H_2SO_4(aq) at (a) $PtPd$ and (b) Pt electrodes. Reprinted from Reference,[69] Copyright (2003), with permission from IOP.

state (i.e. kinetic current). For a quasi-reversible system, the i vs. t curve can be linearized by using mathematical treatments and the kinetic current can be obtained from interception of the linear plot. Figure 1.10 shows examples of potential step studies of FAOR on Pt and Pt/Pd nanoparticles conducted by Zhao et al..[69] They conducted stepped potential experiments at a range of potentials and recorded the current until it reached a fairly steady state. Then they investigated the mechanism of FAOR and the activity of both electrodes by using Tafel plots extracted from CA experiment data. More valuable information can be achieved by CA studies of SOM in addition to kinetic studies, such as activity and rate of electrode poisoning, as well as long-term stability of the catalyst.[70,71]

1.4.3 Rotating Disc Voltammetry

In the cases where the current density is relatively high, such as with thick catalyst layers or highly active electrode materials, concentration polarization (mass transport) can limit the current. Therefore, it becomes beneficial to apply a technique that can determine kinetic parameters independent of mass transport limitations. Moreover, as has been shown in previous hydrodynamic studies,[6,24] oxidation of organic fuels is not typically diffusion controlled which warrants the application of a technique that can extract pure kinetic controlled parameters.

Rotating disk voltammetry (RDV) is the most convenient and widely used hydrodynamic technique. In rotating disk voltammetry (RDV) a disk electrode rotation creates a radial force which drags solution containing reactants towards the center of the electrode. By this technique, higher mass transport to the electrode,

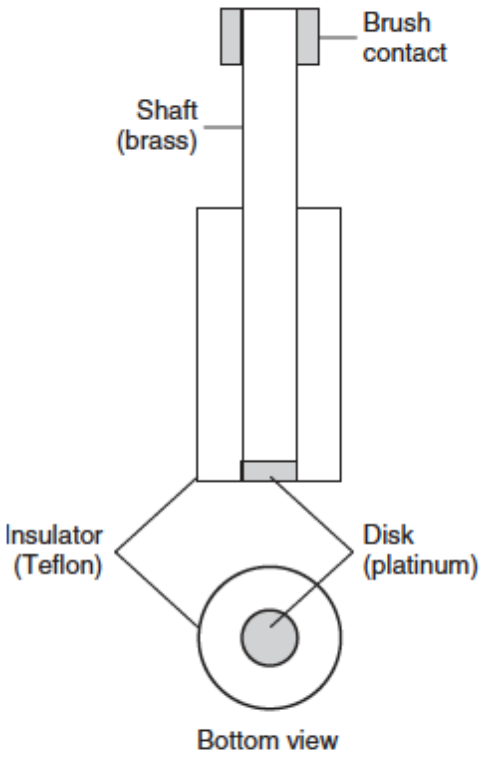

Figure 1.11: Rotating disk electrode (RDE).[55]

compared to the stationary electrode, is provided and more importantly the rate of mass transport can be controlled.[55] A rotating disk electrode (RDE) is illustrated in (Figure 1.11). The Koutecky-Levich equation (K-L) (eq. 1.29) is a mathematical treatment used for RDE rotation and provides important kinetic information.[55] By using the K-L equation, the overall current can be separated into kinetic (i_k) and mass transport limited (i_{lim}) components.

$$1/i = 1/i_k + 1/(0.62nFAD^{2/3}\nu^{-1/6}C\omega^{1/2}) \tag{1.29}$$

Parameters of this equation include; i_k for the kinetic current, n for the number

of electrons transferred, F for the Faraday constant, D for the diffusion coefficient, ν for the kinematic viscosity ($1.0 \times 10^{-2}\ cm^2\ s^{-1}$),[72] ω for angular velocity and C for the concentration of the reactant.[55] RDV can be a complement to cyclic voltammetry in catalyst performance evaluation. This method is widely used for oxygen reduction reaction (ORR) studies as a cathode reaction in a fuel cell.[73–75] In contrast, only limited RDV studies have been reported on catalytic electrooxidation of organic fuels.

1.4.3.1 ORR RDV

As mentioned in Section 1.2.4, ORR is a critical reaction occurring at the cathode of a PEMFC, and so far, a wide range of studies have been reported in order to understand its mechanisms. RDV is primarily used as an electrochemical technique for electrocatalysis studies of ORR.[73–76] A study on quantification of the activity of Pt electrocatalysts for ORR has been reported by Garsany et al.[73] using the RDV method. In this study, a three-electrode system (working, counter and reference electrode) was applied to compare the performance of three different coatings of Pt catalyst layer in ORR. They compared uniform, partially uniform, and nonuniform catalyst coatings by recording ORR polarization curves in O_2 saturated solution at various electrode rotation rates (ca. 400, 900, 1600, 2500, and 3600 rpm). By means of the K-L equation, they could calculate the mass transport corrected kinetic current for each catalyst layer, which indicates their efficiency. They showed the effectiveness of the catalyst layer became poorer as the catalyst film became less uniform. As a result, RDV could provide a convenient and accurate approach for the evaluation of various catalyst performances.

Pavel et al. applied a rotating ring disk electrode (RRDE) to study the ORR

mechanism on Pt nanoparticles attached to carbon nanotubes/nanofilaments.[74] In RRDE, the disk electrode is surrounded by a ring of conductive material with the option of independent potential control. As the electrode rotates, reactants first reach the surface of the disk electrode and some reacts, then the products reach the ring due to centrifugal forces and can be further oxidized or reduced. The ring provides the opportunity of detecting the H_2O_2 escape rate from the diffusion layer, and a better understanding of the mechanism can be achieved. The n value for ORR they obtained fell between 2 and 4. This means a mixture of the direct (eq. 1.30) and indirect (eq. 1.31-1.32) mechanisms of ORR occurs, which is primarily dependent on Pt loadings and potential. Figure 1.12 shows briefly the potential dependency of the ORR mechanism on Pt nanoparticles.[74]

$$O_2 + 4\ H^+ + 4\ e^- \rightarrow 2\ H_2O \quad (direct) \tag{1.30}$$

$$O_2 + 2\ H^+ + 2\ e^- \rightarrow 2\ H_2O_2 \quad (indirect) \tag{1.31}$$

$$H_2O_2 + 2\ H^+ + 2\ e^- \rightarrow 2\ H_2O \tag{1.32}$$

Zhou et al. also studied RDV and RRDV of ORR to determine the efficiency of oxygen conversion and understand its mechanism by obtaining the number of transferred electrons (n).[75] The n value is an essential factor since a low n value means incomplete oxidation and high concentrations of hydrogen peroxide, which has a detrimental effect on the proton exchange membrane in fuel cells. They applied two different catalysts, including Ru and Au, for this study. They showed that n values obtained by RDV (using K-L plot) were dependent on rotation rate and therefore unreliable. Also, they showed that n values obtained through the RRDV

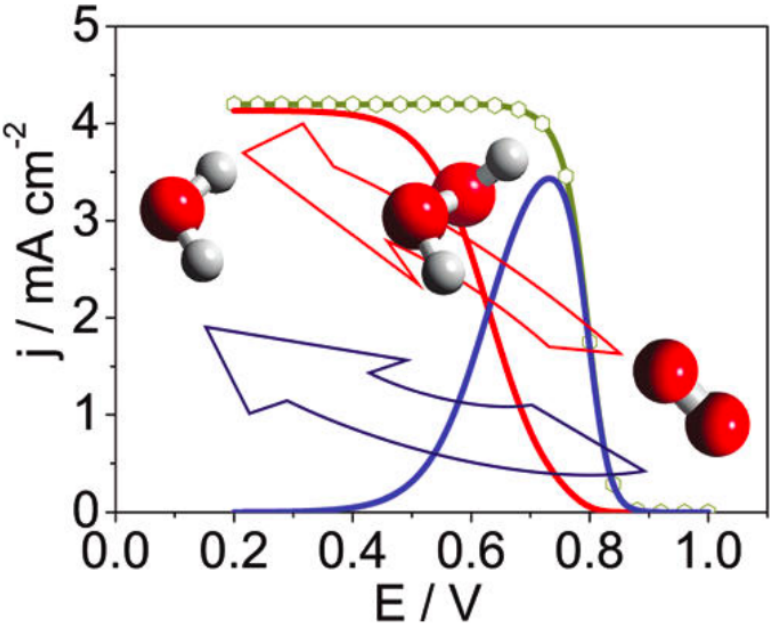

Figure 1.12: Schematic representation of the contribution of direct (blue) and series (red) paths to the overall ORR current (green). Reprinted with permission from Reference,[74] Copyright (2011), American Chemical Society.

method using a properly biased Au ring were theoretically and experimentally more reasonable and accurate.

Mohan and Cindrella studied linear sweep voltammetry (LSV) and CA of ORR on $PtNiO - A$, $PtCoO - A$, $PtCeO_2 - A$ and $Pt - A$ catalysts in acidic media by RRDE.[76] A is a cubic zeolite-A applied as a support for the catalyst preparation. ORR and the oxidation of hydrogen peroxide to H_2O were probed at disk and ring electrodes, respectively. As the electrode was rotated, the current of both disk and ring showed an increase. The n for all four catalysts measured to be 4. By calculation of i_k, they could compare the activity of the above-mentioned catalysts.[76]

1.4.3.2 FAOR RDV

Although RDV has been used as a powerful technique for ORR electrocatalytic studies, only a few reports can be found on RDV studying of the electrocatalytic oxidation of organic fuels. Pavese and Solis[77] reported that the FAOR current decreased at a palladium ring while the electrode was rotating. The decrease in current was attributed to the strong adsorption of oxidation intermediates, and therefore less available active surface area of the electrode.[77] Shin et al. also observed a decrease in FA oxidation current at a Pt disk electrode with rotation and attributed this to a decline in the accumulation of oxidizable intermediates.

Seland et al. reported an increase in oxidation current with electrode rotation for both positive and negative potential scans for formic acid oxidation at a Pt disk electrode, but K-L plots were not investigated.[78] A few more studies also reported normal RDV behavior with K-L plots, but in some cases, the K-L plots were not linear, or their slope was not interpreted.[79,80] Tian et al. studied the electrochemical oxidation of formic acid on regular carbon supported Pd electrode and modified one using RDV.[81] The FAOR peak current showed an increase and a slight shift to higher potentials as a result of electrode rotation (Figure 1.13).[81] K-L plots reported in this study were linear and parallel at low potentials. However, at higher potentials, slopes of the K-L plots decreased. Based on these observations, they concluded that mass transport through diffusion is the rate determining step (RDS) in FAOR. They also calculated kinetic currents using the intercepts of K-L plots to compare activity of two catalysts toward ethanol oxidation.

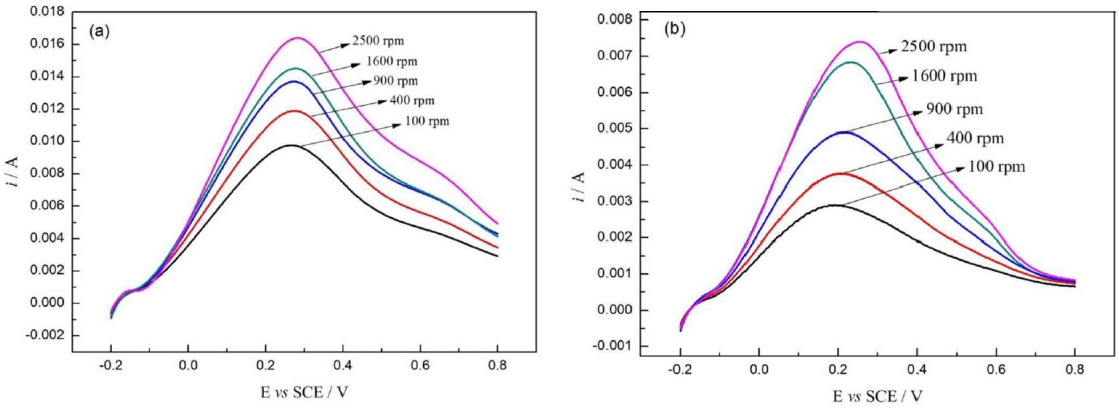

Figure 1.13: Cyclic voltammograms of 0.5 M formic acid in 0.5 M H_2SO_4(aq) at the surface of modified Pd (a) and carbon supported Pd (b) electrodes at various rotation rates. Reprinted from Reference,[81] Copyright (2018), with permission from IOP.

1.4.3.3 MOR RDV

Early studies of methanol RDV reported unusual behavior that depended on the type of electrode employed. Gojcovic has reported an extreme decrease in MOR current with the rotation of smooth Pt[82] and Pt_3Co[83] electrodes. This was ascribed to convective removal of intermediates (i.e., formic acid and formaldehyde) from the surface of the electrode. The same influence has been reported by Velazquez-Palenzuela et al. using $PtRu$ alloy nanoparticles on Vulcan XC-72 carbon black.[84] Seland et al. also observed a current decrease in both positive and negative going potential scans with electrode rotation for MOR at a Pt disk electrode.[78]

There are also research studies reporting either a significant increase in MOR current[85] or normal RDV behavior[86] with the rotation of the electrode. However, there are some unexplained points in these studies, such as applying a much lower apparent diffusion coefficient than is reasonable. Mohan and Cindrella also

investigated LSV and CA of MOR on v$PtNiO-A$, $PtCoO-A$, $PtCeO_2-A$ and $Pt-A$ catalysts in acidic media by RRDE.[76] They reported a decrease in MOR current at the disk electrode and positive shift of the onset potential by increasing the rotation rate. They ascribed the decrease in the current to the diffusion of intermediates away from the disk surface. On the other hand, they observed an increase in ring current, which originated from further oxidation of MOR intermediates. The higher the rotation rate, the lower the disk current, and the higher the ring current were observed in this study.[76]

Puthiyapura et al.[6] studied electrooxidation of methanol, ethanol, n-butanol, and 2-butanol using RDE. They applied either a carbon supported Pt film or electrodeposited Pt film on glassy carbon electrodes in a three-electrode system for this study. The MOR current for both anodic peaks decreased (Figure 1.14)[6] with rotation rate increase (in the range of 0 to 900 rpm) at the electrodeposited Pt film. This observation was ascribed to the diffusion of oxidation intermediates away from catalyst surface, preventing their further oxidation. It has been said that there is a competition between the diffusion of methanol to and diffusion of intermediates away from the electrode surface. Also, they said that at high rotation rates, CO_2 formation happened only through oxidation of CO_{ads} while at a stationary electrode, both parallel mechanisms are involved in CO_2 formation (Section 1.2.1). They observed the same trend of MOR current decrease vs. rotation rate increase at carbon supported Pt as well (Figure 1.13).[6]

Recently Xu et al. studied the effect of scan rate and mass transport on MOR.[87] They studied MOR at both low and high potential scan rates at a smooth polycrystalline Pt electrode (Figure 1.15).[87] A significant decrease in oxidation

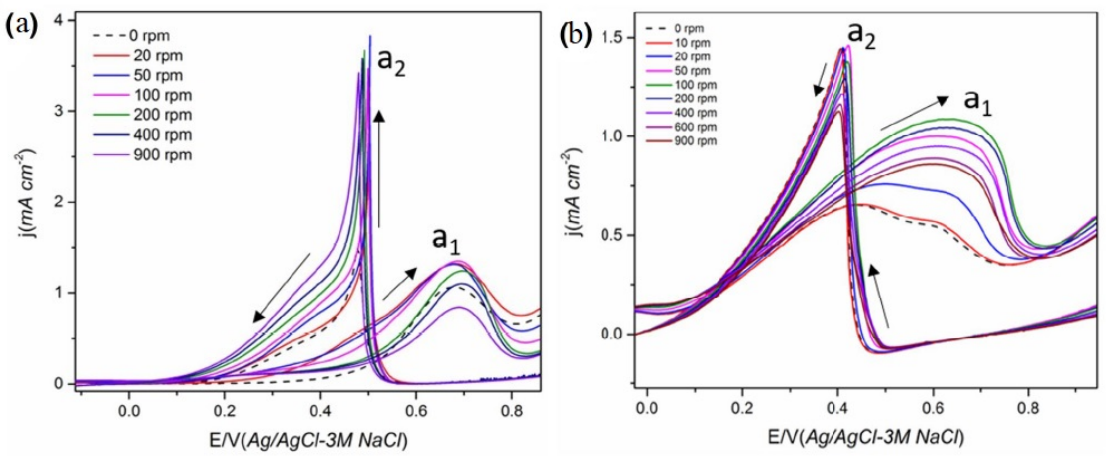

.

Figure 1.14: Cyclic voltammograms of 0.1 M methanol oxidation in 0.1 M $HClO_4$ at the surface of electrodeposited Pt film (a) and carbon supported Pt (b) electrodes at various rotation rates.[6]

current was observed with increasing rotation rate at overpotentials higher than 0.25 V and low potential scan rate (10 $mV\ s^{-1}$). No change in current appeared at low overpotentials (-0.2 to 0.25 V) at low scan rate and was attributed to deactivation of the electrode due to adsorption of MOR intermediates. Opposite behavior was observed for high potential scan rate (400 $mV\ s^{-1}$). They reported that adsorption of intermediates such as CO was less pronounced at low overpotentials for high scan rates due to the fast electrochemical reaction process. Therefore, intermediates are removed away from the electrode surface by rotation of the electrode and more free active sites became available, resulting in a MOR current increase. While at low scan rates, intermediates are absorbed firmly and MOR occurs through soluble species ($HCHO$ and $HCOOH$) pathways. This means that both rotation rate and potential scan rate effect mass transport and therefore the MOR pathways.

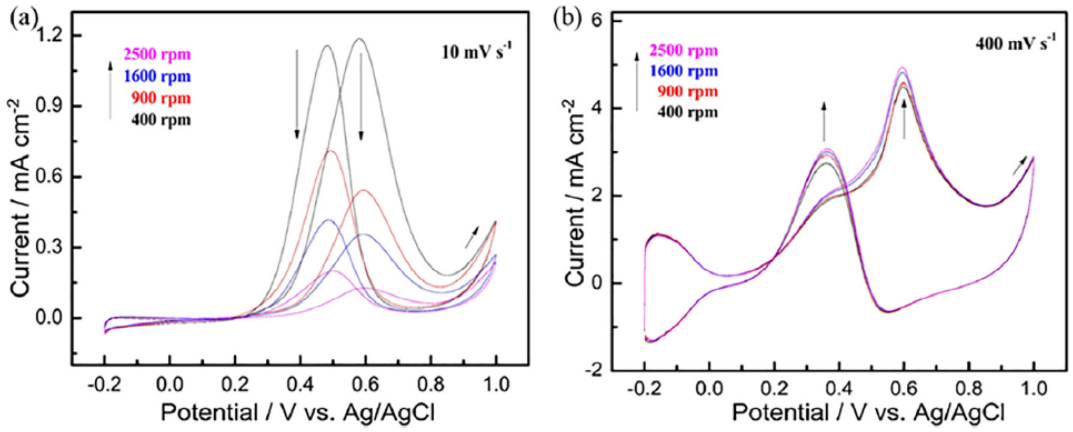

Figure 1.15: Dependence of anodic oxidation peak current of methanol on RDE rotating rate at different potential scan rates (10 $mV\ s^{-1}$ and 400 $mV\ s^{-1}$) at a Pt electrode. Reprinted from Reference,[87] Copyright (2020), with permission from Elsevier.

1.4.3.4 EOR RDV

There have only been a few reports on RDV of ethanol, and the results show either a decrease in oxidation current with electrode rotation[88] or an insignificant effect.[87] Shieh and Hwang have investigated ethanol electrooxidation kinetics at a ruthenium oxide RDE in alkaline solutions at 0, 100, 300, 500, and 1500 rpm at 26 $°C$.[88] In this study, the reaction current decreased as the rotation rate was increased, and it remained constant above 500 rpm. Convective removal of the acetaldehyde intermediate before it gets a chance to become further oxidized was assumed to be the main reason. Zheng et al. reported that rotation of Pt and Pt/Sn coated GC electrodes (100- 2500 rpm) increased the current for EOR in acidic solution and gave linear K-L plots.[85]

Seland et al. have reported the opposite effect of rotation rate on current in

anodic versus cathodic voltammetric scans.[89] They have ascribed strongly adsorbed intermediates such as CO to the current decay with the rotation of the electrode in the anodic scan, and slow formation of adsorbed intermediates to the current increase during the cathodic scan of potential. McClure et al. studied EOR in alkaline media on various homemade Pd_xAu_{1-x} catalysts using RDE. In this study the electrode was rotated at a constant rate (i.e. 900 rpm) to obtain a consistent hydrodynamic boundary layer.[90]

In an RDV study of EOR, Puthiyapura et al.[6] reported contradicting effects of rotation on the electrooxidation current for ethanol at carbon supported Pt and electrodeposited Pt film catalysts. At the electrodeposited Pt film, the oxidation current peak in the anodic scan (a_1) decreased with an increase in rotation rate (Figure 1.16),[6] similar to methanol. However, in contrast to methanol, the peak in the cathodic scan (a_2) increased with increasing rotation rate up to 100 rpm and then remained constant at higher rotation rates. They stated that in contrast to MOR, where the a_2 peak current is the result of the fast formation of CO_2, in EOR the current is due to the slow formation of acetic acid and acetaldehyde from freshly adsorbed ethanol. The stability of the current with rotation rate increase is attributed to a non-mass transport controlled EOR process. At Pt/C, the current increased for both oxidation peaks (Figure 1.15).[6] This contrasting response of the catalysts was attributed to rough carbon surface at Pt/C, which facilities longer residence times of adsorbed intermediates and, therefore more complete EOR. Pushkarev et al. applied RDE to study electrooxidation of ethanol on 20% Pt/C to assess various catalysts activity and determine n values involved in the reactions.[91] They applied different rotation rates at a range of constant potentials (i.e. 0.6-0.9 V vs. the

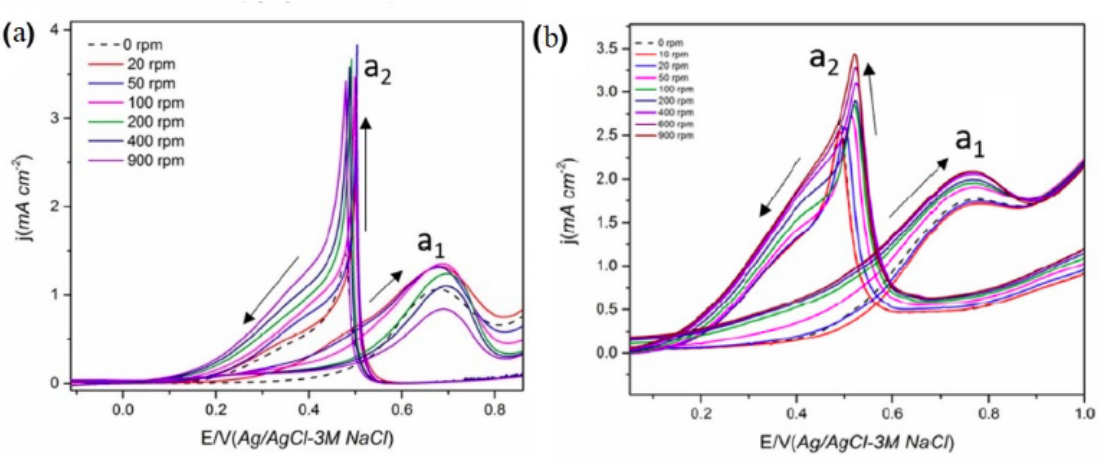

Figure 1.16: Cyclic voltammogram of 0.1 M ethanol oxidation in 0.1 M $HClO_4$(aq) at the surface of electrodeposited Pt film (a) and carbon supported Pt (b) electrodes at various rotation rates.[6]

standard hydrogen electrode (SHE)). Current increased with rotation rate and fairly linear but non-parallel K-L plots were obtained. They extracted kinetic current and n values from K-L plots for each studied catalysts for performance assessment and comparisons. Through RDV studies they showed n value is dependent on potential, and it increases for $SnPt$ electrode compared to Pt electrode.

1.5 Flow Cells

Methodologies with the ability to produce controlled mass transport are required for a better understanding of catalytic activity towards the electrooxidation of organic fuels. These techniques provide the opportunity for determination of kinetic parameters without concentration polarization (mass transport) limitation.[55] RDE which is discussed in section 1.4.3, despite its all advantages, still has some

deficiencies. For instance, product collection is very challenging for RDE, due to the escape of volatile oxidation intermediates from the rotator gasket. Moreover, mass transport by rotation of a RDE occurs through a relatively thick diffusion layer. On the other hand, in a flow cell, the flow of the analyte past or through the electrode can provide more effective mass transport. It also can be designed with various beneficial features, such as highly efficient collection of products.[92,93] Particularly, it can be designed quite similarly to a fuel cell system and provide more relevant data for fuel cell development purposes. The flow rate of the electrolyte solution into the cell can be controlled easily with an external pump, and products can be collected from cell exhaust.[92,93]

Sun et al. have investigated the electrooxidation of ethanol at a carbon-supported Pt/Vulcan catalyst with a high-pressure/high-temperature differential electrochemical mass spectroscopy (DEMS) set-up.[94] They applied a thin-layer channel flow cell "under reaction and transport conditions" relevant to fuel cells. However, they were not able to discriminate between acetaldehyde and acetic acid as partial oxidation products.

An electrochemical flow cell was designed based on a wall-jet configuration by Temmel et al. to investigate the ORR on various Pt catalysts.[95] Their new design was applicable for non-conductive substrates, and the atmosphere in which the experiments were conducted could be controlled. Bondue et al. designed a two-compartment flow-through cell combined with DEMS.[96] This flow cell, which consisted of 6 electrodes, was applied for ORR studies as well. Gisela et al. studied FAOR kinetics on Pt using a flow cell.[97] However, only electrochemical measurements were conducted in this study. Recently, Cychy et al. designed a spectrochemical flow

cell to study electrooxidation of the alcohols.[98] A plastic pump was applied to pump electrolyte solution through the center of a borehole electrode. They studied ethanol oxidation at a Ni_xB catalyst, and reported that flow of the electrolyte at a desirable rate provided effective mass transport of reactants to the surface of the electrode. They also reported that the flow prevents heterogeneous pH distribution.[98]

Among various flow cell designs, flow-through cells provide maximum utilization of the catalyst, and more even potential and current distributions. Since electrolyte passes through the working electrode, intermediates have more chance to react further, and higher efficiency can be achieved. The cell can also be designed to minimize the solution resistance.[92]

1.6 Thesis Outline

This project was based on two main parallel objectives. One of the objectives was to develop new methodologies for evaluating the intrinsic activity of various catalysts applied for formic acid (Chapter 5), methanol(Chapter 3), and ethanol (Chapters 4 and 6) oxidation. It is important to establish a reliable and inexpensive method for assessing fuel cell catalysts' activity through the determination of their pure kinetic currents. Therefore, we aimed to establish a simple system which can emulate the fuel cell hydrodynamics and provide separation of overall current into its kinetic and mass transport components. Developing reliable mathematical models was also required to determine corrected kinetic currents.

Another objective of this project was developing a simple and novel method to determine the n_{av} of ethanol oxidation. n_{av} is a crucial parameter which represents

the faradaic efficiency of the fuel. The investigation of n_{av} and the effect of various catalysts on its variation are of fundamental importance in improving DEFC's efficiency. Designing a simple electrochemical cell (Chapter 7), which can provide an efficient collection of oxidation products and is applicable in elevated temperatures, was also one of our main focuses. Thus establishing an efficient model which allows for the determination of the mass transport and kinetic parameters of a current for various catalysts in relation to formic acid oxidation was required. These parameters are crucial and can be applied for the determination of the n_{av} involved in complex oxidation reactions such as ethanol oxidation on the same catalyst.

Chapter 2

Experimental Methods

2.1 Chemicals and Materials

Solutions were prepared using anhydrous ethanol (Commercial Alcohols Inc.), methanol (Fisher Scientific), formic acid, hydrochloric acid (Sigma-Aldrich). Industrial grade nitrogen (Air Liquide) was used for oxygen removal from solutions during experiments.

Chemicals applied for catalyst ink preparation include: commercial carbon-supported Pt (20% Pt/C; Etek), commercial $Pt - Ru$ black (Ru : Pt = 50:50, Alfa Aesar), commercial carbon supported Pt (70% Pt/C, HiSPEC^{TM} 13100, 70% Pt on a high surface area advanced carbon support, Alfa Aesar, Lot# M22A026) and commercial carbon supported $PtRu$ alloy catalyst (75% $PtRu/C$) which was HiSPEC^{TM} 12100, 50% Pt and 25% Ru on a high surface area advanced carbon support, Alfa Aesar, Lot# P17B047). 1-propanol (J.T. Baker), and Nafion^{TM} solution in a mixture of lower aliphatic alcohols (5.14% from DuPont) were also applied for dispersion and adhesion of catalyst purposes respectively.

Carbon fiber paper (CFP; Toray^{TM}, TGP-H-090; 0.26 mm) and Pt black electrodes (proprietary) consisted of 4 $mg\ Pt\ cm^{-2}$ with a PTFE binder on wet-proofed CFP were used as electrode materials. CO_2 (Air Liquide) was used in detector calibration. Fumaric acid (Sigma) was used as an internal standard for product analysis.

2.2 Rotating Disk Voltammetry

2.2.1 Cell Compartments

A three-compartment glass cell was operated with a Pine Instruments RDE4 potentiostat and ASR Analytical Rotator. The working electrode was a glassy carbon rotating disk electrode (0.196 cm^2; Pine Instruments) loaded with catalyst ink. A piece of Pt wire was applied as a counter electrode. The reference electrode was either a saturated calomel electrode (SCE) (241 mV vs. SHE) or mercury sulfate electrode in 3.8 M sulfuric acid (MSE) (Koslow; 635 mV vs. SHE). All potentials reported in this thesis are given relative to the standard hydrogen electrode (SHE).

2.2.2 Preparation of Catalyst Ink

Catalyst inks were prepared by dispersing weighed amounts of catalyst powder in either a Nafion solution or a mixture of 1-propanol and Nafion solution. The mixture was homogenously sonicated in an ultrasonic bath for 1-3 h. The surface of a glassy carbon disk electrode was polished with an alumina slurry (0.3 μm, Sturbridge Metallurgical Services, Inc.) before the catalyst application.

For each experiment, the required amount of catalyst ink was applied with an Eppendorf micropipette (or fine paint brush) onto the polished surface of the RDE in several small aliquots. After using each aliquot, the electrode was rotated at a rate of 100 rpm for 15 min and then at 600 rpm for 5 min to achieve a homogeneous dispersion layer of catalyst on the surface. Between each application, the ink was sonicated for a minimum of 10 min to prevent precipitation. 4 μL of Nafion solution

was pipetted onto the catalyst layer and allowed to dry for 30 *min* at ambient temperature to improve the catalyst attachment.

2.2.3 Electrochemical Measurements

Either an EG&G model, 273A Potentiostat/Galvanostat, or RDE4 potentiostat was applied for electrochemical records. A Pine Instruments ASR Analytical Rotator was also used for the rotating working electrode. An EG&G Model 5210 Lock-in Amplifier and Power-Suite commercial software were used for cell impedance measurement.

2.3 Flow Cell

2.3.1 Cell Compartments

2.3.1.1 Three-Electrode Flow-Through Cell

A three-electrode flow cell was designed using two separate pieces of graphite blocks for anode and cathode compartment with a hole passing through the center for the electrolyte solution to flow (Figure 2.1). A wider hole was used in the cathode side to facilitate the removal of gas bubbles. Conical cavities adjacent to each graphite block dispersed the solution over the CFP layer supporting the anode catalyst (first electrode), and collected solution and gases from the cathode. Both the anode and cathode were circular pieces of carbon fiber paper (0.196 cm^2) coated with an intended catalyst layer, held in place by two layers of the gasket. A layer of Lexan plastic (6 *mm* thickness), with a hole in the center, was placed between the blocks to hold a reference electrode, which is attached from the side into the hole in a way that the

reference electrode locates between anode and cathode catalyst.

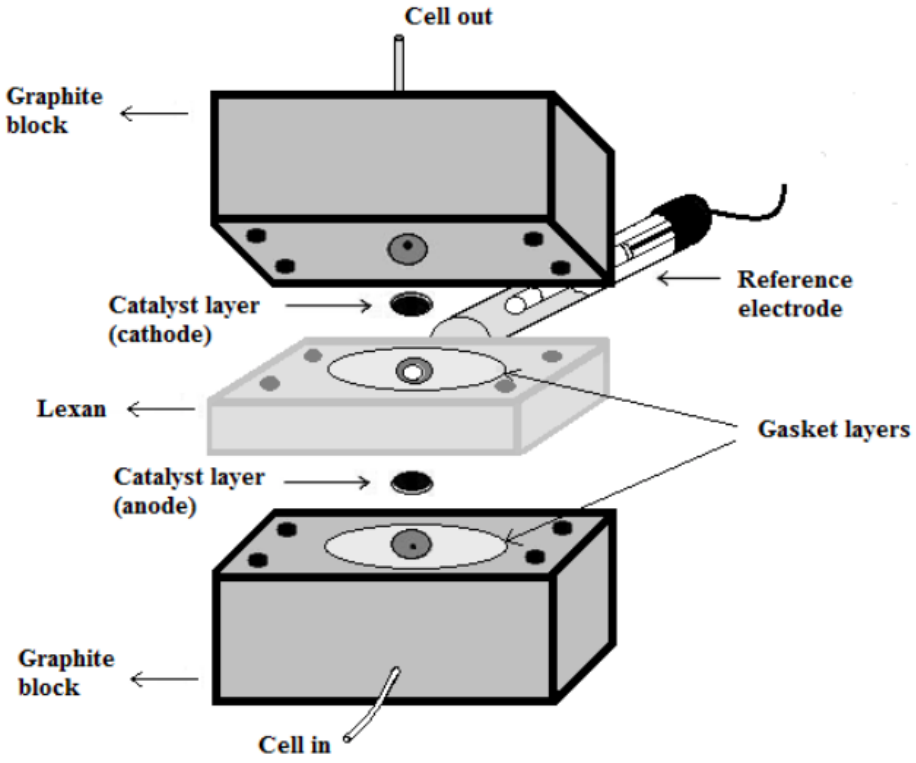

Figure 2.1: Schematic representation of the three-electrode flow-through cell.

In typical operation, the electrolyte solution was passed through the anode first and exited through the cathode. Carbon dioxide and hydrogen gas bubbles are produced through fuel oxidation at the anode and proton reduction at the cathode respectively and can interfere with electrochemical measurements. One of the beneficial approaches to the design in Figure 2.1 is that carbon dioxide and hydrogen bubbles can be flushed out of the cell by temporarily increasing the flow rate.

2.3.1.2 Two-Electrode Flow-Through Cell

The cell consisted of two stainless steel cylinders (anode and cathode) with a diameter of 3 cm and a thickness of 1 cm and conical cavities in the center. Catalyst layers for both anode and cathode were the same as for three-electrode cell held in place and separated by three silicone gaskets (Figure 2.2).

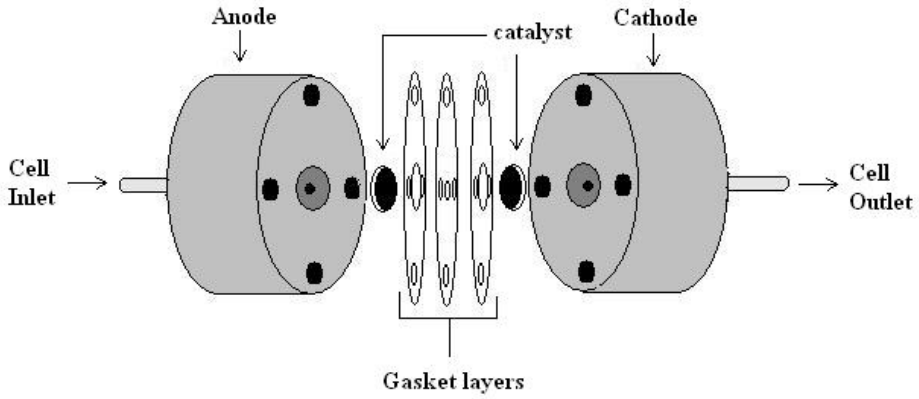

Figure 2.2: Schematic representation of the two-electrode flow-through cell.

2.3.2 Electrode Preparation

Either a custom made electrode or a commercial one was applied in flow cells. The commercial catalyst layer consisted of 4 $mg\ Pt\ cm^{-2}$ with a PTFE binder on wet-proofed CFP. Homemade catalyst inks were prepared by dispersing weighed amounts of catalyst powder in a mixture of 1-propanol and Nafion solution on circular pieces of CFP (0.196 cm^2).

2.3.3 Electrochemical Measurements

EG&G model 273A Potentiostat/Galvanostat was applied for electrochemical measurements. The EG&G Model 5210 Lock-in Amplifier and Power-Suite commercial software were used for cell impedance measurement.

2.3.4 Product Analysis

2.3.4.1 CO_2 Analysis

For CO_2 measurements, a Non-dispersive Infrared (NDIR)[99] Carbon Dioxide detector (commercial Telaire 7001) was applied, and CO_2 signals were recorded by Logger Pro3 software. This detector has a gas through inlet in which a gas stream of N_2 carries produced CO_2 into the detector, where a dual-beam absorption infrared method is used for detection. An IR source delivers light through the gas tube, and IR waves are absorbed by the CO_2 leading to a decrease in light detected. Beer's law represents the correlation between the intensity of light and analyzed concentration.

2.3.4.2 NMR Analysis

Proton nuclear magnetic resonance (^{1}H-NMR) spectroscopy was applied for the analysis of residual organic fuel, uncompleted oxidation products, and their derivatives. Uncompleted oxidation products consisted of acetic acid and acetaldehyde for ethanol. Formic acid and formaldehyde are bi-products of incomplete methanol oxidation. During each experiment, chemicals were collected in the cell outlet in a sealed container covered with a mixture of ice and dry ice in order to provide minimum loss of chemicals, especially acetaldehyde, which is very volatile. A

100 μL of the cell's exhausts was added to a 400 μL of fumaric acid solution in D_2O in an NMR tube for measurement purposes.

^{1}H-NMR spectra of collected samples were recorded by a Bruker AVANCE III 300 MHz with a BACS auto-sampler. A Topspin 3.0 with ICON was used as the software. The concentrations of the organic fuel and reaction products were measured against the peak area of the internal standard, which was fumaric acid in D_2O with a singlet in the spectra at 6.72 ppm. Spectra were referenced to sodium 3-(trimethylsilyl)-2,2,3,3-tetradeuteropropionic propionate at 0 ppm.

Chapter 3

Evaluation of Methanol Oxidation Catalysts by Rotating Disc Voltammetry

All experiments in this chapter were conducted by Azam Sayadi. Data analysis was performed by Azam Sayadi and Prof. Peter G. Pickup. This chapter has been published as (Sayadi, A.; Pickup, P. G. Evaluation of methanol oxidation catalysts by rotating disc voltammetry. *Electrochim. Acta* **2016**, *199*, 12-17). Prof. Peter G. Pickup was the corresponding author and Azam Sayadi contributed to writing of the first draft.

3.1 Introduction

The electrochemical oxidation of methanol is of fundamental importance in the development of our understanding of the electrochemistry of small organic molecules,[29,100–102] and central to the development of direct methanol fuel cells (DMFC).[19,103–106] The development of more active catalysts for methanol oxidation[106,107] requires efficient methodologies for evaluating large numbers of new formulations in sufficient depth to identify candidates for further development.[108] Typically, new catalysts for methanol oxidation are assessed by cyclic voltammetry and chronoamperometry, with the latter method providing data most relevant to DMFCs.[108] However, neither of these techniques provides a clear separation of kinetic and mass transport effects. Rotating disc voltammetry (RDV) is much more suitable for this, and so has become the normal method for evaluating oxygen reduction catalysts.[73,109,110] Although it should be possible to apply RDV similarly to methanol oxidation, and extract both steady-state kinetic parameters and stoichiometry (the number of electrons per methanol molecule), there are a number of complications. Consequently, there are few reports on methanol oxidation at rotating electrodes. Gojkovic reported that electrode rotation decreased the current for methanol oxidation at smooth Pt[82] and Pt_3Co alloy[83] electrodes, and attributed this to convective removal of partially oxidized products (mainly formaldehyde). Oxidation of methanol to formaldehyde produces only two electrons (eq. 3.1; $n = 2$) relative to the six electrons for complete oxidation to carbon dioxide (eq. 3.2; $n = 6$), and formic acid (eq. 3.3; $n = 4$) can also be produced. The number of electrons released during methanol oxidation (n_{av}), and hence the current produced,

is determined by the product distribution.

$$CH_3OH \rightarrow 2\ H^+ + 2\ e^- + HCHO \tag{3.1}$$

$$CH_3OH + H_2O \rightarrow 6\ H^+ + 6\ e^- + CO_2 \tag{3.2}$$

$$CH_3OH + H_2O \rightarrow 4\ H^+ + 4\ e^- + HCO_2H \tag{3.3}$$

Since both formaldehyde and formic acid can be further oxidized to CO_2, n_{av} depends strongly on the mass transport conditions, with thick catalyst layers and slow mass transport leading to more complete oxidation of the methanol (higher n_{av}).[111–113] Consequently, rotation of the electrode had less (negligible) influence when the electrode is coated with a layer of carbon supported Pt catalyst.[82,85] Electrode rotation has also been reported to have an insignificant effect on methanol oxidation at a $PtRu$ alloy on Vulcan XC-72 carbon black.[84] In contrast, a significant increase in current was seen with electrode rotation at a carbon supported Pt_9Sn catalyst.[85] In that work, a Koutecky-Levich plot was used to obtain the kinetic current, but the mass transport behaviour was not analysed. However, the methanol diffusion coefficient can be estimated to be ca. $1 \times 10^{-7}\ cm^2\ s^{-1}$ from that plot, which is much too low (the literature value is ca. 1.5×10^{-5}).[114]

Experiments in a flow cell, with arrays of catalytically active cylindrical Pt nanostructures at two different densities, paralleled the RDV results at Pt disc electrodes.[115] Simultaneous measurement of the CO_2 produced by differential electrochemical mass spectrometry (DEMS) showed that the efficiency for complete oxidation of the methanol decreased with increasing flow rate, and increased when the density of Pt nanostructures was increased. This was explained by a "desorption-readsorption-reaction" model in which reactive intermediates that desorb from the

electrodes can either be readsorbed or can diffuse into the bulk solution.[115]

Seland et al.[89] found that an increase in rotation rate caused a transient increase in current for the oxidation of 1 M methanol in 0.5 M H_2SO_4 at a Pt disc. This was attributed to the increased mass transport rate (i.e. the normal effect of electrode rotation), while the decrease in current with time was attributed to an increasing coverage of adsorbed intermediates.

Hou et al.[86] reported seemingly normal RDV behaviour for 1 M methanol (in 0.5 M H_2SO_4) at a polycrystalline Pt rotating disc electrode (RDE). Substantial increases in current were obtained over the range of 400–1600 rpm, with the data providing parallel Koutecky-Levich plots over the range of 0.4–0.6 V vs. RHE, and a linear Tafel plot with a slope of 125 $mV\ decade^{-1}$. However, the slopes of Koutecky-Levich plots gave an unreasonably low number of electrons of (ca. 10^{-5}) for the reaction, or an apparent diffusion coefficient of ca. $5 \times 10^{-12}\ cm^2\ s^{-1}$ (for $n = 6$). This was attributed to "counter diffusion of gaseous CO_2 and other intermediates in a thin film adjacent to the electrode surface".[86] Using a diffusion coefficient of $5.37 \times 10^{-12}\ cm^2\ s^{-1}$, obtained from chronoamperometry, they found that n_{av} increased from ca. 1.8 at 0.41 V to ca. 5.4 at 0.6 V.

The purpose of the work described here was to further develop RDV as a method for evaluating methanol oxidation catalysts, and in particular to address the very low apparent diffusion coefficient that has been reported[86] and the reliability of n_{av} values that are obtained. n_{av} is a central parameter in determining the energy efficiency of a DMFC, since the faradaic efficiency is proportional to n_{av} (efficiency for oxidation to $CO_2 = n_{av}/6$).[22,116] It also provides an indication of by-product[117] and harmful emission levels.[118] However, it is very difficult to measure n_{av} experimentally.[119]

Consequently, RDV would be a powerful techniques for catalyst evaluation if it could provide reliable n_{av} values. Here we demonstrate that methanol oxidation at thick layers of a carbon supported Pt catalysts, and $PtRu$ black, shows mixed mass transport and kinetic control of the current with a normal methanol diffusion coefficient. n_{av} values are consistent with reported product distributions.

3.2 Experimental

3.2.1 Materials and Solutions

Solutions were prepared by using methanol (95–98% from ACP Chemical Inc.), sulfuric acid (98% from ACP Chemical Inc.) and deionized water. Nafion^{TM} solution in a mixture of lower aliphatic alcohols (5.14% from DuPont), commercial carbon supported platinum (20% Pt/C; Etek) and commercial platinum-ruthenium black ($Ru : Pt$ = 50:50, Alfa Aesar) were used for catalyst ink preparation. Electrodes were polished with an alumina slurry (0.3 μm, Sturbridge Metallurgical Services, Inc.).

3.2.2 Electrode Preparation

Catalyst inks were prepared by dispersing weighed amounts of catalyst powder (ca. 50 $mg\ mL^{-1}$ for carbon supported Pt; 63 $mg\ mL^{-1}$ for $PtRu$) in a Nafion solution homogenously by sonicating in an ultrasonic bath for 1 h. For each experiment, the required amount of catalyst ink was applied with an Eppendorf micropipette (or fine paint brush for $PtRu$) onto the polished surface of a glassy carbon disk electrode

(0.196 cm^2; Pine Instruments) in several small aliquots. Before depositing each aliquot, the catalyst ink was sonicated again for 10 min. Each aliquot was allowed to dry for 20 min at ambient temperature. To improve the catalyst attachment, 4 μL of Nafion solution was pipetted onto the catalyst layer and allowed to dry for 30 min at ambient temperature. The catalyst loading amounts were 7.6 and 10 $mg\ cm^{-2}$ for the carbon supported platinum catalyst and ca. 8 $mg\ cm^{-2}$ for the $PtRu$ black catalyst.

3.2.3 Electrochemistry

Electrochemical measurements were at ambient temperature in a three-compartment glass cell operated with a Pine Instruments RDE4 potentiostat and ASR Analytical Rotator. The working electrode was a catalyst loaded glassy carbon rotating disk electrode and the counter electrode was a platinum wire. The reference electrode was either a saturated calomel electrode or mercury sulfate electrode in 3.8 M sulfuric acid. However, all potentials are given relative to SHE. Rotating disk cyclic voltammetery and constant potential experiments were run in 0.1 M methanol solutions with 1 M sulfuric acid as the electrolyte. Before each experiment, the solution was de-aerated by passing N_2 gas into the solution for 15 min and over the surface of the solution continuously during the experiments.

3.3 Results and Discussion

3.3.1 Carbon Supported Platinum (20% Pt/C)

From literature reports, it appears that electrode rotation begins to increase the current for oxidation of methanol when the Pt loading on the electrode reaches ca. 0.25 $mg\ cm^{-2}$.[82,85] Consequently, much higher loadings of a commercial carbon supported Pt catalyst were employed here, leading to significant increases in currents with increasing rotation rate. This is illustrated by the voltammograms in Figure 3.1 for 2 $mg\ Pt\ cm^{-2}$ (10 $mg\ cm^{-2}$ of 20% Pt/C). Although the current did not reach a mass transport limited plateau, rotation of the electrode did increase the current significantly at potentials above ca. 0.4 V. The current peaked in the 0.7–0.9 V region due to the formation (forward scan) and stripping (reverse scan) of an oxide layer on the Pt surface, which strongly inhibits methanol adsorption and oxidation.[86] The voltammogram of the electrode in the the absence of methanol in Figure 3.1 is distorted by resistance effects within the very thick catalyst layer, and so is not typical of other Pt/C voltammograms in the literature.[73]

Although voltammograms recorded over a range of electrode rotation rates could be analyzed to provide acceptable Koutecky-Levich plots in some cases, the small differences in currents relative to the large background current (in the absence of methanol) subtraction resulted in unacceptable uncertainty. Consequently, steady-state currents (i) were measured at constant potentials over a range of rotation rates (ω), as illustrated in Figure 3.2. Koutecky-Levich plots (i^{-1} vs. $\omega^{1/2}$) for data at various potentials are shown in Figure 3.3. These are approximately parallel, indicating that the diffusion characteristics did not vary significantly with potential.

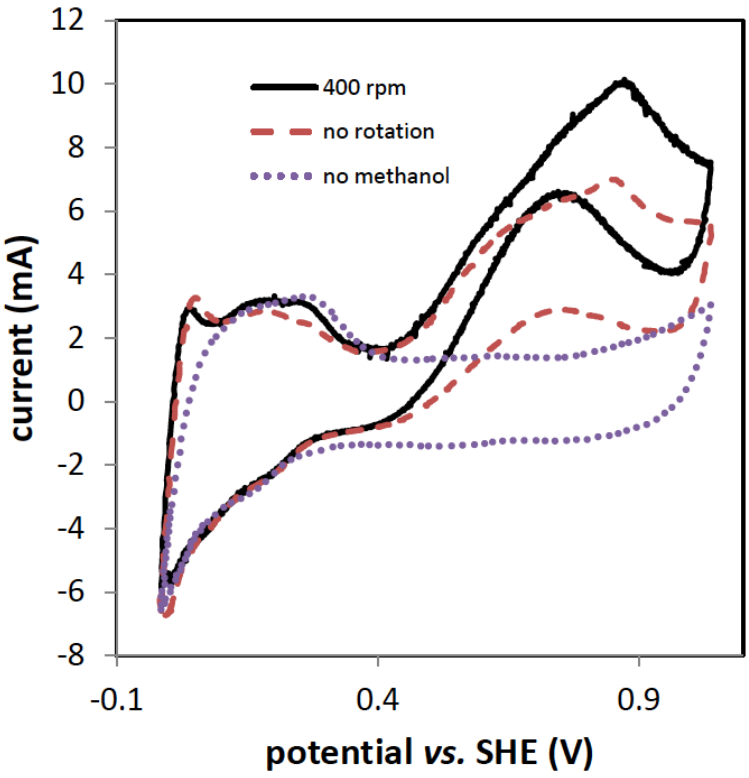

Figure 3.1: Cyclic voltammograms (10 $mV\ s^{-1}$) of a $GC/Pt/C$ (10 $mg\ cm^{-2}$) electrode in 1 M H_2SO_4(aq) (dotted), and with 0.1 M methanol without rotation (dashed) and at 400 rpm (solid).

Analysis of the slopes and intercepts according to the Koutecky-Levich equation (eq. 3.4) provided the diffusion and kinetic parameter listed in Table 3.1.

$$1/i = 1/i_k + 1/(0.62 n_{av} F A D^{2/3} \nu^{-1/6} C \omega^{1/2}) \tag{3.4}$$

where i_k is the kinetic current, D is the methanol diffusion coefficient, ν is the kinematic viscosity of the solution ($1.0 \times 10^{-2}\ cm^2\ s^{-1}$), C is the methanol concentration, and ω is the angular velocity. If it is assumed that the methanol is completely oxidized to CO_2 (eq. 3.2; $n_{av} = 6$), the data in Figure 3.3 give an

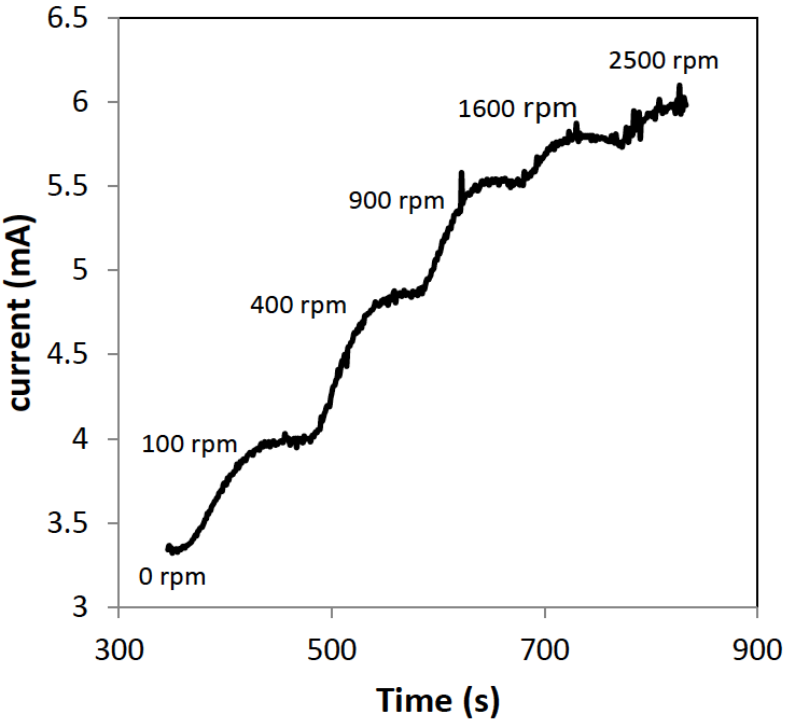

Figure 3.2: Current vs. time at 0.64 V and various rotation rates for the oxidation of 0.1 M methanol in 1 M H_2SO_4(aq) at a $GC/Pt/C$ (10 $mg\ cm^{-2}$) electrode.

average (apparent) diffusion coefficient of $(5.3 \pm 1.3) \times 10^{-6}\ cm^2\ s^{-1}$ (Table 3.1), which is unreasonably low. Literature values for the diffusion of methanol in water at ca. 22 $°C$ are ca. 1.4 *to* $1.5 \times 10^{-5}\ cm^2\ s^{-1}$.[114] Use of $D = 1.45 \times 10^{-5}\ cm^2\ s^{-1}$ in eq. 3.4 yields an average n_{av} of 3.1 ± 0.5. This indicates that the oxidation of methanol was inefficient, and that large amounts of formaldehyde plus formic acid were formed. The n_{av} values in Table 3.1 do not show at clear trend with potential, relative to the uncertainly of the measurement.

The n_{av} values reported in Table 3.1 are within the range expected from literature reports of product distributions at ambient temperature measured in differential

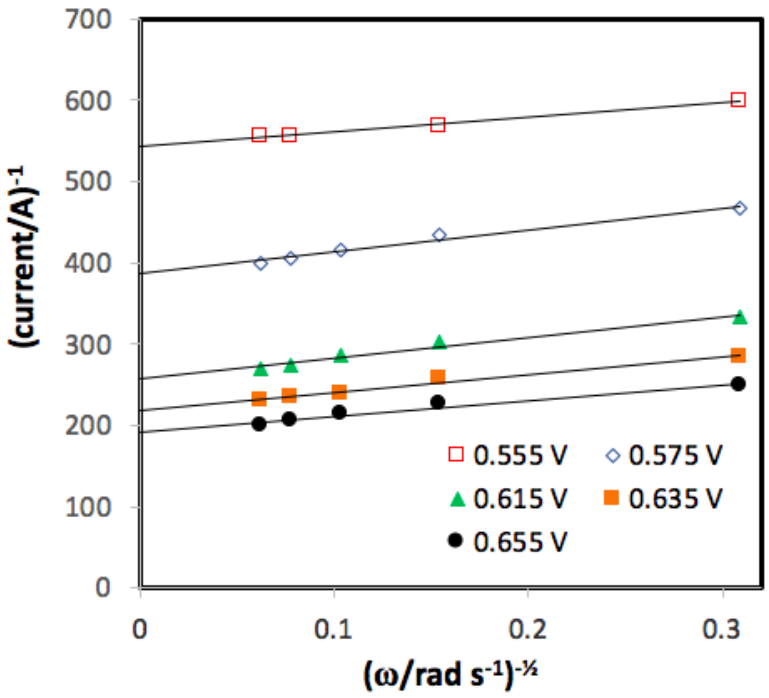

Figure 3.3: Steady-state Koutecky-Levich plots (i^{-1} vs. $\omega^{-1/2}$) for constant potential oxidation of 0.1 M methanol in 1 M H_2SO_4(aq) at a $GC/Pt/C$ (7.6 $mg\ cm^{-2}$) electrode.

electrochemical mass spectrometry (DEMS) studies.[112,113,120,121] Eq. 3.5[120] can be used to obtain n_{av} from the chemical yields of formaldehyde (y_{FAL}), formic acid (y_{FA}), and CO_2 (y_{CO2}).

$$n_{av} = 2y_{FAL} + 4y_{FA} + 6y_{CO2} \tag{3.5}$$

Wang et al. reported an n_{av} (z in ref.[120]) of 2.6 for oxidation of 0.1 M methanol at a Pt disc electrode[120], and faradaic CO_2 yields of 30% (2.5 $<n_{av}<$4.4) at a Pt disc and 88% (4.8 $<n_{av}<$5.7) at carbon supported Pt.[112] Jusys and Behm[121] reported that ca. 9.2 electrons were required to produce each CO_2 molecule in the oxidation

Table 3.1: Apparent diffusion coefficients (D_{ap}; for $n_{av} = 6$), kinetic currents (i_k), and n_{av} (for $D = 1.45 \times 10^{-5}\ cm^2\ s^{-1}$)[114] from the Koutecky-Levich plots (eq. 3.4) for 20% Pt/C shown in Figure 3.3.

E vs. RHE (V)	i_k (mA)	D_{ap} ($10^{-6}\ cm^2\ s^{-1}$)	n_{av}
0.555	1.8	7.0	3.7
0.575	2.6	3.8	2.5
0.615	3.9	4.2	2.6
0.635	4.6	5.2	3.0
0.655	5.2	6.2	3.4

of 0.1 M methanol at a 20% Pt/C catalyst layer. This puts n_{av} between 3.5 and 5.1, depending on the formic acid to formaldehyde ratio, which could not be quantified. In a later study it was reported that the CO_2 yield increased from 54% to 85% as the loading of catalyst was increased, and formic acid and formaldehyde yields were also reported.[113] The product distributions measured under potentiostatic conditions[113] yield n_{av} values ranging from 3.3 to 5.5 as the catalyst loading was increased.

The kinetic currents in Table 3.1 are presented as a Tafel plot in Figure 3.4. The Tafel slope of 200 $mV\ decade^{-1}$ is significantly higher than the value of 125 $mV\ decade^{-1}$ reported for RDV of 1 M methanol at a Pt disc,[86] and other literature summarized in that work. Gojkovic[122] reported 136 $mV\ decade^{-1}$ from cyclic voltammetry at 5 $mV\ s^{-1}$ for carbon supported Pt, but lower values were obtained with increasing time at constant potential. To investigate this apparent discrepancy with the literature, a Tafel plot was obtained from a background (no methanol) corrected cyclic voltammogram (CV; no rotation). The effect of rotation in the

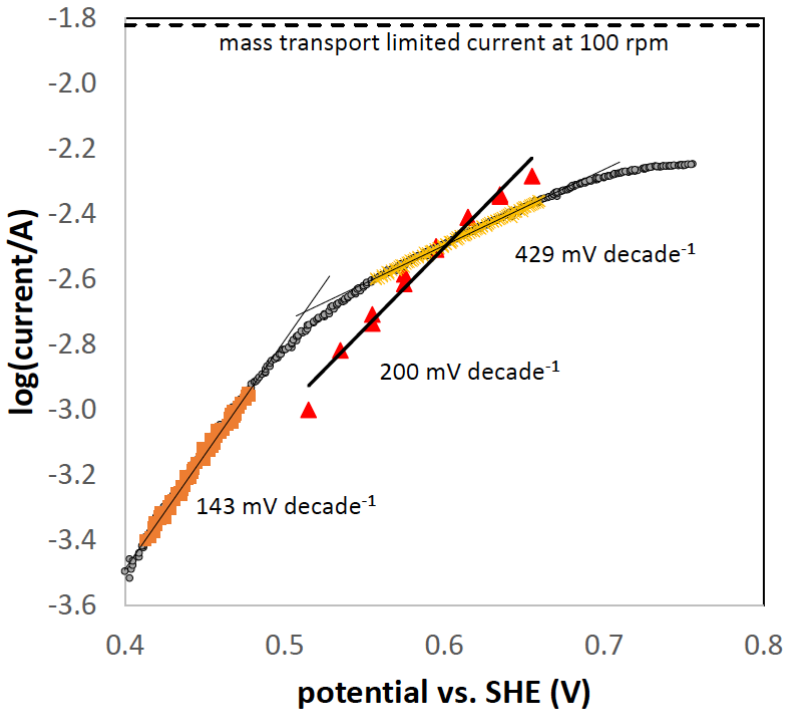

Figure 3.4: Tafel plots for the data in Table 3.1 (and additional data collected for the same electrode; 7.6 $mg\ cm^{-2}$ $Pt/C(\triangle)$, and a background corrected cyclic voltammogram (10 $mV\ s^{-1}$) for the same electrode ($\circ$)).

kinetically controlled region (below 0.5 V) was too small to provide reliable Koutecky-Levich plots, and so correction of kinetic currents for mass transport was not possible, or required, in this region. The two techniques are therefore complementary, in that electrode rotation is not required in the kinetic region (<10% of the mass transport limit), while correction for mass transport (eq. 3.4) is required at higher potentials. The Tafel plots from CV and RDE (fixed potential) are compared in Figure 3.4.

The Tafel slope in Figure 3.4 for the CV data between 0.41 and 0.48 V is 143 mV $decade^{-1}$, which is similar to literature values (above) from RDV at a Pt disc[86] and CV at carbon supported Pt.[122] At higher potentials, the slope decreased to 429 mV

$decade^{-1}$ (0.55 to 0.66 V) and then levelled off. The first change in slope occurs at ca. 0.51 V, at a current of ca.1.7 mA, which corresponds to ca. 11% of the calculated mass transport limited current at 100 rpm (for $n_{av} = 3.1$). Consequently, the CV data at potentials above ca. 0.49 V do not provide accurate kinetic currents, and the Tafel data above this potential is meaningless. Only the RDV Tafel data are accurate in the higher potential region. The somewhat higher slope of the RDV data relative to the low potential CV data can presumably be attributed to the effects of Pt oxide formation, while the positive offset on the potential axis may be due to a higher coverage of adsorbed CO due to the longer timescale of the RDV experiments.

The RDV method provides steady state Tafel parameters that are more relevant to methanol oxidation in fuel cells than those obtained by cyclic voltammetry. The optimal operational region for a fuel cell balances efficiency with power output, both of which increase to a peak with increasing current density.[105,123] Consequently, the cell should be operated in the mixed kinetic mass transport region where the kinetic current rises sharply, but there are not large mass transport losses. This typically occurs between ca. 40% and 60% of the mass transport limited current.[123]

3.3.2 PtRu Black

Previously,[86] it has been reported that RDV of methanol at a Pt disc yields anomalously low diffusion coefficients of ca. 5×10^{-12} cm^2 s^{-1}. Consequently, the accuracy of the n_{av} values reported in Table 3.1 may be questionable, since we have assumed the diffusion coefficient to be the average literature value for methanol in water. To investigate this further, an electrode with a high loading of a $PtRu$ black

catalyst was used. The presence of Ru decreases the onset potential for methanol oxidation,[120] which provides a wider potential window for measuring rotation effects before interference from Pt oxide formation. It is also expected to increase the efficiency of methanol oxidation,[112,120,124] with n_{av} expected to be close to the value of 6 for complete oxidation to CO_2.[125] Figure 3.5 shows cyclic voltammograms of the

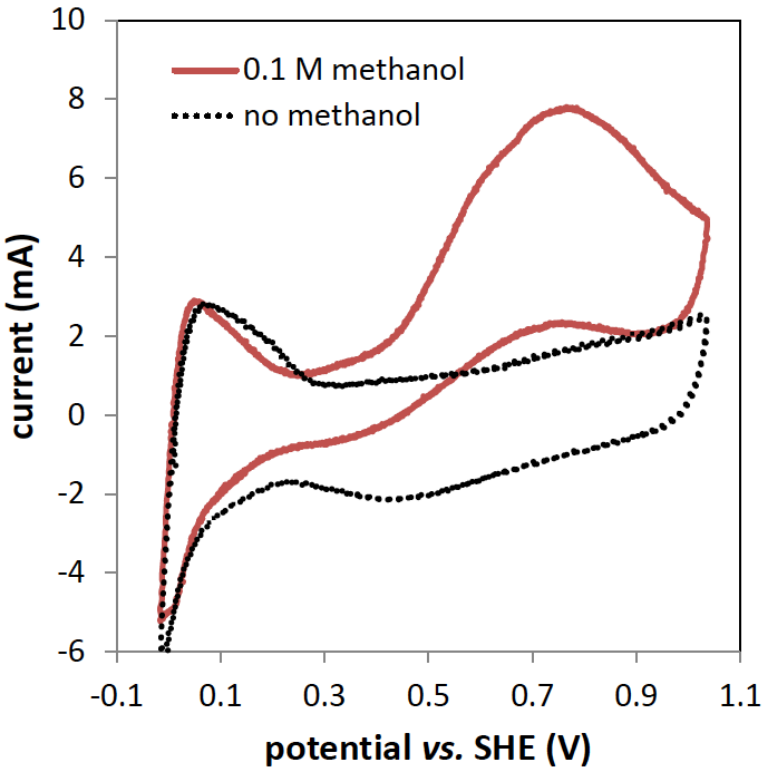

Figure 3.5: Cyclic voltammograms (10 $mV\ s^{-1}$) of a $GC/PtRu$ black (ca. 8 $mg\ cm^{-2}$) electrode in 1 M H_2SO_4(aq) (dotted), and with 0.1 M methanol (solid). The electrode was not rotated.

$PtRu$ coated electrode in H_2SO_4(aq) in the absence and presence of methanol. In comparison with the data in Figure 3.1 for 20% Pt/C, the onset of methanol oxidation

occured at a lower potential (ca. 0.27 V vs. ca. 0.39 V at Pt/C). Although the peak currents are similar, the peak potential is ca. 100 mV lower at the $PtRu$ electrode, and currents in the 0.45 to 0.75 V region are significantly higher.

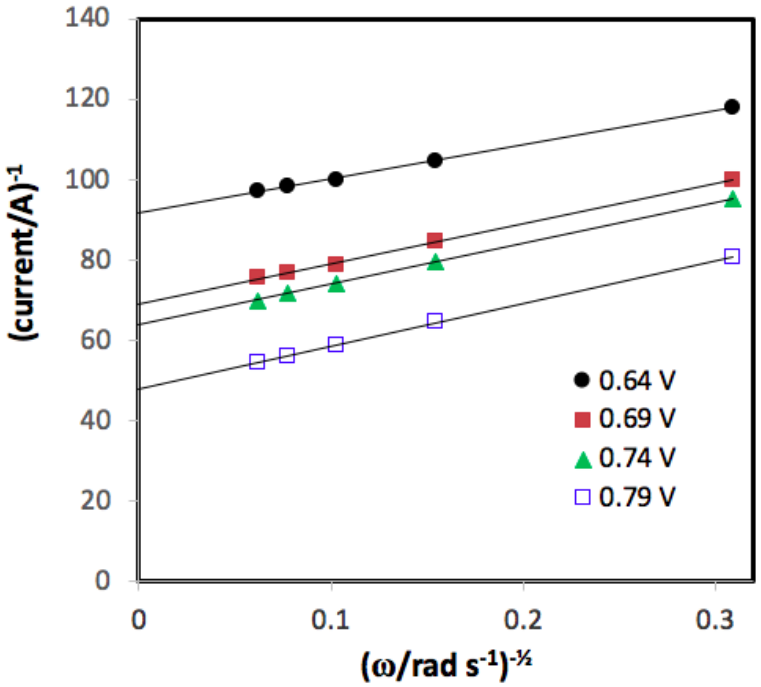

Figure 3.6: Steady-state Koutecky-Levich plots (i^{-1} vs. $\omega^{1/2}$) for constant potential oxidation of 0.1 M methanol in 1 M H_2SO_4(aq) at a $GC/PtRu$ black (ca. 8 $mg\ cm^{-2}$) electrode.

Figure 3.6 shows Koutecky-Levich plots for the $PtRu$ electrode obtained from potentiostatic RDE experiments in a 0.1 M methanol solution. The data at different potentials show similar slopes, indicating that n_{av} is approximately constant. Furthermore, the intercepts ($1/i_k$) decrease with increasing potential, showing that the kinetic current was still increasing over this potential range (0.64 to 0.79 V),

which corresponds to the approach to the top of the broad peak in the voltammogram (Figure 3.5), where the current was not changing greatly. Clearly, the current in this region was still significantly influenced by the electron transfer kinetics.

Table 3.2: Diffusion coefficients (for $n_{av} = 6$) and kinetic currents from the Koutecky-Levich plots for $PtRu$ black shown in Figure 3.5.

E vs. RHE (V)	D_{ap} (10^{-5} cm^2 s^{-1})	i_k (mA)
0.64	2.27 $\pm$ 0.16	11.0 $\pm$ 0.2
0.69	1.69 $\pm$ 0.01	16.2 $\pm$ 2.4
0.74	1.62 $\pm$ 0.07	15.9 $\pm$ 0.9
0.79	1.75 $\pm$ 0.36	22.0 $\pm$ 1.0

Table 3.2 presents diffusion coefficients for = 6 and kinetic currents from the Koutecky-Levich plots shown in Figure 3.6. Although the diffusion coefficients are all somewhat higher than the expected range of 1.4 to 1.5 $\times$ 10^{-5} cm^2 s^{-1}, there are significant uncertainties in both the literature values,[114] and the values reported in Table 3.2. The global average for the data in Table 3.2 of $(1.79 \pm 0.29) \times 10^{-5}$ cm^2 s^{-1} is not statistically different from literature values. It can therefore be concluded that methanol oxidation at the $PtRu$ black electrode produced CO_2 exclusively.

Observation of a faradaic efficiency of 100% here for the oxidation of methanol to CO_2 confirms that complete coverage of the electrode with active catalyst was achieved, since any inactive areas would have caused a decrease in the apparent n_{av}.[73] The use of thick catalyst layer films makes it easier to completely cover the electrode, and thinner regions can still support the required current density.

The oxidation of methanol occurring within the catalyst layer is very complicated, with multiply pathways and poisoning species, all of which are potential dependent. This could lead to inaccuracy of the n_{av} values that are obtained even when Koutecky-Levich plots are linear.[126] To avoid this, we have obtained data for Koutecky-Levich analysis at constant potentials. This allows i_k to approach a steady-state value based on the concentration of methanol at the catalyst layer surface determined by mass transport in the solution diffusion layer. Because the reaction occurs primarily within the bulk of the catalyst layer, blocking of the catalyst particles (e.g. by CO) will influence i_k, but will not block the geometric surface area that determines mass transport in the solution. This interpretation is supported by the reasonable agreement of the n_{av} values with expectations from the literature. Although it is possible that there are inaccuracies due to changes in i_k over the course of each constant potential experiment, these would be expected to result in variations in the Koutecky-Levich slope with potential.[126]

The kinetic currents reported in Table 3.2 are not suitable for Tafel analysis because of the high potentials that were employed in order to produce a strong mass transport effect. They cover the region in which the current peaks due the effect of Pt oxide formation. Lower potentials were not investigated here since the purpose was to evaluate whether the literature diffusion coefficient is applicable to RDV of methanol, which it is. Where a comparison can be made between the two catalysts, it can be seen that the kinetic current was significantly larger at the $PtRu$ black catalyst layer (11 mA at 0.640 V in Table 3.2) than at the Pt/C catalyst layer (4.6 mA at 0.635 V in Table 3.1). This difference is notably higher than the difference seen in cyclic voltammetry without rotation (6.6 mA for $PtRu$ vs. 5.4 mA for Pt at 0.64

V in Figures 3.5 and 3.1, respectively). This illustrates the importance of correction for mass transport effects for proper comparison of the activities of different catalyst layers.

The use of thick catalyst layers in this work complicates the interpretation of i_k because it includes the effects of mass transport through the catalyst layer.[73] This does not mean that the kinetic data are incorrect. Rather, it makes them more relevant to applications in fuel cells, etc., where thick layers are required. Methods are available for separating i_k into its kinetic and mass transport components.[55]

3.4 Conclusions

Rotating disc voltammetry of methanol oxidation at thick catalyst layers has been shown to accurately account for mass transport effects and provide a simple measure of the average number of electrons lost per molecule. The method reproduces the higher efficiency for oxidation to CO_2 (higher n_{av}) for $PtRu$ relative to Pt reported in differential electrochemical mass spectrometry (DEMS) studies. The RDV method complements cyclic voltammetry (and chronoamperometry) in the evaluation of catalysts for methanol oxidation by providing mass transport corrected kinetic currents at high potentials, in addition to providing n_{av} values. From a practical perspective, this is extremely important because we can now accurately determine the number of electrons released per methanol molecule, which is crucial for fuel cell applications. In addition, RDV provide mass transport corrected kinetic currents in the potential region of most importance for fuel cell applications (mixed kinetic-mass transport region). This has not been possible previously, because of the inaccurate

slopes of the Koutecky-Levich plots in previous work.[85,86]

Although n_{av} is the key parameter that determines the faradaic efficiency of methanol oxidation, it does not provide the distribution of products between formaldehyde, formic acid and carbon dioxide unless the faradaic yield of one of these products is known. Complementary analytical techniques, such as DEMS, infrared spectrometry, or chromatography, are therefore required to determine the product distributions to gain a full characterization.

Chapter 4

Evaluation of Ethanol Oxidation Catalysts by Rotating Disc Voltammetry

All experiments in this chapter were conducted by Azam Sayadi. Data analysis was performed by Azam Sayadi and Prof. Peter G. Pickup. This chapter has been published as (Sayadi, A.; Pickup, P. G. Evaluation of ethanol oxidation catalysts by rotating disc voltammetry. *Electrochim. Acta* **2016**, *215*, 84-92). Prof. Peter G. Pickup was the corresponding author and Azam Sayadi contributed to writing of the first draft.

4.1 Introduction

Ethanol is an attractive liquid fuel for sustainable energy systems since it is renewable, readily available, and non-toxic. It is currently produced on a large scale from biomass, and since it is a liquid, storage and transportation are not issues for concern.[20] Ethanol has a high energy density (8.0 $kWh\ kg^{-1}$), high solubility in aqueous electrolytes, and is a promising green energy source for direct ethanol fuel cells (DEFC).[20,49,127,128] A comprehensive understanding of the ethanol oxidation reaction (EOR) is of fundamental importance in determining and enhancing the commercial potential of these fuel cells.

The complete EOR to carbon dioxide produces twelve electrons according to equation 4.1.

$$CH_3CH_2OH + 3\ H_2O \rightarrow 2\ CO_2 + 12\ H^+ + 12\ e^- \tag{4.1}$$

However, this reaction has not been achieved exclusively on the surface of any anode material at temperatures that are compatible with proton exchange membrane fuel cell (PEMFC) technology. To understand this, numerous experimental techniques have been applied,[36,129] and there have been a number of computational studies.[130–136] For example, in situ Fourier transform infrared spectroscopy (FTIRS)[37–39,137–151] and differential electrochemical mass spectrometry (DEMS),[151–153] have been used to identify adsorbed intermediates on the electrode, and DEMS and chromatography[37,139,154–159] have been used to determine product distributions. As a result of these and many other studies, the oxidation mechanism of ethanol in acid solution may be summarized in the parallel reactions shown in eqs. 4.2 and 4.3, where $C1_{ad}$ and $C2_{ad}$ represent adsorbed fragments with one and two carbon atoms,

respectively.

$$CH_3CH_2OH \rightarrow [CH_3CH_2OH]_{ad} \rightarrow C1_{ad}, C2_{ad} \rightarrow CO_{ad} \rightarrow CO_2 \ [total\ oxidation] \tag{4.2}$$

$$CH_3CH_2OH \rightarrow [CH_3CH_2OH]_{ad} \rightarrow CH_3CHO \rightarrow CH_3COOH \ [partial\ oxidation] \tag{4.3}$$

Due to the strong bond between the two carbon atoms in the ethanol molecule, the complete electro-oxidation of ethanol to CO_2 occurs to only a small extent under ambient conditions.[36,38,94] Instead, acetaldehyde (two-electron oxidation) and acetic acid (four-electron oxidation) are the main products, which decreases the faradaic efficiency due to the lower number of electrons transferred per molecule.[160] Although the yield of CO_2 can be increased to >80% at elevated temperatures,[72,94,161] and catalyst activity can be increased by alloying platinum with other metals, such as Ru and Sn,[36,129] better catalysts are needed for the development of efficient DEFCs.

Electrochemical investigations of ethanol oxidation have largely relied on cyclic voltammetry and chronoamperometry which provide details of both the potential and time dependence of the reaction rate. However, data analysis and interpretation of the results is hampered by the time dependent interplay of electrode kinetics and mass transport. In other areas, rotating disk voltammetry (RDV) is commonly used to separate kinetic and mass transport currents.[55] RDV is a hydrodynamic method in which a rotating disk electrode (RDE) provides well-defined, steady-state mass transport of the reactant to the electrode surface. Generally, the Koutecky-Levich equation (eq. 4.4) can be applied to separate the kinetic and mass transport

parameters,

$$1/i = 1/i_k + 1/(0.62 n_{av} F A D^{2/3} \nu^{-1/6} C \omega^{1/2}) \tag{4.4}$$

where i is the measured current, i_k is the kinetic current, n_{av} is the average number of electrons transferred, F is the Faraday constant, D is the diffusion coefficient, ν is the kinematic viscosity ($1.0 \times 10^{-2}\ cm^2\ s^{-1}$),[55] ω is angular velocity and C is the concentration of the reactant. The mass transport limited current ($i_{lim} = 0.62 n_{av} F A D^{2/3} \nu^{-1/6} C \omega^{1/2}$) and kinetic current are obtained from the slope and intercept, respectively, of a plot of i^{-1} vs. $\omega^{1/2}$. RDV has become a particularly important technique in the evaluation and study of catalysts for oxygen reduction.[73,109,110,162] It is surprising therefore that there have only been a few reports of ethanol oxidation at RDEs.[85,88,89,163,164]

Shieh and Hwang[88] reported that the current for ethanol oxidation at ruthenium oxide in KOH(aq) decreased as the rotation rate was increased, and became constant above 500 rpm. This was attributed to convective removal of the acetaldehyde intermediate ($n = 2$) before it could be further oxidized to acetic acid ($n = 4$). In contrast, rotation had an insignificant effect on ethanol oxidation at a nickel electrode in $NaOH$(aq),[163] but increased the current at a Pt electrode.[164] In the latter work, a rotating ring-disc electrode was used to monitor pH changes during ethanol oxidation in $NaOH$(aq).[164] For ethanol oxidation at a Pt disc electrode in H_2SO_4, Seland et al.[89] found that electrode rotation decreased the current on the forward voltammetric scan but increased it on the reverse scan. This difference was attributed to slow formation of adsorbed intermediates during the reverse scan, since it was concluded that the decrease in the forward scan was due to the accumulation

of strongly adsorbed intermediates (e.g. CO) that block ethanol oxidation. Zheng et al.[85] have reported linear Koutecky-Levich plots ($i^{-1} \propto \omega^{1/2}$) for ethanol oxidation at glassy carbon electrodes coated with Pt and $PtSn$ nanoparticles, but did not analyze the mass transport characteristics.

Similarly contradictory effects have been reported for RDV of methanol oxidation,[82,85,86,89,165] and this can be attributed largely to the thickness of the catalytic layer on the electrode. Flat Pt electrodes generally show decreased currents with increasing rotation rate,[82] due to removal of intermediates by convection, while thick layers of higher surface area catalysts provide normal Koutecky-Levich behavior.[165] In the latter work, n_{av} was determined to be 6.0 for methanol oxidation at a $PtRu$ black catalyst layer and 3.1 at a carbon supported Pt layer.[165]

In this work we investigate ethanol electro-oxidation by RDV using thick layers of carbon supported Pt and $PtRu$ black catalysts on a glassy carbon (GC) electrode, in order to explore the interplay between kinetic and mass transport effects and determine parameters that will be useful in the development of anode catalysts for DEFCs. The use of thick catalyst layers on the electrode not only increases current densities into the range required for DEFCs, but also provides total coverage of the electrode surface, which improves the accuracy of the kinetic and mass transport parameters.[165] Of particular importance is the average number of electrons (n_{av}) transferred, which plays a central role in determining the energy efficiency of a DEFC.[119] It is clear from studies of the film thickness dependence of n_{av} for oxygen reduction,[74] and borohydride oxidation,[166] that thicker catalyst layers favor the conversion of intermediates to the final product. Consequently, n_{av} increases with increasing catalyst layer thickness, and values obtained with thick catalyst layers are

more representative of the behavior of the catalyst in a fuel cell.

4.2 Experimental

4.2.1 Materials

Anhydrous ethanol and sulfuric acid were obtained from ACP Chemicals Inc. Catalyst inks were prepared from a Nafion^{TM} solution in a mixture of lower aliphatic alcohols (5.14%; DuPont), 1-propanol (J.T. Baker), and commercial carbon supported platinum (20% Pt; Etek) or commercial platinum-ruthenium black ($Ru : Pt$ = 50:50, Alfa Aesar). Prior to application of each catalyst ink, the electrode was polished with an alumina slurry (0.3 μm; Sturbridge Metallurgical Services, Inc.).

4.2.2 Electrode Preparation

Catalyst inks were prepared by dispersing weighed amounts of catalyst powder (ca. 62 $mg\ mL^{-1}$) homogenously in either a Nafion solution or a mixture of 1-propanol and Nafion solution by sonication in an ultrasonic bath for 1 h. The electrode was prepared by applying the required amount of catalyst ink, with an Eppendorf micropipette, onto the polished surface of a glassy carbon disk electrode (0.196 cm^2; Pine Instruments). Each catalyst layer was allowed to dry for at least 30 min at ambient temperature. Where loadings higher than 1.5 $mg\ cm^{-2}$ were required, the catalyst ink was applied in several aliquots, with ultrasonic re-dispersion of the ink for 10 min. Specified catalyst loadings do not include the mass of Nafion used as a binder, which varied from 17% to 50% of the catalyst layer mass as specified.

4.2.3 Electrochemistry

Electrochemical experiments were conducted at ambient temperature in a three-compartment glass cell operated with a Pine Instruments RDE4 potentiostat and ASR Analytical Rotator. The working electrode was a catalyst coated glassy carbon electrode, the counter electrode was a platinum wire and a mercury sulfate electrode in 3.8 M sulfuric acid (Koslow; 635 mV vs. SHE) was used as a reference electrode. All potentials are given relative to the standard hydrogen electrode (SHE). Rotating disk cyclic voltammetry and constant potential experiments were carried out in 0.1 M ethanol solutions with 1 M sulfuric acid as the electrolyte. Prior to all experiments, the solution was de-aerated by passing N_2 into the solution for 15 min, and then over the surface of the solution continuously during the experiments. Steady-state cyclic voltammograms, obtained after repeated potential sweeps, are shown.

4.3 Results and Discussion

4.3.1 Comparison of Thick Layers of Carbon Supported Pt and PtRu Black Catalysts

Carbon supported Pt was employed here as a typical baseline catalyst for ethanol oxidation, while $PtRu$ black was chosen for comparison due to its higher activity, particularly at low potentials. $PtRu$ was previously shown to provide very efficient oxidation of methanol in RDE experiments.[165] Initially, high catalyst loadings and high Nafion contents were employed to maximize the efficiency of ethanol oxidation.[165]

As is illustrated by the voltammograms in Figure 4.1 and Figure 4.2, rotation of

the electrode can significantly increase the current for ethanol oxidation at both Pt/C and $PtRu$ electrodes, although the effects were less pronounced for Pt/C than $PtRu$ black. For $PtRu$ black (Figure 4.1) the increase in current with electrode rotation began at very low potentials (ca. 0.1 V) and was observed on both the forward and reverse scans. For Pt/C, the current did not begin to increase as the rotation rate was increased until potentials above ca. 0.5 V. In both cases, the formation of an oxide layer on the Pt surface, starting at ca. 0.7–0.8 V, inhibits ethanol absorption and a mass transport limited plateau was not achieved. The effect of oxide formation was more pronounced for Pt/C than $PtRu$. In the reverse potential scan, the adsorbed oxide layer on the surface of the electrode is stripped and the ethanol oxidation current increases to a broad peak between 0.8 and 0.4 V. Interestingly, this reverse peak was more sensitive to rotation rate than the forward peak, particularly at Pt/C.

Additional experiments with thicker $PtRu$ layers (up to 13 $mg\ cm^{-2}$) and rotation rates as low as 30 rpm were performed, but a mass transport limited plateau was not obtained. This can be attributed primarily to the low potential dependence of the kinetic current over the 0.2 to 0.6 V region, where the Tafel slope is very high (see below). Consequently, the mass transport limited region is shifted to potentials beyond the decrease in i_k due to oxide formation. Although i_k initially increased as the $PtRu$ layer thickness was increased, it became independent of thickness at ca. 6 $mg\ cm^{-2}$.

Since it was not possible to obtain pure mass transport control of the current, n_{av} could not be obtained from the Levich equation. Consequently, the Koutecky-Levich equation was used to separate the kinetic and mass transport components of the current measured at potentials between 0.53 and 0.89 V. In order to achieve

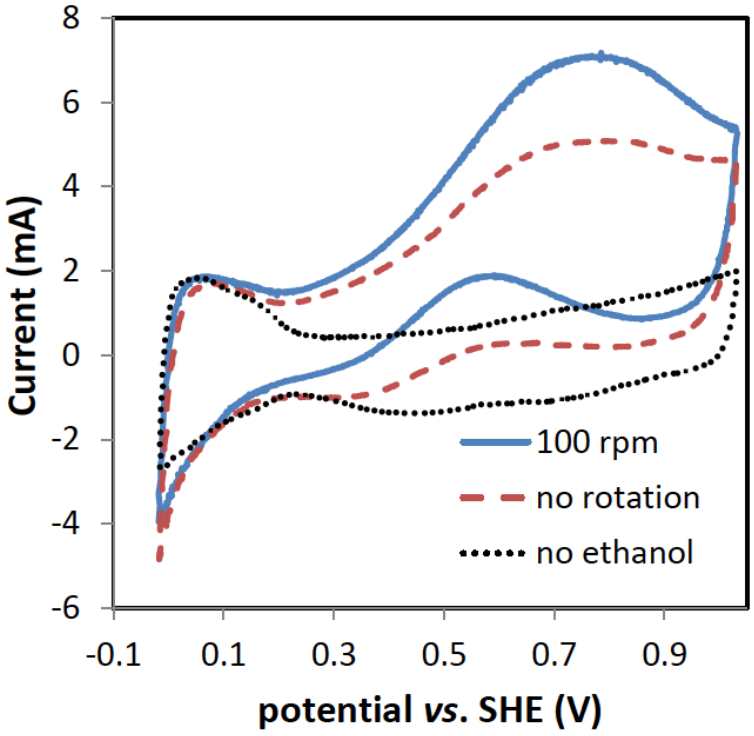

Figure 4.1: Cyclic voltammograms (10 $mV\ s^{-1}$) of a $GC/PtRu$ black (2.0 $mg\ cm^{-2}$; 30% Nafion) electrode in 1 M H_2SO_4(aq) (dotted), and with 0.1 M ethanol without rotation (dashed) and at 100 rpm (solid).

steady state conditions, and avoid errors from the large background currents due to the surface electrochemistry of the catalyst seen in voltammetry (Figure 4.1), steady-state currents (i) were measured at constant potentials over a range of rotation rates (ω). Figure 4.3 displays an example of the steady-state current change with rotation rate at a constant potential of 0.785 V. Koutecky-Levich plots (i^{-1} vs. $\omega^{1/2}$) (eq. 4.4) of these experiments were applied to extract the kinetic current (i_k) and stoichiometry (n_{av}). A literature diffusion coefficient of $1.22 \times 10^{-5}\ cm^2\ s^{-1}$ for aqueous ethanol at 25 $°C$ was employed.[167] Koutecky-Levich plots obtained from potentiostatic RDE

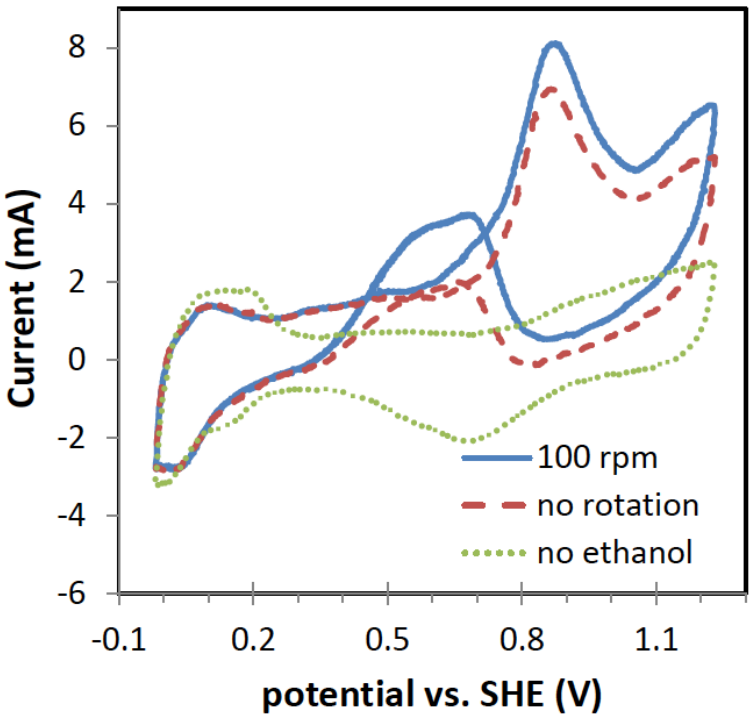

Figure 4.2: Cyclic voltammograms (10 $mV\ s^{-1}$) of a $GC/Pt/C$ (6.0 $mg\ cm^{-2}$; 43% Nafion) electrode in 1 M H_2SO_4(aq) (dotted), and with 0.1 M ethanol without rotation (dashed) and at 100 rpm (solid).

experiments using the $PtRu$ black catalyst are displayed in Figure 4.4, while n_{av} and i_k values obtained from the slopes and intercepts (eq. 4.4) are plotted in Figures 4.5 and 4.6, respectively. n_{av} was independent of potential between 0.585 V and 0.885 V at ca. 3.6. This is consistent with product analysis results from a DEMS study of ethanol oxidation at carbon supported $PtRu$, which also indicated that n_{av} was independent of potential.[52] The reported product distribution gives an average n_{av} of 3.0 $\pm$ 0.1 between 0.4 and 0.7 V vs. RHE. The somewhat higher n_{av} here suggests that the $PtRu$ black catalyst layer was more efficient than the carbon supported

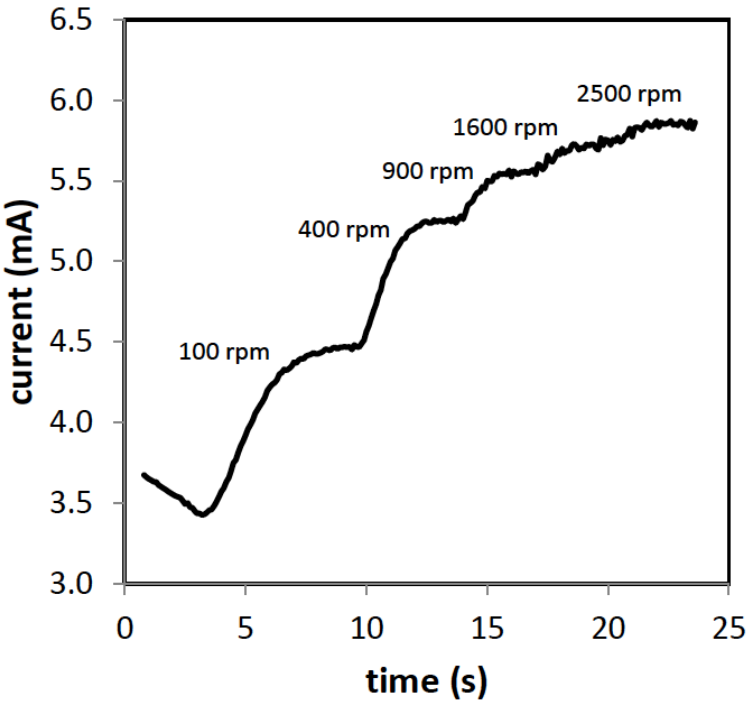

Figure 4.3: Current vs. time at 0.785 V and various rotation rates for the oxidation of 0.1 M ethanol in 1 M H_2SO_4(aq) at a $GC/PtRu$ black (2.0 $mg\ cm^{-2}$; 30% Nafion) electrode.

$PtRu$ layer employed in.[52] Differences in efficiencies have previously been reported for different carbon supported $PtRu$ catalysts.[168] In addition, the efficiency will depend on the thickness and structure of the catalyst layer.[74,166,169]

The n_{av} of 3.6 obtained from the Koutecky-Levich plots for $PtRu$ corresponds to a limiting current of 15.6 mA at 100 rpm. This is significantly higher than the maximum current of 7.1 mA seen in the voltammogram at 100 rpm (Figure 4.1) or the maximum current of 5.6 mA obtained in the potentiostatic experiments at 100 rpm. This confirms that the mass transport limit was not reached in these experiments.

Examples of Koutecky-Levich plots of steady state data for 6.0 $mg\ cm^{-2}$ Pt/C

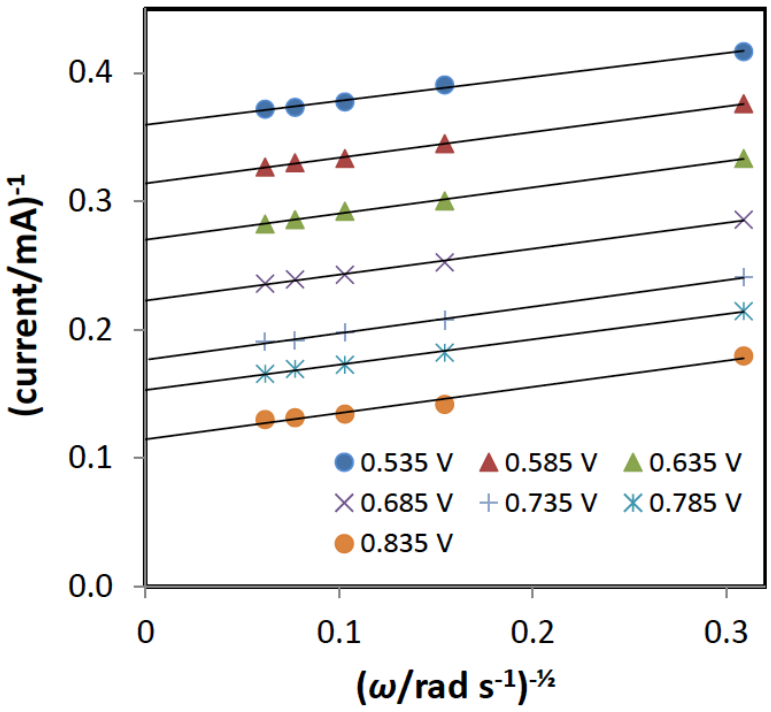

Figure 4.4: Steady-state Koutecky-Levich plots for constant potential oxidation of 0.1 M ethanol in 1 M H_2SO_4(aq) at a $GC/PtRu$ black (2.0 $mg\ cm^{-2}$; 30% Nafion) electrode.

are shown in Figure 4.7. Although these plots are linear at most potentials, they are not parallel, indicating that n_{av} was potential dependent. There is significant curvature at the lowest potentials, and this leads to unreasonably low values of n_{av} (Figure 4.5) which should not be less than 2 (i.e. for 100% conversion of ethanol to acetaldehyde). The origin of this curvature is explored in Section 4.3.3. For the Pt/C electrode, n_{av} values from eq. 4.4 increased from <2 to 3.5 with increasing potential (Figure 4.5), which is consistent with reports that the ratio of acetic acid to acetaldehyde increases with increasing potential.[37,139,160] However, a decrease in the acetic acid to acetaldehyde ratio at 0.7 V vs. RHE was also reported[160], and a DEMS

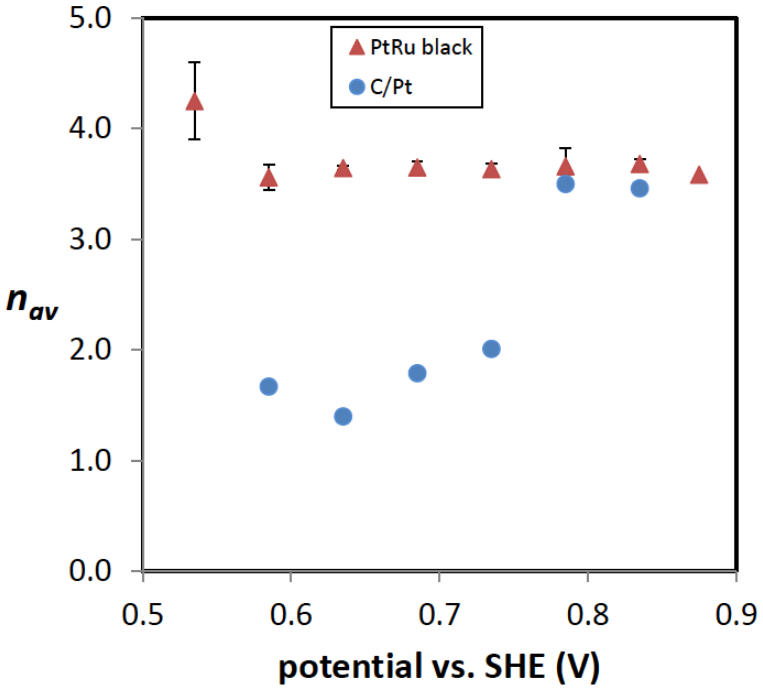

Figure 4.5: n_{av} vs. potential for oxidation of 0.1 M ethanol in 1 M H_2SO_4(aq) at $GC/PtRu$ black (2.0 $mg\ cm^{-2}$; 30% Nafion) and $GC/Pt/C$ (6.0 $mg\ cm^{-2}$; 43% Nafion) electrodes. Error bars for the $PtRu$ electrode are standard deviations for two or more data sets at each potential.

study indicated that the acetic acid to acetaldehyde ratio was constant between 0.5 and 0.7 V,[52] which means that n_{av} was also constant over this range of potentials. Product distributions reported in that work give $n_{av} = 2.7 \pm 0.1$, which is consistent with the range in Figure 4.5. A n_{av} of 2.7, averaged over a full cyclic potential scan, was also reported in another DEMS study.[38] These discrepancies in the potential dependence of n_{av} can be attributed to variations in the product distributions with time and the experimental protocol.[38] Consequently, it can be concluded that the n_{av} values reported in Figure 4.5 for Pt/C at potentials above ca. 0.7 V are reasonable.

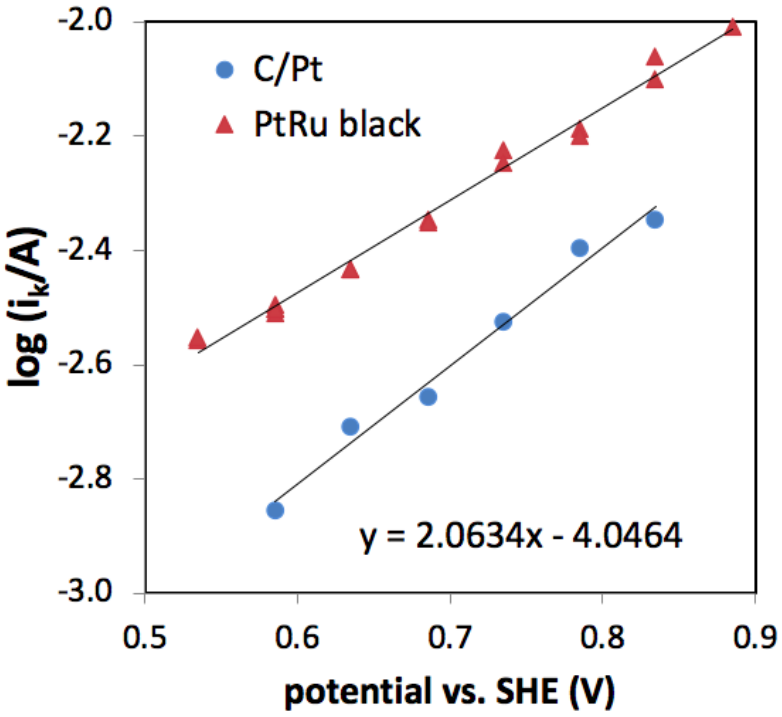

Figure 4.6: i_k vs. potential for oxidation of 0.1 M ethanol in 1 M H_2SO_4(aq) at $GC/PtRu$ black (2.0 $mg\ cm^{-2}$; 30% Nafion) and $GC/Pt/C$ (6.0 $mg\ cm^{-2}$; 43% Nafion) electrodes.

However, a quantitative comparison cannot be made here because the thicknesses and structures of the catalyst layers were different. The variation of product distributions with the thicknesses and structure of the catalyst layer, and the experimental protocol, make it very difficult to obtain reliable estimates of n_{av} that can be used to verify or dispute the values from Koutecky-Levich plots. Unlike the oxygen reduction reaction, the EOR does not form an intermediate or products that can be selectively monitored at a ring electrode. Analysis of products by other means is hampered by significant losses of CO_2 and acetaldehyde from the cell during electrolysis at the RDE.

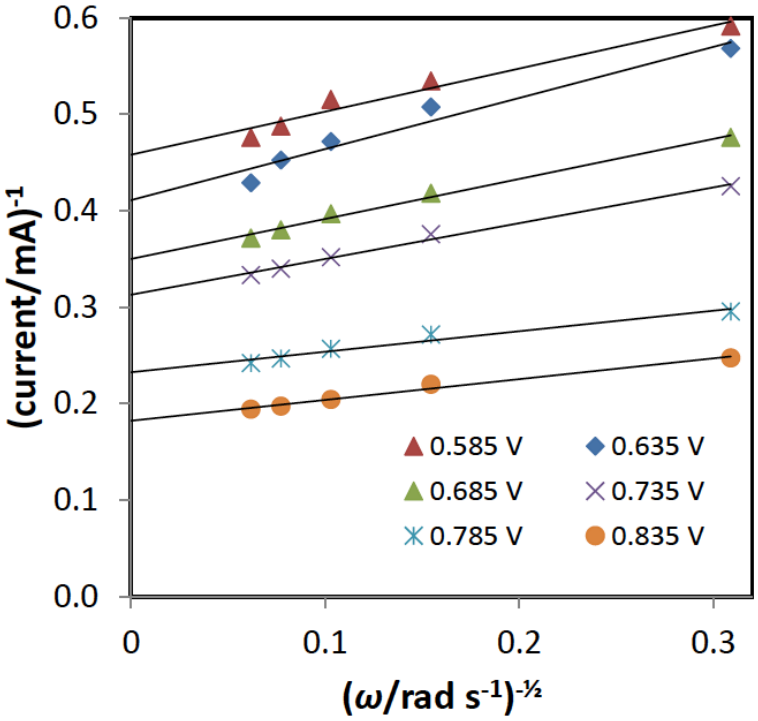

Figure 4.7: Steady-state Koutecky-Levich plots for constant potential oxidation of 0.1 M ethanol in 1 M H_2SO_4(aq) at a $GC/Pt/C$ (6.0 $mg\ cm^{-2}$; 43% Nafion) electrode.

The complete oxidation of ethanol to CO_2 is a very minor pathway at Pt and $PtRu$ electrodes at ambient temperature and the current is due primarily to dehydrogenation of ethanol to produce acetaldehyde and oxidation to acetic acid, which results in 2 and 4 electrons, respectively.[37,38,52,160]

Kinetic currents extracted from the Koutecky-Levich plots for both $PtRu$ (Figure 4.4) and Pt/C (Figure 4.7) are presented as Tafel plots in Figure 4.6. The slope of 613 $mV\ decade^{-1}$ for $PtRu$ is much higher than a value of 165 $mV\ decade^{-1}$ reported for a Ru modified platinized platinum electrode,[170] and also higher than values that have been report for Ru-decorated carbon-supported Pt catalysts, which

range from 215–500 $mV\ decade^{-1}$.[171] The slope of 629 $mV\ decade^{-1}$ for Pt/C is also much higher than literature values which range from of 137 to 310 $mV\ decade^{-1}$ for carbon supported Pt.[147,170–172] It corresponds to a transfer coefficient (a) of 0.12, which is much lower than the value of 0.44 reported by Hitmi et al. for a smooth Pt electrode.[139] It has been suggested that a Tafel slope of 420 $mV\ decade^{-1}$ for ethanol oxidation at a $Pt - Rh - SnO_2/C$ catalyst could indicate that the rate limiting step involves breaking of the $C - C$ bond,[173] although that seems highly unlikely here based on the low n_{av} values. The high slopes here are more likely to be due to the formation of Pt oxide at the high potentials employed. Several reports[168,172] show a transition to a higher Tafel slope in the 0.5 to 0.9 V region covered by the data in Figure 4.6. It should also be noted that the Tafel slope could be dependent on the product distribution, which was presumably different in each of these studies. To the best of our knowledge, there are currently no theoretical or mechanistic models available for interpreting Tafel slopes for the EOR at Pt in acid. However, a first principles model is available for methanol oxidation,[174] and this provides some basis for understanding the wide range of Tafel slopes that are observed experimentally.

4.3.2 Ethanol Concentration Dependence

The application of eq. 4.4 is based on the assumption that the reaction order is unity: i.e. that $i_k = n_{av}FAkC$, where k is the rate constant. However, literature values for the reaction order of ethanol range from 0.5 to 1.1,[38,139,175] and show a potential dependence[139]. The effect of ethanol concentration was therefore investigated here in order to assess the validity eq. 4.4. Figure 4.8 displays cyclic voltammograms at

a Pt/C electrode for ethanol at various concentrations. On the forward potential scan, the currents increased linearly with increasing ethanol concentration ($R^2 > 0.95$) over the potential range of 0.63 to 0.84 V, indicating that the reaction order was unity under these conditions. However, the current did not depend significantly on concentration at 0.56 V and decreased with increasing concentration at lower potentials. This can be attributed to the blocking effects of adsorbed intermediates (e.g. CO), which is also reflected in the suppression of the hydrogen under-potential deposition and desorption waves (between 0 and 0.2 V) with increasing ethanol concentration.

4.3.3 Dependence on Catalyst Loading

Studies of methanol oxidation at RDEs coated with thin catalyst layers have shown little or no dependence of the current on electrode rotation,[82,84,85] and this has been attributed to loss of reaction intermediates (formaldehyde and formic acid) by convection.[82] A similar effect would be expected for ethanol oxidation, where enhanced diffusion of acetaldehyde away from the electrode with increasing rotation rate would be expected to decrease n_{av}. Such an effect could be responsible for the curvature of the Koutecky-Levich plots at low potentials in Figure 4.7, which leads to underestimation of n_{av}.

To explore the effects of convective removal of acetaldehyde, the loading of Pt/C on the electrode was decreased relative to the electrodes described in Section, 4.3.1 and the dependence on loading was investigated. In these experiments, the percentage of Nafion in the catalyst layer was also decreased, in order to increase the rate of ethanol

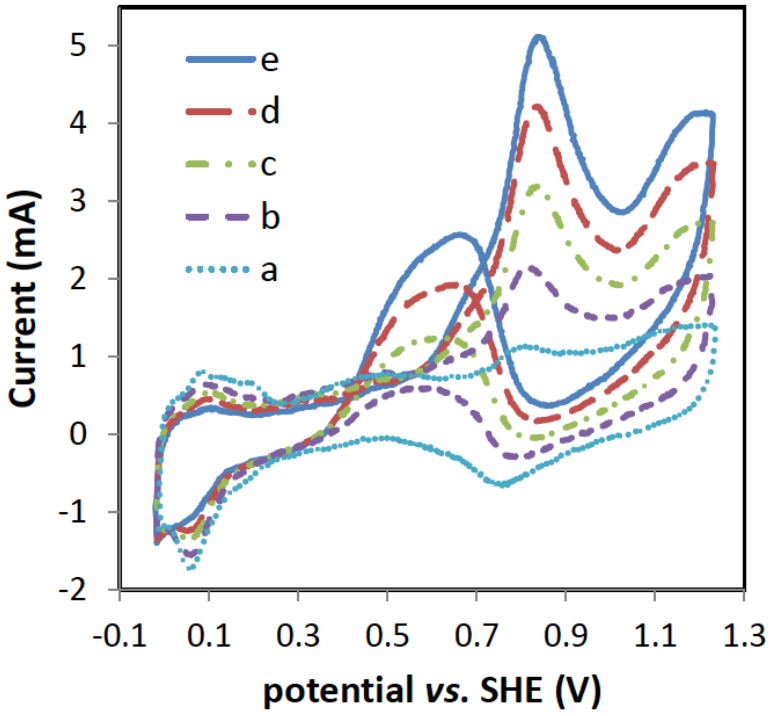

Figure 4.8: Cyclic voltammograms (10 $mV\ s^{-1}$) of a $GC/Pt/C$ (2.8 $mg\ cm^{-2}$; 17% Nafion) electrode in 1 M H_2SO_4(aq) containing ethanol at (a) 0.02 M, (b) 0.04 M, (c), 0.06 M, (d), 0.08 M, (e), 0.1 M.

and product diffusion in the layer. By analogy with the effects of electrode rotation on methanol oxidation,[82,85] oxygen reduction,[74] and borohydride oxidation,[166] the balance between the opposing effects of faster ethanol transport to the electrode and faster acetaldehyde removal is expected to shift towards the latter as the catalyst layer thickness is decreased. Figure 4.9 shows voltammograms of ethanol oxidation at Pt/C electrodes with a range of loadings. Currents increased linearly with increasing catalyst loading, indicating that the entire catalyst layer was active for ethanol oxidation. There was no evidence of the activity levelling off, which would occur

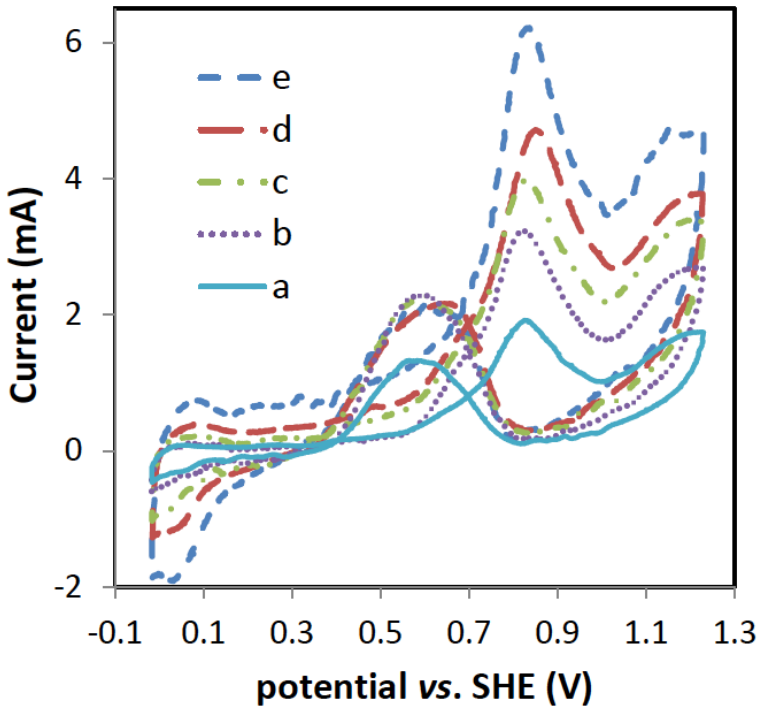

Figure 4.9: Cyclic voltammograms (10 $mV\ s^{-1}$; no rotation) for oxidation of 0.1 M ethanol in 1 M H_2SO_4(aq) at $GC/Pt/C$ electrodes with 17% Nafion and Pt/C loadings of (a) 0.6 $mg\ cm^{-2}$, (b) 1.1 $mg\ cm^{-2}$, (c) 1.6 $mg\ cm^{-2}$, (d) 2.1 $mg\ cm^{-2}$, (e) 2.8 $mg\ cm^{-2}$.

if a large fraction of the ethanol was consumed before reaching the glassy carbon support. This indicates that over this range of loadings the whole of the catalyst layer was involved in ethanol oxidation. Although RDE measurements at constant potential showed strong dependences on rotation rate for all loadings, they did not provide linear Koutecky-Levich plots, as illustrated by the data set shown in Figure 4.10. Since eq. 4.4 could not be reasonably applied here (and it gave n_{av} values below

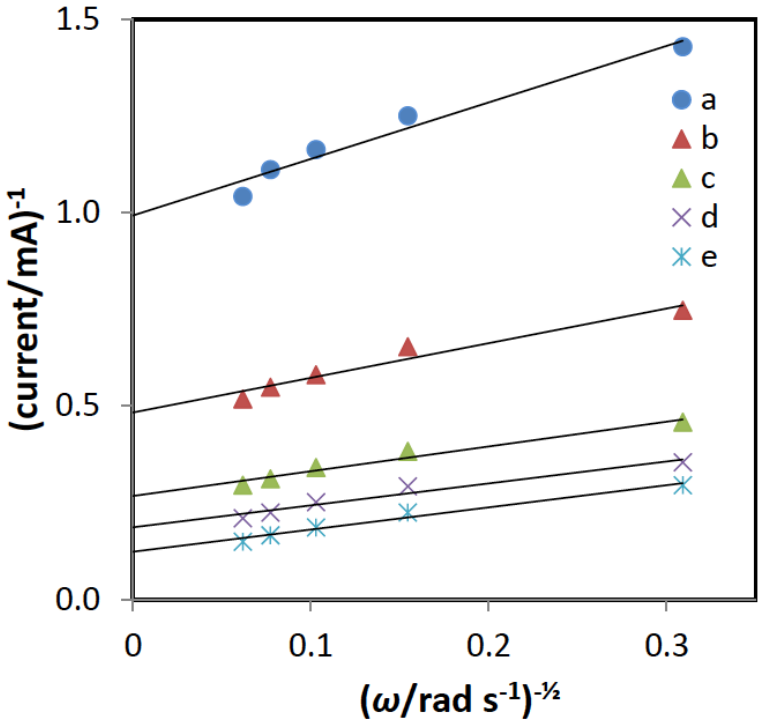

Figure 4.10: Steady-state Koutecky-Levich plots for oxidation of 0.1 M ethanol at 0.735 V in 1 M H_2SO_4(aq) at $GC/Pt/C$ electrodes with 17% Nafion and Pt/C loadings of (a) 0.6 $mg\ cm^{-2}$, (b) 1.1 $mg\ cm^{-2}$, (c) 1.6 $mg\ cm^{-2}$, (d) 2.1 $mg\ cm^{-2}$, (e) 2.8 $mg\ cm^{-2}$.

2), each data point was fitted to eq. 4.5.[55]

$$i = i_{lim}(C - C_0)/C \tag{4.5}$$

where i_{lim} is the mass transport limited current ($0.62n_{av}FAD^{2/3}\nu^{-1/6}C\omega^{1/2}$) and C_0 is the ethanol concentration at the interface between the catalyst layer and the solution. To allow for a possible deviation in the reaction order (m) from unity, i_k and i are

expressed as eqs. 4.6 and 4.7, respectively.

$$i_k = n_{av} F A k C^m \tag{4.6}$$

$$i = n_{av} F A k C_0^m \tag{4.7}$$

Combining eqs. 4.5–4.7 yields eq. 4.8.

$$i_k = i/(1 - i/i_{lim})^m \tag{4.8}$$

These relationships were used in a spreadsheet to explore how the parameters n_{av}, i_k, and m influenced the calculated Koutecky-Levich plots, and to fit the experimental data. It was found that simulated Koutecky-Levich plots were linear for all values of m. Varying n_{av} or m with rotation rate over reasonable values ($2 < n_{av} < 12$; $0.5 < m < 2$) could not reproduce the curvature of the experimental Koutecky-Levich plots, while small variations in i_k with rotation rate could be used to reproduce the experimental data. This is illustrated in Figure 4.11, which shows i_k values, calculated from the experimental currents by using eq. 4.8 with various n_{av} and m values, vs. $\omega^{1/2}$ for a typical data set. It can be seen that variation of n_{av} and/or m had only a small influence, and so it is not possible to extract meaningful values of these parameters from the data. The almost linear increase in i_k with the mass transport rate (proportional to $\omega^{1/2}$) seen in Figure 4.11, suggests that transport of a product away from the electrode may be responsible, since the effect of ethanol transport to the electrode is accounted for by eq. 4.5.

These results raise two key questions. Firstly, what causes the variation in i_k with rotation rate? Secondly, why was this problem not encountered under most conditions for the thick catalyst layers employed in Section 4.3.1? The variation in i_k

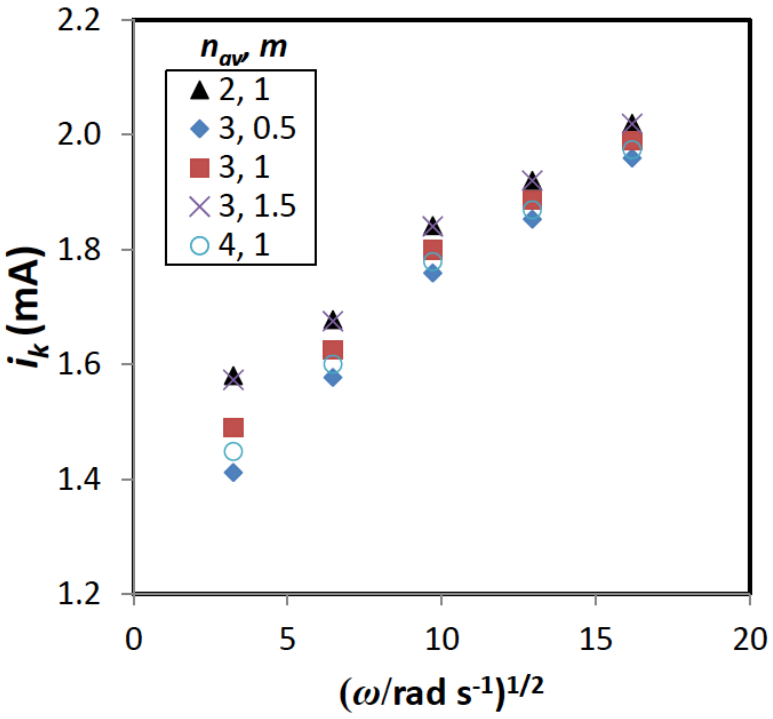

Figure 4.11: Kinetic current (i_k), calculated from the experimental currents by using eq. 4.8 with various n_{av} and m values, vs. $\omega^{1/2}$ for oxidation of 0.1 M ethanol at 0.735 V in 1 M H_2SO_4(aq) at a $GC/Pt/C$ (1.1 $mg\ cm^{-2}$; 17% Nafion) electrode.

is opposite to the effect of rotation on the convective removal of acetaldehyde away from the electrode. This would cause n_{av} to decrease with increasing rotation rate, which would also decrease i_k (eq. 4.6). Consequently the most reasonable explanation of the rotation rate effect on i_k is that acetaldehyde in the catalyst layer acts as a poison. This is supported by a report on the effect of acetaldehyde on the oxidation of ethanol in a fuel cell, where addition of acetaldehyde was found to decrease the performance of the cell.[176]

The effect of increased acetaldehyde removal by convection would have been much

less significant at the thicker catalyst layers with high Nafion loadings used in Section 4.3.1. The oxidation of ethanol would have occurred throughout the layer, and most of the acetaldehyde would have been oxidized to acetic acid (and small amounts of CO_2) before it could diffuse into the solution. This is supported by the high n_{av} values that were obtained from the linear Koutecky-Levich plots.

4.3.4 Effect of Nafion Content in the Catalyst Layer

Since different Nafion contents were used for the electrodes in Sections 4.3.1 and 4.3.3, it was important to assess the role that this could have played in changing the RDE behavior. Figure 4.12 shows cyclic voltammograms of 0.1 M ethanol at electrodes with the same amounts of Pt/C (2.0 $mg\ cm^{-2}$), but different Nafion to Pt/C ratios. When there was no rotation, the ethanol oxidation current was higher for the electrode with less Nafion at all potentials, except for the region between 0.8 and 0.9 V on the forward scan where the currents were similar. The effect of Nafion content was most pronounced in the regions between 0.4 and 0.8 V on the forward scan, and 0.4 to 0.7 V on the reverse scan. These results indicate that a higher Nafion content slows the diffusion of ethanol into the catalyst layer. Since i_k contains a component due to ethanol transport in the catalyst layer (see discussion), this would decrease i_k, and reduce the effect of electrode rotation. Consequently, when the electrodes were rotated at 400 rpm, the increases in current were less pronounced for the higher amount of the Nafion. The clear and expected effect of Nafion content on ethanol diffusion in the catalyst layer seen in Figure 4.12 would also occur for diffusion of products out of the catalyst layer. In particular, higher Nafion contents would slow the diffusion of

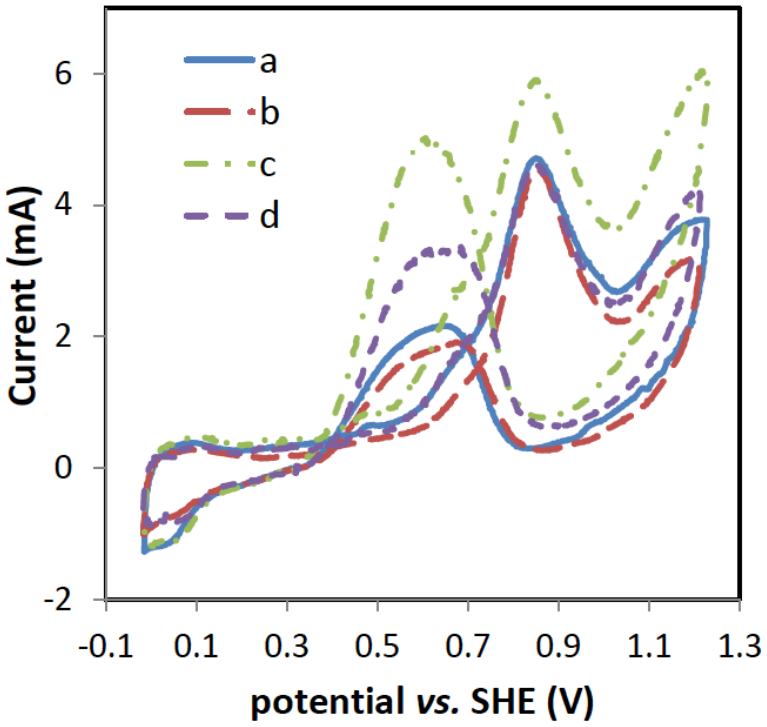

Figure 4.12: Cyclic voltammograms (10 $mV\ s^{-1}$) for oxidation of 0.1 M ethanol in 1 M H_2SO_4(aq) at $GC/Pt/C$ (2.0 $mg\ cm^{-2}$) electrodes. (a) 17% Nafion by mass without rotation, (b) 50% Nafion without rotation, (c) 17% Nafion at 400 rpm, and (d) 50% Nafion at 400 rpm.

acetaldehyde out of the catalyst layer, and decrease the effect of electrode rotation. This would increase the electrochemical conversion of acetaldehyde to acetic acid (and small amounts of CO_2), and therefore produce higher n_{av} values. In addition, the effect of electrode rotation on i_k would be decreased. It can therefore be concluded that both the thickness of the catalyst layer and its Nafion content play important roles in determining whether linear Koutecky-Levich plots are obtained. Thick layers with high Nafion contents (Section 4.3.1) are required to determine meaningful n_{av}

values.

4.3.5 Discussion

The observation of linear Koutecky-Levich plots for ethanol oxidation at thick layers of $PtRu$ black and carbon supported Pt in Section 4.3.1, and the observation of n_{av} values that are consistent with literature reports of product distributions, suggests that the Koutecky-Levich treatment is appropriate under these conditions. This is expected from theoretical treatments of RDV at electrodes coated with catalytic layers, which show that linear Koutecky-Levich plots should be obtained and that the kinetic current consists of an electron transfer component (i_e) coupled with a component due to diffusion of the reactant through the catalytic layer (i_s) according to eq. 4.9.[177]

$$i_k = (i_s i_e)^{1/2} \tanh(i_e/i_s)^{1/2} \tag{4.9}$$

Consequently, the slope of a Koutecky-Levich plot should provide an accurate value of n_{av}, and there should be no effect of rotation rate on i_k.

For multi-step reactions, n_{av} values from linear Koutecky-Levich plots do not generally provide the total number of electrons that would be determined from exhaustive coulometric electrolysis.[126] That is clearly the case here, since all of the acetaldehyde intermediate would be oxidized to acetic acid or CO_2 during electrolysis. However, the value from RDV is more relevant to oxidation of ethanol in a fuel cell because they are both hydrodynamic methods in which the product distribution is influenced by convection, and the thickness and structure of the catalyst layer.

Zhou et al.[75] have shown that for oxygen reduction, n_{av} values from Koutecky-

Levich plots are inaccurate, and show by modelling that the diffusion of hydrogen peroxide away from the electrode, and reversibility of the reduction to H_2O_2, lead to deviations from Koutecky-Levich behavior. Although this raises concerns regarding the accuracy of the Koutecky-Levich equation to multi-step/pathway reactions in general, the relevance to the EOR is unclear, since the reduction of acetaldehyde back to ethanol is not possible under the conditions of the experiments presented here, and we have used very thick catalyst layers. The observation of linear Koutecky-Levich behavior for these thick films can be attributed to restriction of the current by slow mass transport through the catalyst layer, which is not dependent on rotation rate. This, together with the low acetaldehyde yield, would result in a low concentration gradient of acetaldehyde in solution, and therefore only a small effect of electrode rotation on the diffusion of acetaldehyde away from the catalyst layer. Although small increases in n_{av} presumably occur as the rotation rate is increased, it has been shown in Section 4.3.3 that these cannot account for the non-linearity of the Koutecky-Levich plots.

The non-linearity of the Koutecky-Levich plots obtained for the thinner Pt/C layers in Section 4.3.3 (Figure 4.10), and thick Pt/C layers at low potentials in Section 4.3.1 (Figure 4.7), does not appear to be due to the effects of diffusion through the catalyst layer,[177] nor the multistep mechanism.[126] Furthermore, as shown in Section 4.3.3, it cannot be due to a rotation rate dependence of either m or n_{av}. It is consistent, however, with a variation in i_k that could arise from poisoning of the catalyst by acetaldehyde produced as an intermediate.

This hypothesis is supported by the known inhibitory effect of acetaldehyde on ethanol oxidation,[176] the effect of varying the catalyst layer thickness (Section 4.3.3),

and the potential dependence seen for Pt/C in Figure 4.7, where non-linear Koutecky-Levich plots are observed only at low potentials, where the acetaldehyde production is high. The measured n_{av} values indicate that the main product was acetic acid at $PtRu$ all potentials, and for Pt/C at high potentials. In both of these cases, the Koutecky-Levich plots were linear. However, non-linear Koutecky-Levich plots were observed for Pt/C at lower potentials, where acetaldehyde is expected to be the major product, and the slopes yield low n_{av} values.

Although this work has focused on n_{av}, an equally important application of linear Koutecky-Levich plots is the determination of mass transport corrected kinetic currents. This is particularly important in the evaluation of fuel cell catalysts, which are generally operated under mixed kinetic and mass transport control of the current. The i_k values reported here therefore complement those in the literature that have been determined under kinetic control at lower potentials. It should be noted that we, and others,[147,168,170,172] have reported i_k values that include the effect of mass transport within the catalyst layer, rather than the intrinsic kinetic current (i_e). Extraction and comparison of i_e values would require detailed knowledge of the physical properties of each catalyst layer, including ionic conductivity, ethanol diffusion coefficient, porosity, tortuosity, and partitioning of ethanol.[178]

Finally, it should be noted that the Koutecky-Levich treatment employed here is an approximation. Although the n_{av} values obtained from linear Koutecky-Levich plots are reasonable, and follow trends reported in the literature, they could be inaccurate. It is certainly clear that the n_{av} values obtained from non-linear Koutecky-Levich plots are inaccurate, since some are impossibly low (<2). As with the measurement of n_{av} for oxygen reduction by RDV,[74,75,169,179] and studies of CO

oxidation[180] more sophisticated modelling is required for RDV of ethanol to be more than a semi-quantitative method for comparing different catalyst.

4.4 Conclusions

RDV has been shown to be a convenient and useful method for estimating the average number of electrons per ethanol molecule transferred under hydrodynamic conditions. High loadings of catalyst are required to obtain meaningful results. This makes the method well suited to the evaluation and comparison of catalysts for fuel cells, for which thick catalyst layers are required. Since RDV emulates the hydrodynamic conditions of a fuel cell anode, it provides more relevant stoichiometry and mass transport corrected kinetic parameters than coulometry, cyclic voltammetry, and chronoamperometry.

Thinner catalyst layers, which are better suited to mechanistic studies, show more complex RDV behavior due to the enhanced convective removal of soluble reaction intermediates (primarily acetaldehyde). Analysis of such data should allow differentiation of the various reaction pathways that have been identified,[129,136] but will require more sophisticated modelling to unravel.

Chapter 5

Electrochemical Oxidation of Formic Acid at Carbon Supported Pt Coated Rotating Disk Electrodes

All experiments in this chapter were conducted by Azam Sayadi. Data analysis was performed by Azam Sayadi and Prof. Peter G. Pickup. This chapter has been published as (Sayadi, A.; Pickup, P. G. Electrochemical oxidation of formic acid at carbon supported Pt coated rotating disk electrodes. *Russ. J. Electrochem.* **2017**, *53*, 1054-1060). A partial first draft of the manuscript was written by Azam Sayadi. Prof. Peter G. Pickup finalized and submitted the manuscript.

5.1 Introduction

The electrochemical oxidation of formic acid is the simplest process for the oxidation of an organic molecule to carbon dioxide and therefore serves as an important model for understanding the fundamental steps in the electro-oxidation of organic fuels. Formic acid fuel cells are currently being developed for portable applications,[16,181] and methanol fuel cell technology is now well developed.[105,182]

Fundamental studies of formic acid oxidation have focussed on the use of Pt and Pt-based electrodes and catalysts, and there is now a good understanding of the mechanistic details.[16,183,184] Formic acid oxidation at Pt proceeds through two parallel pathways, direct and indirect, which both occur following the adsorption of formic acid onto an active site on the Pt surface. In the direct pathway (eq. 5.1), formic acid is oxidized directly to carbon dioxide through a dehydrogenation mechanism. On the other hand, the indirect pathway (eq. 5.2) involves dehydration of the adsorbed formic acid molecule to form adsorbed carbon monoxide (CO_{ads}), which is a stable intermediate at low potentials. The resulting CO_{ads} can accumulate on the Pt surface and partially block (poison) formic acid adsorption, which inhibits both pathways for its oxidation. The second step in the indirect pathway, oxidation of CO_{ads} to CO_2, only occurs at a significant rate when the Pt surface begins to oxidize to Pt–OH at potentials above ca. 0.5 V vs. SHE.

$$HCOOH(aq) \rightarrow HCOOH_{ads} \rightarrow 2\ H^+ + 2\ e^- + CO_2 \tag{5.1}$$

$$HCOOH(aq) \rightarrow HCOOH_{ads} \rightarrow CO_{ads} + H_2O \rightarrow 2\ H^+ + 2\ e^- + CO_2 \tag{5.2}$$

The kinetics of these processes, and the activities of different catalysts, are generally investigated by cyclic voltammetry and chronoamperometry. The effects of mass

transport have been assumed to be negligible in most cases, which is reasonable for most flat electrodes. However, highly active electrode materials and thick catalytic layers produce much larger current densities, which can result in a significant reduction in the current due to concentration polarization (mass transport).[79,80] In such circumstances, rotating disk voltammetry (RDV) is generally used to separate the kinetically (i_k) and mass transport limited (i_{lim}) components of the overall current (i) through use of the Koutecky–Levich (K–L) equation 5.3.[55,185–187]

$$1/i = 1/i_k + 1/i_{lim} \tag{5.3}$$

where ($i_{lim} = 0.62nFAD^{2/3}\nu^{-1/6}C\omega^{1/2}$) , n is the number of electrons transferred (n = 2), F is the Faraday constant, A is the electrode area, D is the diffusion coefficient ($1.46 \times 10^{-5}\ cm^2\ s^{-1}$ for aqueous formic acid at 25 $^{\circ}C$),[188] ν is the kinematic viscosity ($1.0 \times 10^{-2}\ cm^2\ s^{-1}$) for water, C is the concentration of the reactant and ω is angular velocity.

There are only a few reports on the effects of electrode rotation on formic acid oxidation, and we have found no analysis of the mass transport rate. Pavese and Solis have investigated oxidation of formic acid on a palladium ring electrode in acid and reported that the oxidation current decreased as a result of increasing the rotation rate.[77] This was attributed to the blocking of the electrode surface by strongly adsorbed intermediates, which is enhanced by the convective increase in the $HCOOH$ concentration at the Pd surface.[77] Shin et al. found that the current at a Pt disk electrode decreased with increasing rotation rate, while poisoning of the electrode (i.e. accumulation of adsorbed, oxidizable intermediates mainly CO_{ads}) decreased.[189] In contrast to these results at Pd and Pt disk electrodes, Casado-Rivera et al. reported

normal RDV behavior and a linear K–L plot (i^{-1} vs. $\omega^{-1/2}$) for formic acid oxidation at an intermetallic $PtBi$ electrode.[80] Matsumoto et al. reported RDV data for formic acid oxidation at electrodes coated with Pt black, Pd black, carbon supported $PtRu$, and intermetallic $PtPb$ nanoparticles.[79] While the $PtPb$ gave a linear K–L plot, there was significant curvature for the other catalysts. In addition, the slopes of the K–L plot were different for each catalyst. Heterogeneous charge transfer rate constants were calculated from the intercepts of the K–L plots, but analysis of the slopes was not reported. A number of other electrochemical studies of formic acid oxidation have been made at rotating disk electrodes (RDE) using a single rotation rate,[190–194] in order to minimize mass transfer limitations,[193] supress re-deposition of Bi when a $PtBi$ alloy electrode was used,[190] or minimize the effect of local pH changes.[194]

We report here on the effects of electrode rotation at a glassy carbon disk electrode coated with a commercial carbon supported Pt catalyst (Pt/C). The goal was to verify that the mass transport rate conformed to the Levich equation, and to explore how the kinetics varied with potential and time. By using eq. 5.3 to obtain mass transport corrected kinetic currents, we have been able to observe the true rate of poisoning of the catalyst surface.

5.2 Experimental

5.2.1 Materials and Solutions

Formic acid (98–100% from Sigma Aldrich), sulfuric acid (95–98% from ACP Chemical), and deionized water were used to prepare solutions. The catalyst ink was

prepared from a Nafion^{TM} solution in a mixture of lower aliphatic alcohols (5.14% from DuPont), 1-propanol (J.T. Baker), and a commercial carbon supported platinum catalyst (20% Pt; Etek). The electrode was polished with an alumina slurry (0.3 μm, Sturbridge Metallurgical Services, Inc.).

5.2.2 Electrode Preparation

For catalyst ink preparation, a weighed amount of catalyst powder (ca. 28 $mg\ mL^{-1}$) was dispersed in a mixture of 1-propanol and Nafion solution homogenously in an ultrasonic bath for 3 h. The required amount of catalyst ink was applied onto the polished surface of a glassy carbon disk electrode (0.196 cm^2; Pine Instruments) with an Eppendorf micropipette and was allowed to dry at ambient temperature for ca. 30 min while it was rotated first at 100 rpm (ca. 15 min) and then at 600 rpm.[195] The catalyst layer contained ca. 1 $mg\ cm^{-2}\ Pt/C$ (0.2 $mg\ Pt\ cm^{-2}$) and ca. 25% Nafion by mass.

5.2.3 Electrochemistry

All electrochemical measurements were conducted at ambient temperature (24-25$^{\circ}C$) in a three-compartment glass cell using a catalyst coated glassy carbon electrode as the working electrode, a platinum wire as the counter electrode and a mercury sulfate electrode in 3.8 M sulfuric acid (Koslow; 635 mV vs. SHE) as a reference electrode. However, all potentials are given relative to the standard hydrogen electrode (SHE). An EG&G model 273A Potentiostat/Galvanostat and Pine Instruments ASR Analytical Rotator were used for rotating disk cyclic voltammetry,

constant potential and pulsed potential experiments in a 0.1 M formic acid solution with 1 M sulfuric acid as the electrolyte. The solution was de-aerated by passing N_2 into the solution for 20 min prior to all experiments, and then over the surface of the solution continuously during the experiments. Cyclic voltammetry was performed at 10 $mV\ s^{-1}$ between 0 and 1.24 V vs. SHE. For RDV, the first cathodic scan and second anodic scan are shown, since the first anodic scan was less reproducible due to variations in the coverage of adsorbed intermediates. The first anodic scan was used to clean and activate the electrode to produce a reproducible surface.

5.3 Results and Discussion

5.3.1 Rotating Disk Cyclic Voltammetry

Figure 5.1 shows cyclic voltammetry of the stationary Pt/C coated glassy carbon electrode in sulphuric acid solution in the absence and presence of formic acid. In the anodic scan, the oxidation current due to the direct pathway for formic acid oxidation commenced at 0.16 V and increased to a plateau at ca. 0.5 V. At higher potentials the oxidative removal of CO as CO_2 caused the current to increase to a peak at 0.75 V, where it is dominated by the direct pathway on the unblocked Pt surface.[45] At this point the increasing oxide coverage of the Pt surface limits the availability of sites for formic acid adsorption, and the current begins to decrease. In the cathodic scan, reduction of the oxide layer begins at ca. 0.8 V and the oxidation of formic acid then proceeds rapidly on the bare platinum sites that are formed. This results in a large anodic peak at ca. 0.5 V due primarily to the direct pathway. In Figure

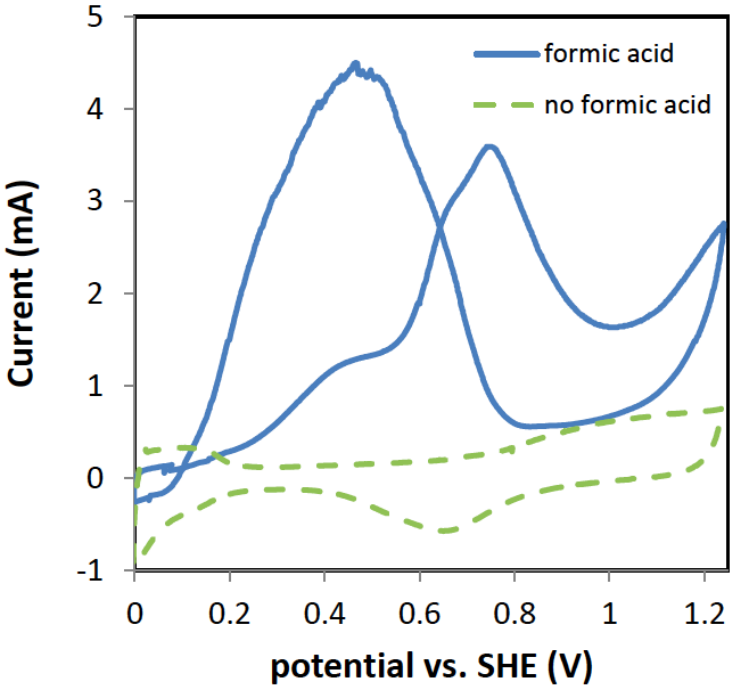

Figure 5.1: Cyclic voltammograms (10 $mV\ s^{-1}$) of a stationary $GC/Pt/C$ (1.04 $mg\ cm^{-2}$) electrode in 1 $M\ H_2SO_4$(aq) (dashed; the 2nd scan is shown), and with 0.1 M formic acid (solid; 1st scan from the open circuit potential of 0.06 V).

5.2, cyclic voltammograms (CV) are shown for formic acid oxidation over a range of rotation rates. On the anodic scans, the current for formic acid oxidation at the CO poisoned surface (i.e. to ca. 0.55 V) is only slightly influenced by rotation of the electrode, while the current for the unblocked surface (>0.55 V) increases sharply with increasing rotation rate. The large anodic peak on the cathodic scan also depends strongly on rotation rate. Although these differences in the rotation rate dependence over the different regions of the voltammogram may appear to be significant, they can simply be accounted for by use of eq. 5.3. When i_k is small, the kinetic term

dominates. Consequently, the effect of changing i_{lim} becomes insignificant when i_k is less than ca. 10% of i_{lim}. In Figure 5.2, i_{lim} increases from 9.8 mA at 100 rpm to 49 mA at 2500 rpm, and so the effect of increasing the electrode rotation rate is only significant when the current is above ca. 1 mA. The rotating disk voltammograms in

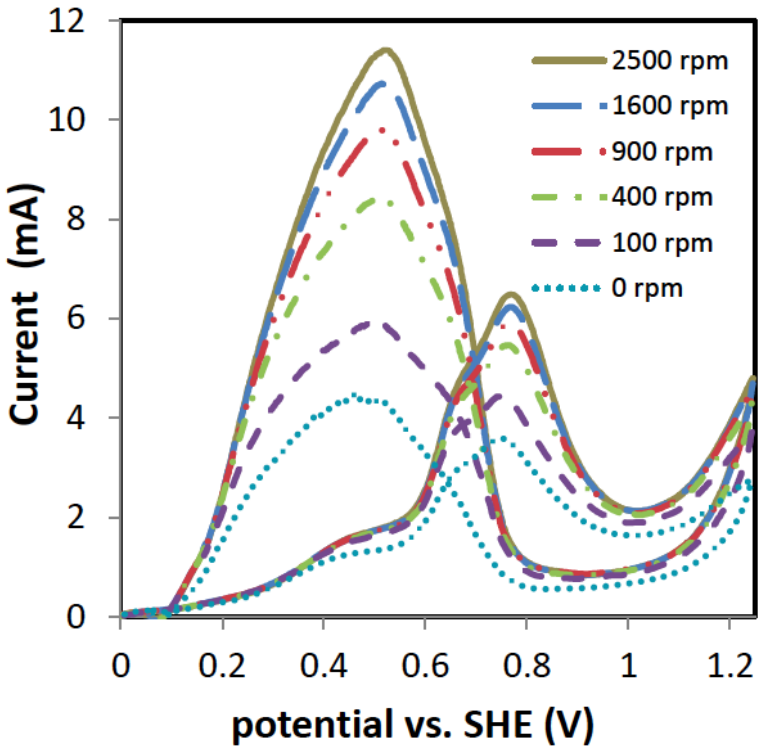

Figure 5.2: Cyclic voltammograms (10 $mV\ s^{-1}$) of 0.1 M formic acid in 1 M H_2SO_4(aq) at a $GC/Pt/C$ (1.04 $mg\ cm^{-2}$) electrode at 100 (1), 400 (2), 900 (3), 1600 (4), and 2500 (5) rpm. The 1st cathodic scan and 2nd anodic scan are shown.

Figure 5.2 are unusual in that they do not reach a constant, mass transport limited current at high potentials. This is due to a decrease in i_k at potentials above 0.75 V due to the formation of an oxide layer on the Pt surface. It can be seen that the

current remains well below i_{lim} (<50%) at all rotation rates.

It is instructive to visualize how the current is affected by concentration polarization, to illustrate the above discussion and to assess the errors that arise if it is assumed that the measured current in the CV at the stationary electrode is the kinetic current (i.e. if it is assumed that there is no mass transport effect). To do this, the CVs at the stationary electrode and at 400 *rpm* were first corrected for the background current due to the charging and electrochemistry of the catalyst layer by subtracting the current at the stationary electrode in the absence of formic acid. Then the CV at 400 *rpm* was corrected for mass transport by using eq. 5.3 to obtain i_k vs. potential. The results are shown in Figure 5.3. The CVs at other rotation rates produced very similar i_k CVs, justifying the use of eq. 5.3 to estimate i_k, and making the selection of the 400 *rpm* data arbitrary. However, it should be noted that the background correction employed here is only approximate because the adsorbed intermediates change the electrochemistry of the *Pt* surface. This is most obvious in the hydrogen adsorption-desorption region below 0.25 V.

It can be seen from Figure 5.3 that the CV at the stationary electrode gives a very poor approximation of the kinetic current, which represents the true activity of the catalyst layer. Consequently, Tafel plots of the CV currents would be very inaccurate, except at very low potentials, and comparisons of the CVs of different catalyst layers would be quite misleading. The application of eq. 5.3 to produce the mass transport corrected voltammogram in Figure 5.3 is based on the assumption that the electron transfer kinetics are first order.[55] This was confirmed by analysis of voltammograms obtained for 0.2 to 1 M formic acid at a stationary electrode. Data at three potentials on the anodic scans and three on the cathodic scans gave an average reaction order

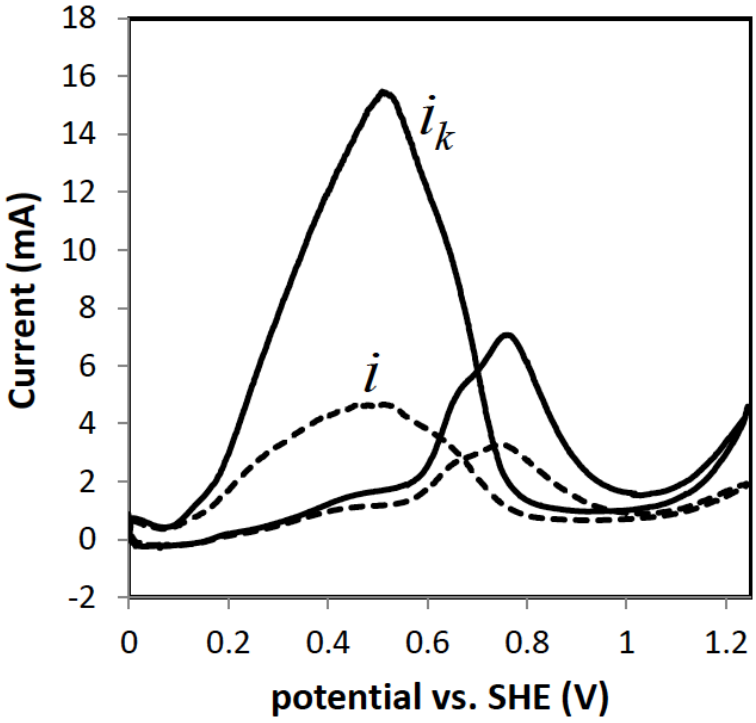

Figure 5.3: Background corrected cyclic voltammogram (10 $mV\ s^{-1}$) of 0.1 M formic acid in 1 M H_2SO_4(aq) at a stationary $GC/Pt/C$ (1.04 $mg\ cm^{-2}$) electrode (dashed) and i_k vs. potential from a background corrected voltammogram at 400 rpm (solid).

of 0.99 $\pm$ 0.13. In order to further test the validity of eq. 5.3 here, K–L plots were made using currents at various potentials on the anodic and cathodic scans of the voltammograms in Figure 5.2, following background correction. Examples are shown in Figure 5.4. These plots were linear and parallel for data collected during the cathodic scan, with slopes corresponding to $n = 2.08 \pm 0.08$, which is within experimental uncertainty of the value of $n = 2$ for oxidation of formic acid to CO_2. There was not a significant dependence of n on potential (Figure 5.5). In contrast, data collected on the anodic scan gave nonlinear K–L plots (Figure 5.4) with slopes

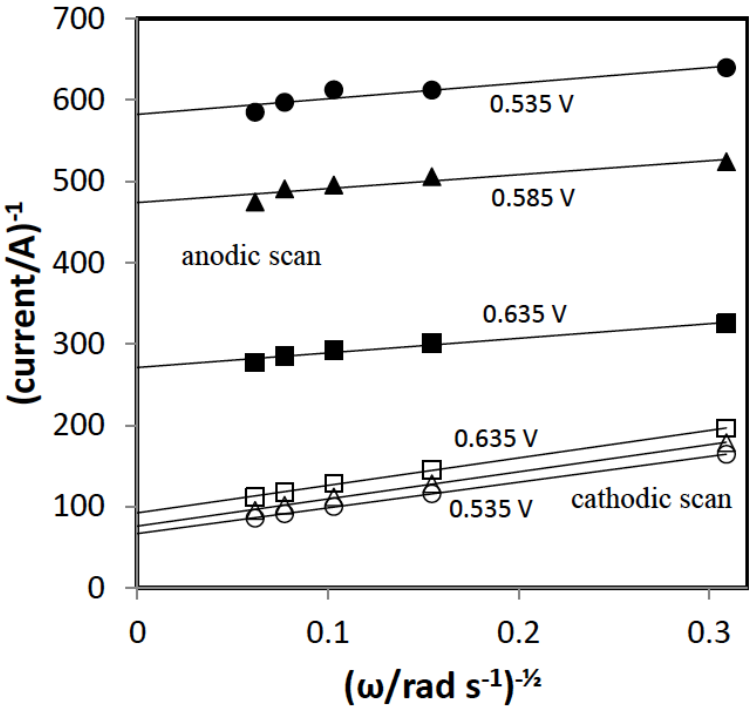

Figure 5.4: Koutecky–Levich plots of background corrected cyclic voltammograms for oxidation of 0.1 M formic acid in 1 M H_2SO_4(aq) at a $GC/Pt/C$ (1.04 $mg\ cm^{-2}$) electrode at 0.535 V (circles), 0.585 V (triangles) and 0.635 V (squares) on the anodic (solid points) and cathodic (open points) scans.

that varied with potential. The apparent number of electrons transferred (Figure 5.5) decreased with increasing potential from 4.7 to 1.2, which is clearly nonsensical. Although this failure of eq. 5.3 for data on the anodic scan could be due to random errors, due to the very small differences in the current with changing rotation rate, the curvature indicates that there was also a systematic error. This is explored in Sections 5.3.2 and 5.4. Kinetic currents (i_k) from the intercepts of the linear K–L plots for the cathodic scans are shown as a Tafel plot in Figure 5.6. This clearly shows that i_k is

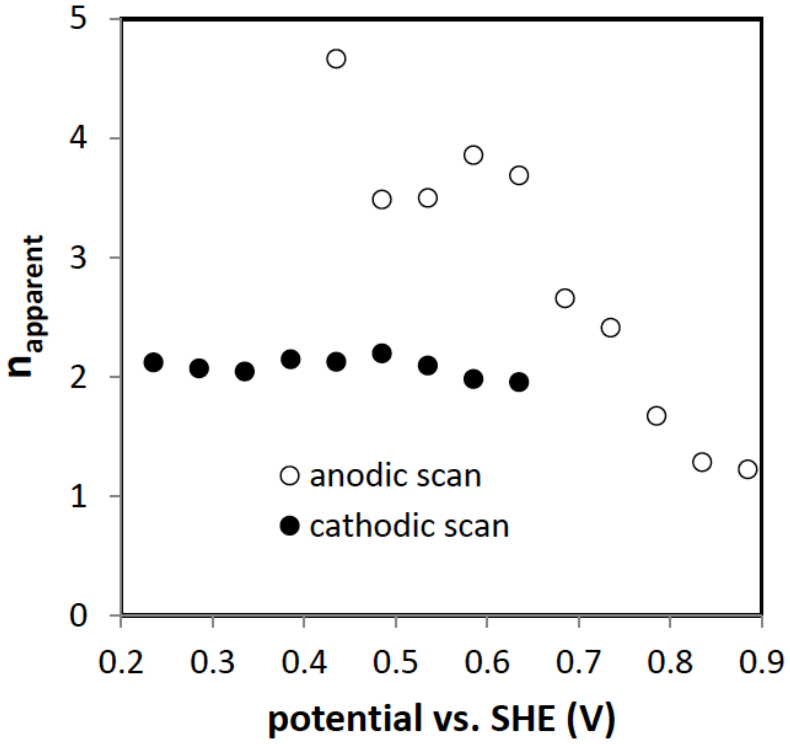

Figure 5.5: Apparent number of electrons transferred (n_{ap}) vs. potential for oxidation of 0.1 M formic acid in 1 M H_2SO_4(aq) at a $GC/Pt/C$ (1.04 $mg\ cm^{-2}$) electrode, from anodic (open points) and cathodic (solid points) voltammetric scans.

lower at higher potentials, when there is an oxide layer on the electrode. The decrease in i_k at low potentials, as the potential was decreased during the cathodic scan, is due primarily to the decreasing overpotential. However, linear Tafel behaviour is not observed due to the increasing coverage of CO_{ads} on the Pt surface during the scan. Kinetic currents for the anodic scan are not shown because they would clearly be very inaccurate. It should be noted that the kinetic currents reported here presumably include a component due to diffusion of formic acid into the thick catalyst layers that have been employed. This does not affect the validity of eq. 5.3,[177] but does provide

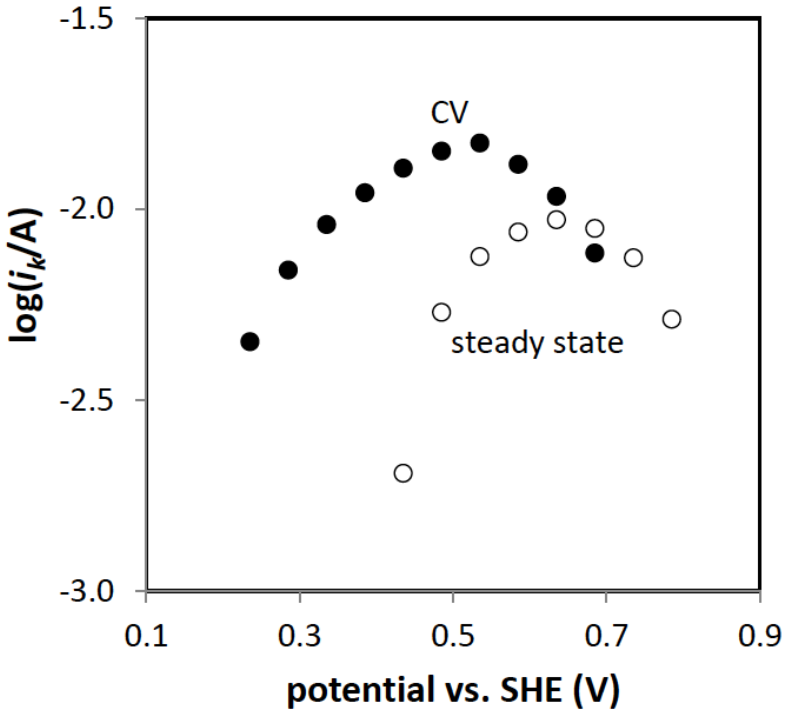

Figure 5.6: Tafel plots for oxidation of 0.1 M formic acid in 1 M H_2SO_4(aq) at a $GC/Pt/C$ (1.04 $mg\ cm^{-2}$) electrode, from the cathodic scans of cyclic voltammograms (solid) and from steady-state currents (open).

data that is most relevant to the use of thick catalyst layers in fuel cells. The intrinsic activity of the catalyst could be extracted if the mass transport characteristics of the catalyst layer were known.[178]

5.3.2 Steady-State Experiments

In addition to cyclic voltammetry, steady-state rotating disk electrode (RDE) experiments were conducted in order to explore why linear K–L plots and reasonable n values were only obtained for the negative voltammetric scan. These experiments

also provide data that is more relevant to applications, particularly in fuel cells, where there is a steady-state coverage of CO_{ads}.

During these experiments, the current was recorded at a constant potential as the rotation rate was increased in a series of steps, as illustrated in Figure 5.7 (inset). This type of experiment was repeated over a range of potentials, with a cyclic scan between 0 and 1.235 V between each experiment to clean and activate the electrode. K–L plots of the steady-state currents showed good linearity (e.g. Figure 5.7), with slopes that were independent of potential and correspond to the transfer of 2.00 ± 0.06 electrons. Kinetic currents from the intercepts are compared with those from CV in Figure 5.6. In the low potential region (0.4 to 0.6 V), they are much lower because the Pt is heavily poisoned with CO_{ads} at steady-state. However, the CV and steady-state values converge in the high potential region where the CO_{ads} coverage is lower and does not change with time. In fact, the steady-state value is higher than the CV value at 0.685 V because of the hysteresis in the oxide coverage, since the oxide layer reduces at lower potentials than for its formation.

Since the steady-state measurements were conducted in the order of increasing potential, and show normal K–L behaviour, the anomalous K–L behaviour in cyclic voltammetry does not appear to be due to the scan direction, per se. Instead, it would appear to be due to the effect of time, which is absent in the steady-state measurements. Previously, it has been reported that the rate of CO_{ads} accumulation on the Pt surface decreases as the rotation rate is increased.[189] This would adequately explain the curvature of the K–L plots, where the current is higher than it should be at high rotation rates.

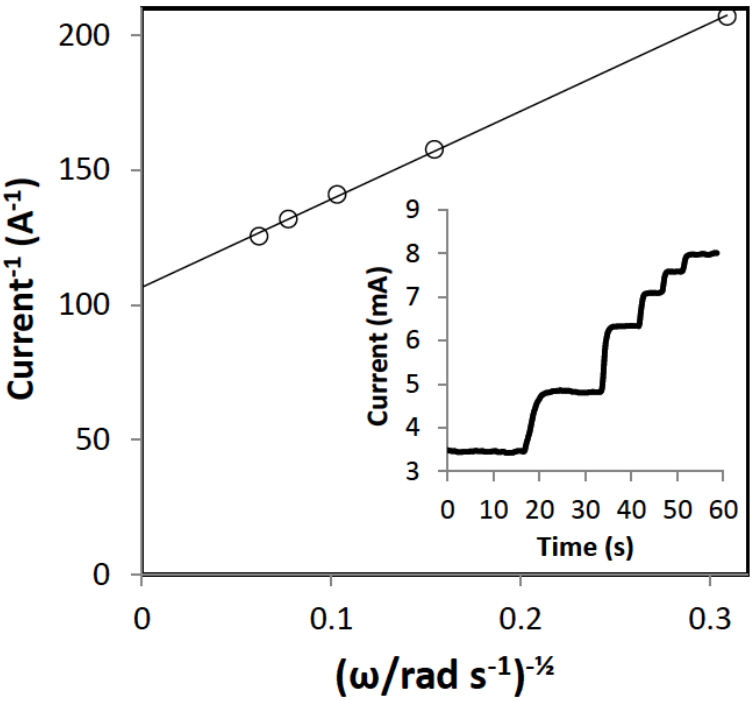

Figure 5.7: Steady-state Koutecky–Levich plot for constant potential oxidation of 0.1 M formic acid in 1 M H_2SO_4(aq) at a $GC/Pt/C$ (1.04 $mg\ cm^{-2}$) electrode at 0.635 V. Inset: current vs. time at 0.635 V and various rotation rates from 0 to 2500 rpm.

5.4 Potential Step Experiments

One of the disadvantages of cyclic voltammetry is that the current at any potential is affected by the history of the electrode at previous potentials. Also, in both CV and steady-state experiments the electrode is exposed to poisoning for relatively long periods of time. Poisoning is affected not only by the potential but also the time at that potential, or its rate of change.[183,196] To evaluate the effect of time on the kinetics of formic acid oxidation, a pulsed potential procedure[45] was used, in order to clean the electrode and restore it to a consistent state before measurements at each rotation

rate and each potential. During these experiments a high potential (1.235 V) was applied to the electrode for a short period of time (10 s) in order to remove CO_{ads} and form an oxide layer. The potential was then stepped to the desired lower potential in order to remove the oxide layer and initiate the oxidation of formic acid at the clean, and activated, Pt surface. This sequence of steps was repeated at different rotation rates at each test potential. Data for 0.435 V, which is close to the peak potential for the direct pathway, is shown in Figure 5.8. It can be seen that the decay rate of the current decreased significantly when the electrode was rotated at 100 rpm, but then appears to increase with increasing rotation rate. This indicates that the rate of poisoning is influenced by the mass transport conditions, as previously reported for a Pt disk electrode.[189]

Because of the dependence of the poisoning rate on rotation rate, K–L plots at different times following the step to the test potential were all slightly curved, and there were small variations in the slope with the measurement time. Consequently, accurate i_k values could not be obtained from K–L plots. Therefore, each i vs. t curve was converted directly to i_k vs. t by using eq. 5.3. Results at 0.485 V, which were similar to those at 0.435 V, are shown in Figure 5.9. It can be seen that the raw i vs. t curves give a misleading impression of the differences in the activities of the catalyst, and that the decay rate of the kinetic current is not dependent on the rotation rate from 400 to 2500 rpm. However, there is a small systematic increase in i_k with increasing rotation rate, which is consistent with the curvature seen in the K–L plots. This same trend was observed at all other potentials (from 0.385 to 0.635 V) that were employed. The data at 100 rpm are anomalous, and this can be attributed to experimental errors. There is greater uncertainly (noise) in i_k at low

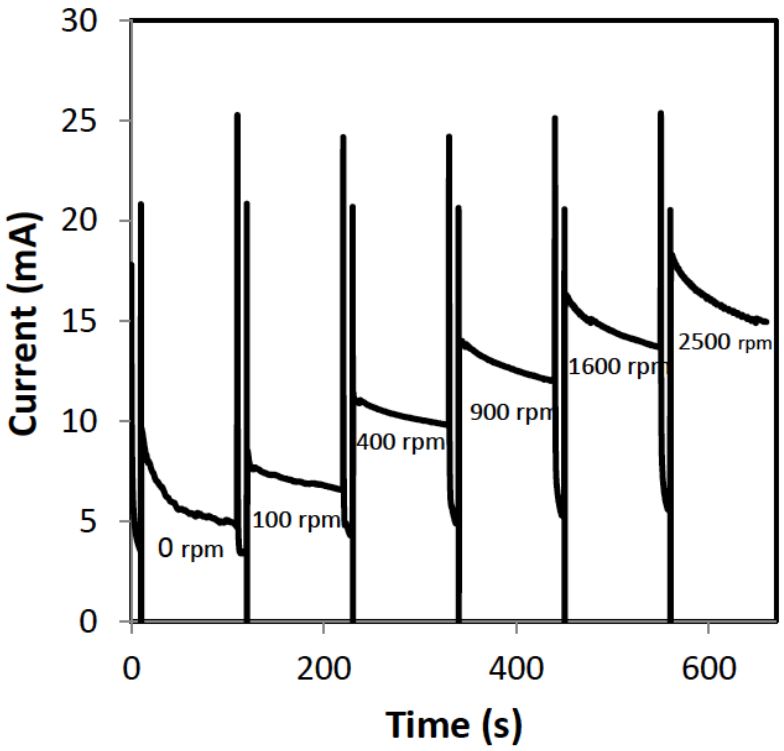

Figure 5.8: Chronoamperometry at 0.435 V for the oxidation of 0.1 M formic acid in 1 M H_2SO_4(aq) at a $GC/Pt/C$ (1.25 $mg\ cm^{-2}$) electrode at 0, 100, 400, 900, 1600, and 2500 rpm. The potential was stepped to 1.235 V for 10 s while the rotation rate was changed.

rotation rates because the measured current is closer to the mass transport limited current. At 100 rpm, i_{lim} was 9.8 mA, while i decreased from 8.9 to 7.3 mA. These relatively small differences between i and i_{lim} lead to large random and systematic errors in i_k. In addition, the thicker diffusion layer at 100 rpm takes longer to be established, which causes a systematic error at short times, and also results in more noise due to vibrations. Consequently, the i_k values obtained at 100 rpm should be regarded as unreliable.

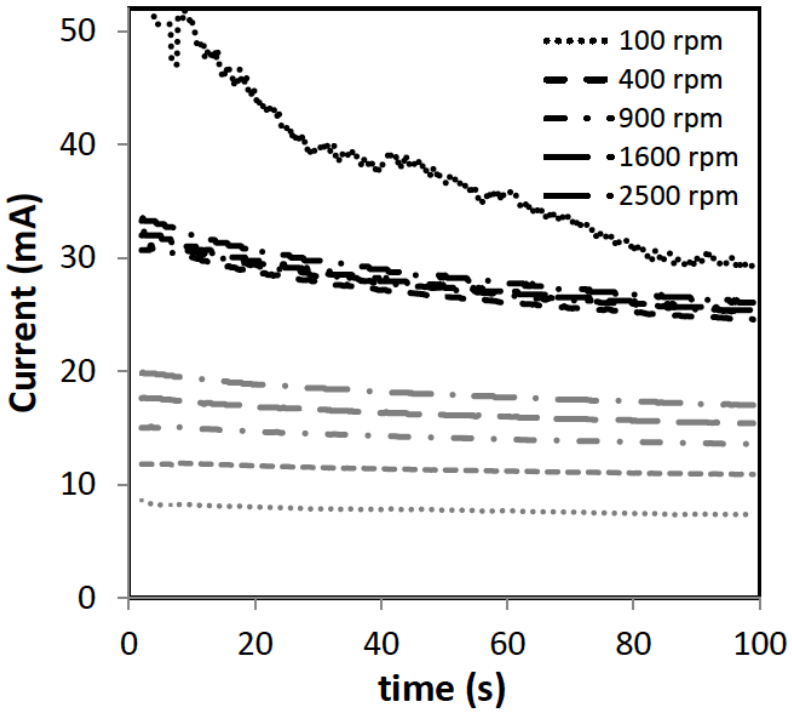

Figure 5.9: Currents (i, grey) and kinetic currents (i_k, black) vs. time for oxidation of 0.1 M formic acid in 1 M H_2SO_4(aq) at 0.485 V at a $GC/Pt/C$ (1.25 $mg\ cm^{-2}$) electrode at 100 (1), 400 (2), 900 (3), 1600 (4), and 2500 (5) rpm. The potential was stepped to 1.235 V for 10 s while the rotation rate was changed. Data for the first 2 s are omitted because of inaccuracy due to the time constant of the cell.

The results in Figure 5.9 further demonstrate the importance of mass transport corrections when conducting kinetic studies at high surface area catalysts. Even at very low potentials, the kinetic current is much higher than the currents measured by cyclic voltammetry or chronoamperometry at a stationary electrode, unless there is severe poisoning.

5.5 Conclusions

Formic acid oxidation at an electrode coated with a layer of carbon supported Pt catalyst with 0.2 $mg\ Pt\ cm^{-2}$ shows substantial mass transport limitations at potentials above 0.1 V vs. SHE unless there is severe poisoning due to adsorbed CO. Although pure mass transport control of the current has not been observed, the Koutecky–Levich equation can be applied to extract mass transport and kinetic parameters. However, changes in the kinetic current with changing rotation rate can cause plots of 1/current vs. $\omega^{-1/2}$ to be non-linear, with inaccurate slopes and intercepts. Under such conditions, the kinetic current can be calculated at each rotation rate by use of the known mass transport limited current.

Chapter 6

Hydrodynamic Studies of Ethanol Oxidation at Pt and PtRu Catalysts at Elevated Temperatures

This work has been published in part as (Sayadi, A.; and Pickup, P. G. Hydrodynamic studies of ethanol oxidation at Pt and PtRu catalysts at elevated temperatures. *ECS Trans* **2020**, 97, 869-875). The experimental part was performed by Azam Sayadi. Data analysis and data interpretation was done by Azam Sayadi and Prof. Peter G. Pickup. Azam Sayadi and Prof. Peter G. Pickup contributed in preparation of the manuscript. Azam Sayadi was the corresponding author of the manuscript. The raw data is provided in Appendix A.

6.1 Introduction

Ethanol has received growing attention as an attractive fuel for direct fuel cell systems in recent years.[2,49,197] It has a number of advantages over other fuels, such as simple production from biomass fermentation, being renewable and safe, and having a high energy density (8.0 $kWh\ kg^{-1}$). Similar to other fuel cells, direct ethanol fuel cells (DEFC) have the potential to produce close to 100% energy efficiency, in theory.[3,4] Nevertheless, despite extensive efforts having been made toward the development of DEFC, they still suffer from incomplete and slow electrochemical oxidation of the ethanol and, therefore, low power output and efficiency. Most of the ethanol is partially oxidized to acetaldehyde and acetic acid (eq. 6.1) in 2- and 4-electron pathways, respectively, vs. the 12-electron pathway for CO_2 production as the final product (eq. 6.2, where $C1_{ad}$ and $C2_{ad}$ represent adsorbed one carbon and two carbon species).[160] Partial oxidation of ethanol leads to a significant decrease in DEFC energy efficiency.

$$CH_3CH_2OH \rightarrow [CH_3CH_2OH]_{ad} \rightarrow C1_{ad}, C2_{ad} \rightarrow CO_2 \quad [total\ oxidation] \tag{6.1}$$

$$CH_3CH_2OH \rightarrow [CH_3CH_2OH]_{ad} \rightarrow CH_3CHO \rightarrow CH_3COOH \quad [partial\ oxidation] \tag{6.2}$$

For enhancement of the energy efficiency, a comprehensive study of the electrocatalytic oxidation mechanisms and the stoichiometry (number of electrons transferred, n) are fundamental. One of the approaches for these studies is applying hydrodynamic methods due to their ability to emulate the hydrodynamic conditions of a fuel cell anode as well as discriminating between the kinetic and mass transport limited components of the measured current. Rotating disk voltammetry (RDV) is a

widely used hydrodynamic technique with straightforward mathematical treatments. The Koutecky–Levich equation (K-L) can be applied to separate the effects of kinetics and mass transport (eq. 6.3).[55]

$$1/i = 1/i_k + 1/i_{lim} = 1/i_k + 1/(0.62nFAD^{2/3}\nu^{-1/6}C\omega^{1/2}) \tag{6.3}$$

Where i is the measured current, i_k and i_{lim} are kinetic and mass transport limited currents, n is the number of electrons transferred, F is the Faraday constant, A is electrode surface area, D is diffusion coefficient, ν is kinematic viscosity and ω is angular velocity. There have been a number of reports on the electrochemical oxidation of ethanol using RDV at ambient temperature.[6,85,88–91,163,165] Since DEFC are operated at high temperatures, in this study, we focused on the electrochemical oxidation of ethanol at various catalysts using RDV at elevated temperatures.

6.2 Experimental

6.2.1 Materials

Solutions were prepared by using anhydrous ethanol and sulfuric acid from ACP Chemicals Inc. Catalyst inks were prepared by dispersion of commercial catalysts in 1-propanol (J.T. Baker) and a Nafion^{TM} solution in a mixture of lower aliphatic alcohols (5.14%, DuPont). Commercial catalysts were carbon supported Pt (70% Pt/C, HiSPEC^{TM} 13100, 70% Pt on a high surface area advanced carbon support, Alfa Aesar, Lot # M22A026) and carbon supported $PtRu$ alloy (75% $PtRu/C$, HiSPEC^{TM} 12100, 50% Pt and 25% Ru on a high surface area advanced carbon support, Alfa Aesar, Lot # P17B047). Prior to application of each catalyst ink,

the working electrode was polished with an alumina slurry (0.3 μm; Sturbridge Metallurgical Services, Inc.).

6.2.2 Electrochemical Measurements

Electrochemical measurements were carried in a three-compartment glass cell operated with an EG&G model 273A Potentiostat/Galvanostat. The working electrode was a catalyst loaded glassy carbon rotating disk electrode (Pine Instruments). A mercury sulfate electrode in 3.8 M sulfuric acid and a platinum wire were applied as reference and counter electrode, respectively. The experiments were carried in 0.1 M ethanol solution in 1.0 M sulfuric acid. Thick layers of catalyst were loaded onto the surface of the electrode with 20% by mass of Nafion as a binder. Prior to each experiment, the solution was de-aerated by passing N_2 gas into the solution for 15 min and over the surface of the solution continuously during the experiments. All of the cyclic voltammetry experiments were recorded at 10 $mV\ s^{-1}$ and all potentials are given relative to SHE. For experiments at elevated temperatures (50 $^{\circ}C$ and 80 $^{\circ}C$), the cell was heated in a water bath, and ice gel packs were wrapped around the neck of the cell to condense vapors.

6.3 Results and Discussion

6.3.1 PtRu/C Catalyst

6.3.1.1 Cyclic Voltammetry

7 $mg\ cm^{-2}$ of 75% $PtRu/C$ catalyst was loaded on the electrode. Figure 6.1 shows cyclic voltammograms at a 75% $PtRu/C$ electrode in sulfuric acid solution without and with ethanol at 0 and 400 rpm. In the forward scan, the oxidation of ethanol at low potentials was hampered by adsorption of poisoning species on the electrode surface, and oxidation commenced at ca. 0.23 V. The double-layer charging current is relatively high for this catalyst because the capacitance is increased by the presence of Ru-oxides.[198] The current increased with potential and peaked at 0.693 V. As can be seen, the oxidation current was increased significantly by rotating the electrode (starting at ca. 0.45 V), and this effect is more visible in the reverse scan. However, a mass transport limited plateau was not achieved in these experiments due to oxide layer formation and suppression of ethanol oxidation at potentials higher than ca. 0.7 V.

The cell was heated to 50 $^{\circ}C$, and voltammograms were recorded at various rotation rates. At 50 $^{\circ}C$, the faradaic current for ethanol oxidation was roughly a factor of 2 higher than at 24 $^{\circ}C$, which can be attributed to the faster reaction kinetics for ethanol oxidation as well as an increase in the ethanol diffusion coefficient (i.e. $D = 2.09 \times 10^{-5}\ cm^2\ s^{-1}$ at 50 $^{\circ}C$, and $D = 3.46 \times 10^{-5}\ cm^2\ s^{-1}$ at 80 $^{\circ}C$ vs. $D = 1.22 \times 10^{-5}\ cm^2\ s^{-1}$ at 24 $^{\circ}C$).[199] Voltammograms at different rotation rates are illustrated in Figure 6.2. The distortion of the voltammograms and increasing

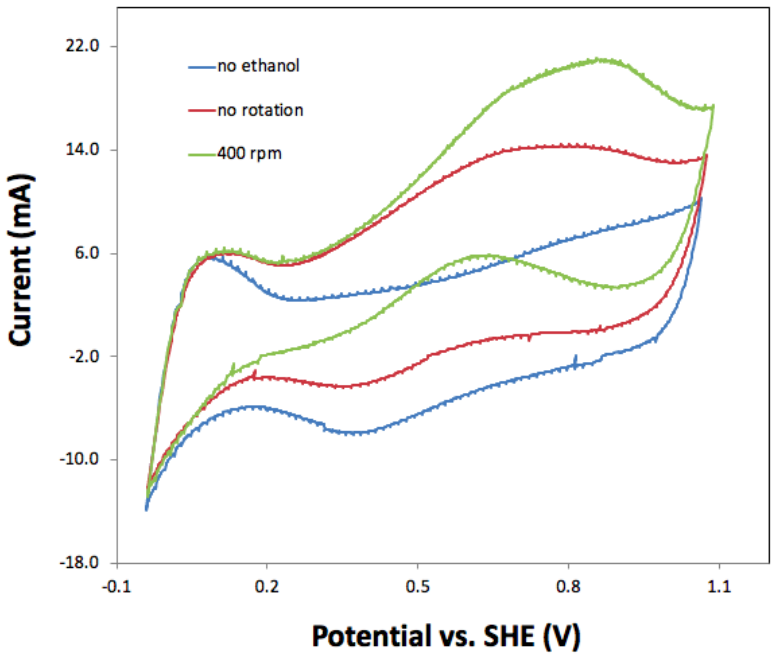

Figure 6.1: Cyclic voltammograms (10 $mV\ s^{-1}$) of a 75% $PtRu/C$ (ca. 7 $mg\ cm^{-2}$) electrode in 1 M H_2SO_4(aq) (blue), with 0.1 M ethanol (red), and 0.1 M ethanol at 400 rpm rotation rate (green) (temperature = 24 $°C$).

peak potentials can be ascribed to the uncompensated resistance, which causes an increasing error in the applied potential as the current increases with increasing temperature and rotation rate. Although the current increased significantly with increasing rotation rate, the mass transport limited current was not achieved at this temperature for any of the rotation rates

A new electrode, with the same catalyst loading, was examined at 80 $°C$, and the oxidation peak current reached 40 mA in a quiescent solution. Cyclic voltammograms at different rotation rates at 80 $°C$ are illustrated in Figure 6.3. A significant increase in the current was observed with the rotation rate increase. The current's fluctuation

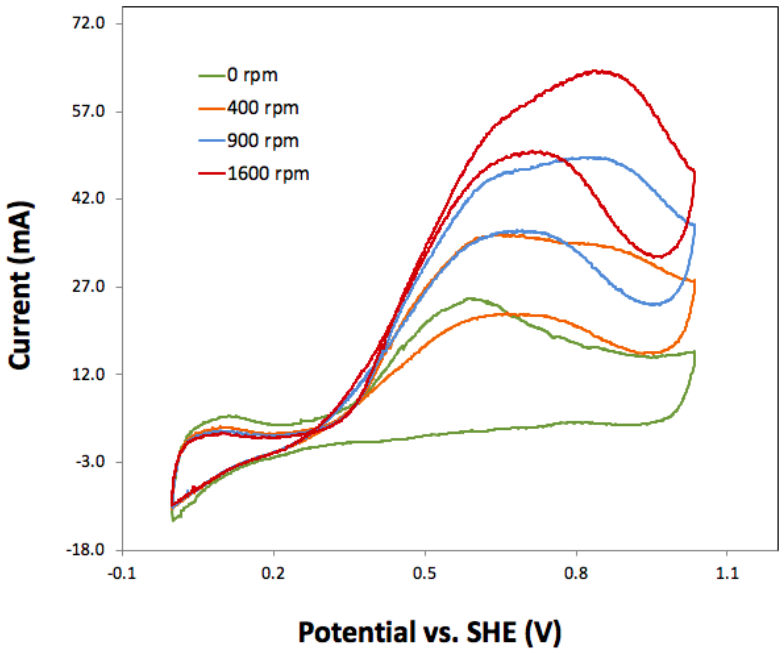

Figure 6.2: Cyclic voltammograms (10 $mV\ s^{-1}$) of the 75% $PtRu/C$ (ca. 7 $mg\ cm^{-2}$) electrode in 0.1 M ethanol in 1 M H_2SO_4(aq) at various rotation rates (temperature = 50 $^{\circ}C$).

between 0.5 to 0.9 V at low rotation rates (i.e. 100 and 400 rpm) can be attributed to CO_2 bubble formation on the electrode surface. The bubbles were removed as the electrode rotated at high rates.

6.3.1.2 Steady-State Measurements

To minimize errors from the large background currents and uncompensated resistance that appeared in cyclic voltammetry, steady-state experiments were conducted to discriminate between the kinetic and mass transport components of the measured current. A constant potential was applied while the electrode rotation was increased in steps, as illustrated in Figure 6.4. Each rotation rate was applied until the current

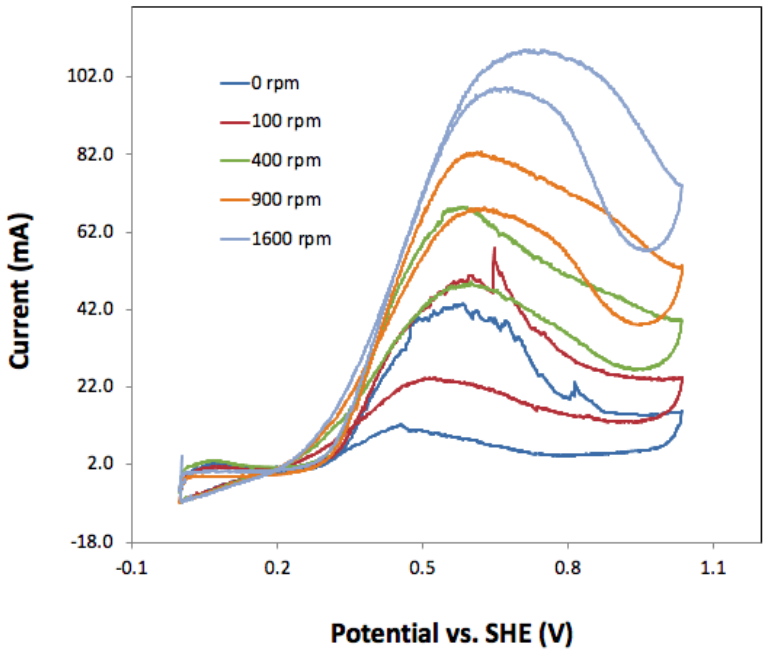

Figure 6.3: Cyclic voltammograms (10 $mV\ s^{-1}$) of a 75% $PtRu/C$ (ca. 7 $mg\ cm^{-2}$) electrode in 0.1 M ethanol in 1 M H_2SO_4(aq) at various rotation rates (temperature = 80 $°C$).

reached a steady-state. These measurements were made over a range of potentials from 0.535 to 0.835 V in 0.05 V intervals at 24, 50, and 80 $°C$. K-L plots were extracted from steady-state experiments, and n values were obtained from the K-L plots slope for all three temperatures (see appendix A).

K-L plots at 80 $°C$ showed fairly good linearity which improved with potential increase over the potential range of 0.535 to 0.685 V. However, at higher potentials, K-L plots showed significant curvature. At these potentials, the slopes of K-L plots are higher; therefore, lower n values were obtained. One of the possibilities is the poisoning of the electrode by the acetaldehyde at higher potentials.[165] The experiments at 80 $°C$ were repeated, and again significant curvature was observed for

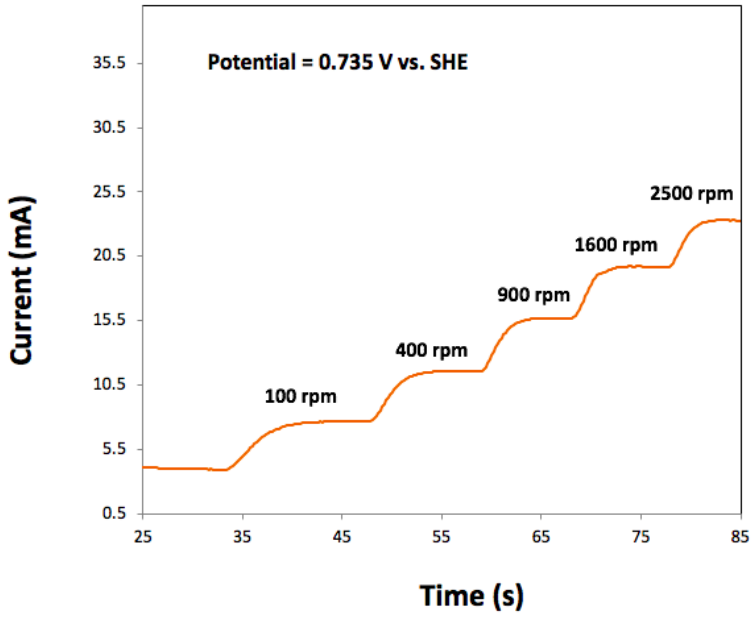

Figure 6.4: Current vs. time at 0.735 V and various rotation rates for the oxidation of 0.1 M ethanol in 1 M H_2SO_4(aq) at a 75% $PtRu/C$ (ca. 7 $mg\ cm^{-2}$) electrode (temperature = 50 $°C$).

the same region. In both experiments, apparent n values decreased with potential increase. K-L plots 80 $°C$ are illustrated in appendix A as Figure A.3.

Figure 6.5 shows K-L plots for three different temperatures at 0.585 V. The decrease in slope with increasing temperature shows an increase in n (stoichiometry). Table 6.1 shows stoichiometries for three more potentials at the same temperature. Values of n obtained at 24 $°C$ are close to 2, indicating that the main product was acetaldehyde ($n = 2$), although the curvature of the K-L plots at this temperature may cause some underestimation of n.[165] At 50 $°C$, the linearity of the K-L plot was better, and n values were higher (ranging from 2.9 to 3.3). The increase in n with temperature indicates that more acetic acid ($n = 4$), and presumably small amounts of

CO_2 ($n = 12$), were formed. At 80 $°C$, n values were even higher, and decreased with increasing potential, from 5.6 to 5.0. Values above 4 indicate that there was increased production of CO_2, and the trend shows that the CO_2 yield decreased with increasing potential. This can be attributed to increasing coverage of the catalyst surface with oxide, which leads to an increase in acetic acid formation.[200] The pronounced potential dependence at 80 $°C$, which is the only temperature at which CO_2 production was detectable (i.e. $n > 4$), indicates that oxide formation inhibits cleavage of the $C - C$ bond of ethanol.

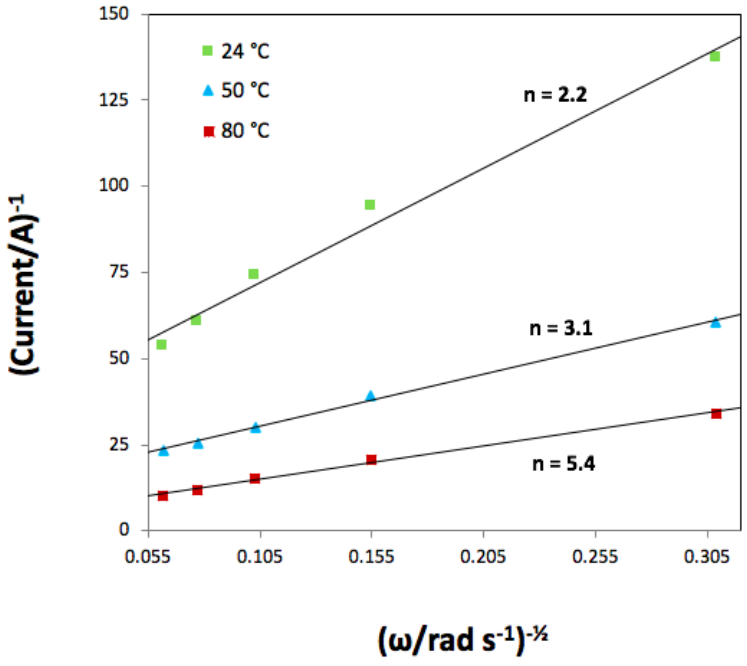

Figure 6.5: Steady-state Koutecky-Levich plots (i^{-1} vs. $\omega^{-1/2}$) for oxidation of 0.1 M ethanol in 1 M H_2SO_4(aq) at a 75% $PtRu/C$ (ca. 7 $mg\ cm^{-2}$) electrode and 0.585 V.

Table 6.1: Stoichiometries obtained from steady-state K-L plots at various temperatures and potentials using 75% $PtRu/C$.

Potential vs. SHE (V)	n *at* 24 °C	n *at* 50 °C	n *at* 80 °C
0.535 V	2.1	3.3	5.6
0.585 V	2.2	3.1	5.4
0.635 V	2.2	2.9	5.2
0.685 V	2.2	3.0	5.0

6.3.2 Pt/C Catalyst

6.3.2.1 Cyclic Voltammetry

The electrode was loaded with 7 mg of 70% Pt/C catalyst (20% by mass Nafion). Figure 6.6 shows cyclic voltammograms of ethanol solution at 70% Pt/C catalyst at 24 °C. The oxidation current began to increase with electrode rotation at higher potential compared to 75% $PtRu/C$ (ca. 0.5 V) and the rotation effect on the current increase was less pronounced for this catalyst.

The cyclic voltammetry experiments at different rotation rates were conducted at 50 °C on the 7 $mg\ cm^{-2}$ 70% Pt/C (Figure 6.7). At 50 °C, the effect of increasing the temperature on the current's increase was more pronounced at lower rotation rates compared to 75% $PtRu/C$ (i.e. 100-400 rpm). The oxidation peak current at 0.80 V reached 33 mA on the stationary electrode at 80 °C (vs. 42 mA at 0.57 V for 75% $PtRu/C$).

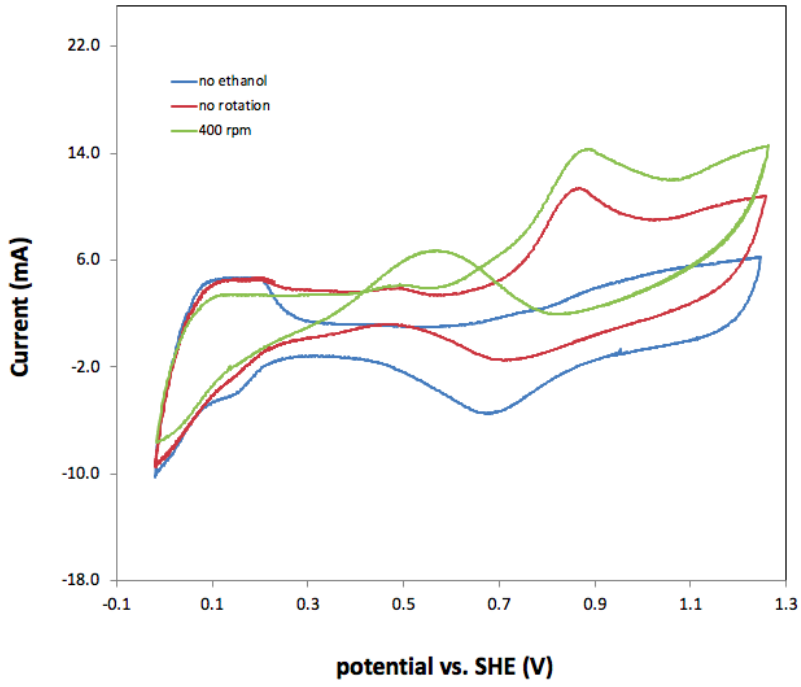

Figure 6.6: Cyclic voltammograms (10 $mV\ s^{-1}$) of a 70% Pt/C (ca. 7 $mg\ cm^{-2}$) electrode in 1 M H_2SO_4(aq) (blue), with 0.1 M ethanol (red), and 0.1 M ethanol at 400 rpm rotation rate (green) (temperature = 24 $°C$).

6.3.2.2 Steady-State Measurements

K-L plots were obtained from steady-state experiments over a range of potentials from 0.535 to 0.685 V for three different temperatures using 70% Pt/C. Those at 0.585 V are shown in Figure 6.8. These plots show good linearity with n increasing as the temperature was increased, as seen for the $PtRu/C$ catalyst. Table 6.2 shows stoichiometries obtained from 0.535 to 0.685 V. Values of n at 24 $°C$ ranged from 2.1 to 2.8 indicating that both acetaldehyde and acetic acid were produced at this temperature, with little CO_2 production. Increasing the temperature to 50 $°C$ increased n to a range of 2.9 to 3.3, indicating increased production of acetic acid.

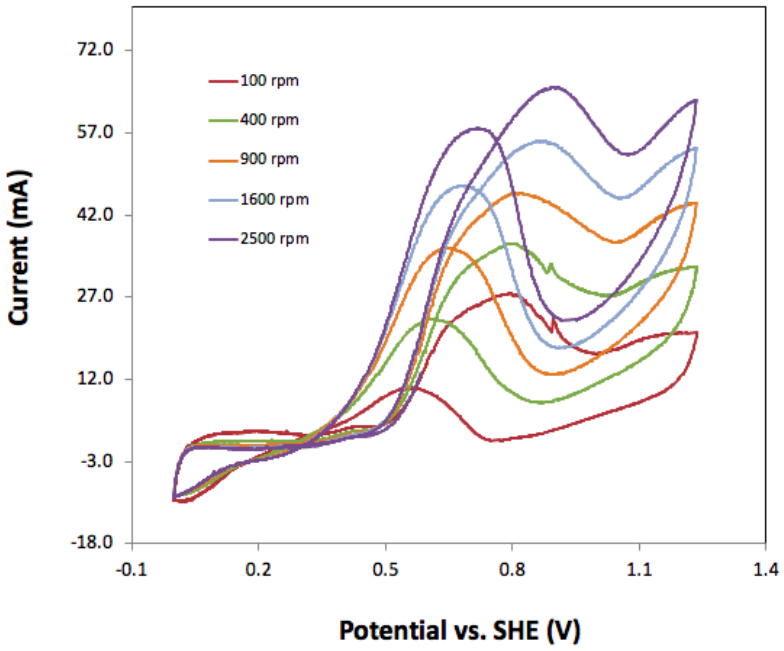

Figure 6.7: Cyclic voltammograms (10 $mV\ s^{-1}$) of the 70% Pt/C (ca. 7 $mg\ cm^{-2}$) electrode in 0.1 M ethanol in 1 M H_2SO_4(aq) at various rotation rates (temperature = 50 $^{\circ}C$).

At 80 $^{\circ}C$, the n values were even higher (3.4 to 4.7), and decreased significantly with increasing potential due to oxide formation. Relative to the $PtRu/C$ catalyst, the Pt/C catalyst appears to give similar product distributions at 24 $^{\circ}C$ and 50 $^{\circ}C$, but lower CO_2 yields at 80 $^{\circ}C$. This may arise from the bifunctional effect. Dissociative adsorption of water occurs at lower potentials by alloying Pt with an oxyphilic metal. $Ru-OH$ groups on the $PtRu$ surface can oxidize adsorbed CO to CO_2 at lower potentials than $Pt-OH$ groups on Pt.

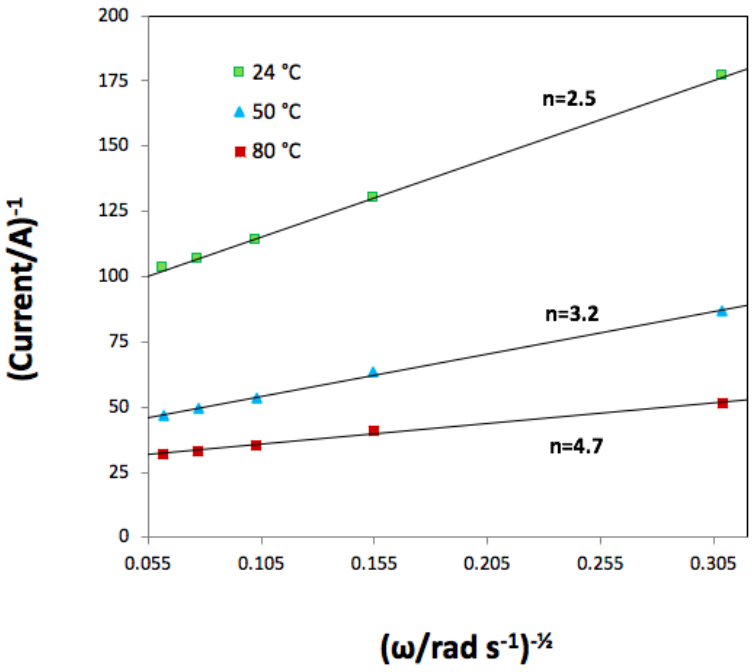

Figure 6.8: Steady-state Koutecky-Levich plots (i^{-1} vs. $\omega^{-1/2}$) for oxidation of 0.1 M ethanol in 1 M H_2SO_4(aq) at a 70% Pt/C (ca. 7 $mg\ cm^{-2}$) electrode and 0.585 V.

Table 6.2: Stoichiometries obtained from steady-state K-L plots at various temperatures and potentials using 70% Pt/C.

Potential vs. SHE (V)	n *at* 24 °C	n *at* 50 °C	n *at* 80 °C
0.535 V	2.7	2.4	4.3
0.585 V	2.5	2.9	4.7
0.635 V	2.1	3.0	4.1
0.685 V	2.8	2.3	3.4

6.4 Conclusions

Steady-state measurements at rotating disc electrodes can provide reasonable estimates of the stoichiometry of ethanol oxidization over a range of temperatures. Increasing values of n observed as the temperature was increased, at both $PtRu/C$ and Pt/C catalysts, indicates that there were increased yields of acetic acid at 50 $^{\circ}C$ vs 24 $^{\circ}C$, and increased CO_2 production at 80 $^{\circ}C$. A significant potential dependence at 80 $^{\circ}C$ can be attributed to the effects of oxide formation, which inhibits breaking of $C-C$ bond of ethanol. The $PtRu/C$ catalyst showed better performances than Pt/C in terms of both activity and the number of electrons transferred at higher temperatures because of the $Ru-OH$ group's role in poison removal (ca. adsorbed CO). The results showed that RDV can provide valuable stochiometric information for the assessment of the completeness of ethanol oxidation.

Chapter 7

Flow Cell Application for Kinetic and Stoichiometric Studies

7.1 Introduction

Small organic molecules (SOM) such as formic acid, methanol and ethanol are known as attractive sources of energy because of their high energy density and convenience of use as liquids.[127,201–203] Therefore, understanding of SOM electrocatalytic oxidation is of fundamental importance to direct organic fuel cell (DOFC) development. The electrochemical oxidation of SOM on various metal catalysts has been broadly investigated with the cyclic voltammetry technique. Despite all the advantages of cyclic voltammetry, its data analysis is restricted by the time-dependent interplay between electrode kinetics and mass transport.[48] On the other hand, hydrodynamic techniques can provide the separation of kinetic and mass transport components of the overall current by providing control of mass transport through either electrode or solution motion.[55] In our previous studies, we have applied rotating disk voltammetry (RDV) for kinetic and stoichiometric studies of formic acid, methanol and ethanol oxidation.[165,204,205] Although RDV is a very straightforward and efficient technique, it is not ideal in many aspects. Moreover, new methodologies are required to assess the validity of RDV findings. Recently, flow cells have received more attention in the assessment of various catalyst performances towards SOM electrochemical oxidation. The flow cell has a similar design to the fuel cell and provides more relevant data for electrocatalytic studies. In this study, we have designed a two and a three-electrode flow-through cell to measure the flow rate dependence of the current and determine stoichiometry of ethanol oxidation on Pt/C. The flow-through cell with a simple design allowed collection of products and real time measurements of CO_2 while providing mass transport control through flow rate change.[92] More advantages

of flow cell applications are available in chapter 1, Section 1.4.

7.2 Experimental

Solutions were prepared by using anhydrous ethanol, (98%) formic acid, (99.8%) methanol, (98%) sulfuric acid from ACP Chemicals Inc., and deionized water. Commercial Pt black electrodes (proprietary) consisting of 4 $mg\ Pt\ cm^{-2}$ with a PTFE binder on wet-proofed carbon fiber paper (CFP) were used as electrode materials. Custom made electrodes were also prepared by dispersing desired amounts of either 70% Pt/C or 20% Pt/C catalyst ink on a circular piece of CFP (0.196 cm^2). More details related to materials and catalyst ink preparation can be found in chapter 2, Sections 2.2 and 2.2.2, respectively.

The organic fuel solution in sulfuric acid was supplied to either the two-electrode or the three-electrode flow-through cell with a syringe pump. Cyclic voltammetry (CV) and staircase voltammetry were carried out on the cells using an EG&G model 273A Potentiostat/Galvanostat for electrochemical study purposes. Flow cell resistance was determined prior to running each set of experiments by the EG&G Model 5210 Lock-in Amplifier and Power-Suite commercial software. Non-dispersive infrared (NDIR) and nuclear magnetic resonance (NMR) spectroscopy were applied for product analysis purposes. Flow cell schemes and applied materials are available in chapter 2, Section 2.3.

7.3 Results and Discussion

7.3.1 Three-Electrode Flow-Through Cell

7.3.1.1 Pt Electrochemistry

To assess the performance of the flow cell, first, CV experiments of Pt electrode were conducted in an electrolyte solution (i.e. 1 M H_2SO_4). An anode was prepared by deposition of 70% Pt/C ink on CFP (10 $mg\ cm^{-2}$). Resistance of the cell was measured prior to running the experiments (see appendix B). The electrolyte solution was passed through the cell at 0.20 $mL\ min^{-1}$ and CVs were recorded at a set of scan rates (Figure 7.1). Potentials (E) in voltammograms were corrected for cell resistance by subtracting resistance (R) times current at each potential (I) from that potential ($E-IR$). Underpotential adsorption and desorption of hydrogen, and oxide formation and reduction are evident in these CVs and there are linear relations between the scan rate and current in voltammograms.

7.3.1.2 Formic Acid Electrochemical Oxidation

Formic acid electrochemical oxidation was studied by cyclic voltammetry using the three-electrode flow-through cell. Figure 7.2 shows the cyclic voltammogram of a 0.1 M formic acid in 1 M sulfuric acid, which was supplied to the flow cell at 0.10 $mL\ min^{-1}$. Oxidation of the formic acid through a direct pathway began at 0.2 V. At higher potentials, the catalyst surface was covered with CO_{ads} and the direct pathway was surpassed by an indirect pathway. As the potential increased, the current increased due to oxidative removal of CO_{ads} and consequently the current

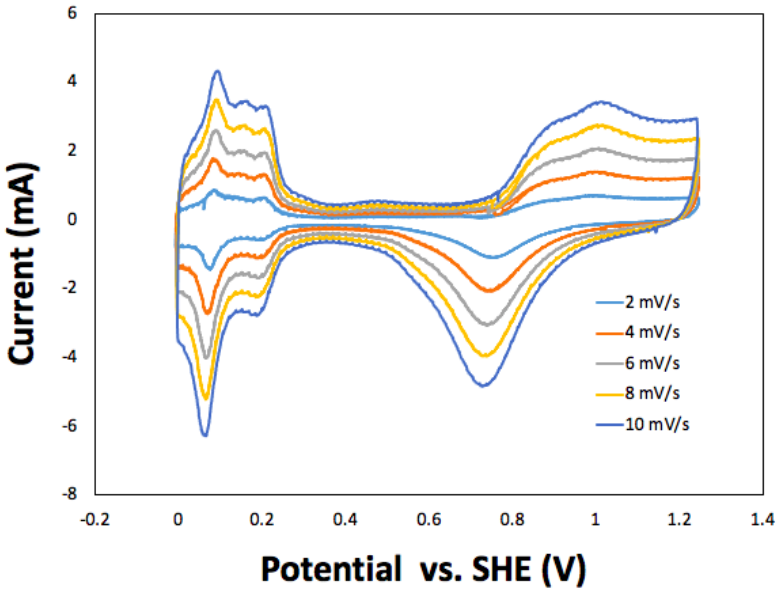

Figure 7.1: Cyclic voltammograms of a 70% Pt (10 $mg\ cm^{-2}$) electrode in 1 M H_2SO_4(aq) (10 $mV\ s^{-1}$), flow rate = 0.20 $mL\ min^{-1}$.

peaked at 0.73 V through direct pathway oxidation on bare Pt sites.[201] However, because of oxide coverage of Pt sites at this region, the mass transport plateau was not achieved. During the cathodic scan, the oxide layer was removed and formic acid oxidation proceeded mainly through the direct pathway, on the bare Pt sites and a broad peak of oxidation current was observed. CVs of formic acid solution at various flow rates were recorded to show flow rate dependency (Figure 7.3). As can be seen, the oxidation current increased with flow rate increase and the fluctuation in current can be attributed to CO_2 bubbles interferences.

7.3.1.3 Methanol Electrochemical Oxidation

Cyclic voltammetry studies of methanol oxidation were conducted by applying the three-electrode flow through cell. Cyclic voltammogram of a 0.1 M methanol solution

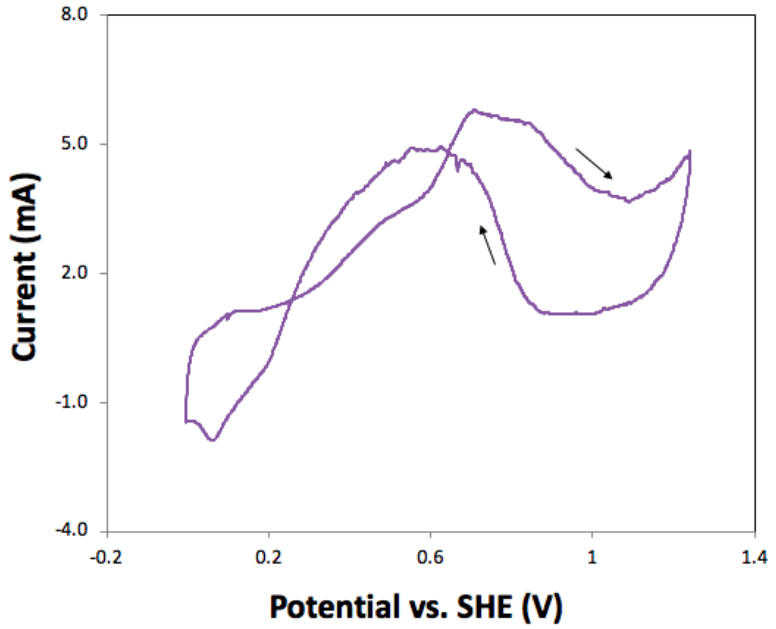

Figure 7.2: Cyclic voltammogram of 0.1 M formic acid in 1 M H_2SO_4(aq) at a 70% Pt (2 $mg\ cm^{-2}$) electrode (10 $mV\ s^{-1}$), flow rate = 0.10 $mL\ min^{-1}$.

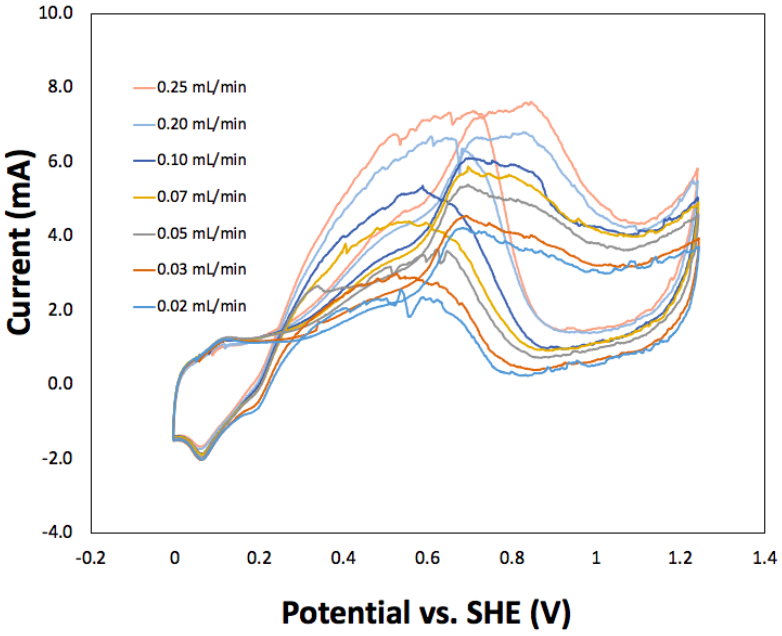

Figure 7.3: Cyclic voltammograms of 0.1 M formic acid in 1 M H_2SO_4(aq) at the 70% Pt (2 $mg\ cm^{-2}$) electrode (10 $mV s^{-1}$) and various flow rates.

passing through the flow cell with a 0.1 $mL\ min^{-1}$ flow rate is illustrated in Figure 7.4. The oxidation current commenced at 0.29 V. The current increased sharply and peaked at 0.83 V. Due to Pt oxide formation, a mass transport plateau was not achieved at this potential. In the reverse scan, as potential decreased and the oxide layer was removed, oxidation of Methanol on bare Pt sites started at 0.87 V and increased to a sharp peak at 0.74 V. Figure 7.5 shows CVs of methanol oxidation at various flow rates. The effect of flow rate on the oxidation current increase was evident in all of voltammograms.

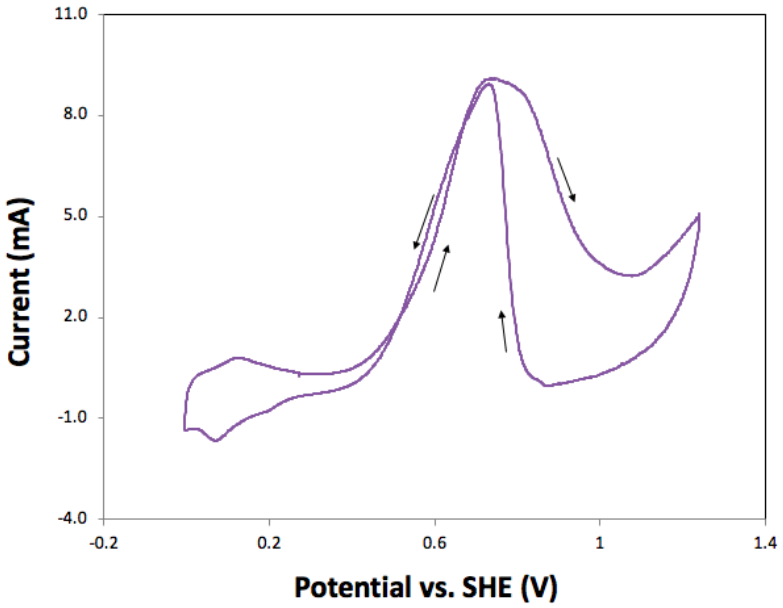

Figure 7.4: Cyclic voltammogram of 0.1 M methanol in 1 M H_2SO_4(aq) at a 70% Pt (2 $mg\ cm^{-2}$) electrode (10 $mV\ s^{-1}$), flow rate = 0.10 $mL\ min^{-1}$.

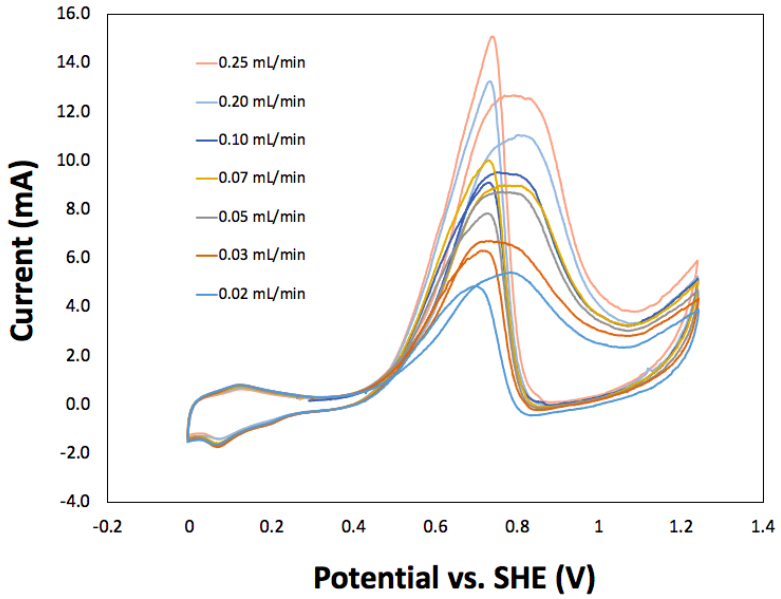

Figure 7.5: Cyclic voltammograms of 0.1 M methanol in 1 M H_2SO_4(aq) at the 70% Pt (2 $mg\ cm^{-2}$) electrode (10 $mV\ s^{-1}$) and various flow rates.

7.3.1.4 Ethanol Electrochemical Oxidation

The electrochemical oxidation of ethanol solution was studied applying cyclic voltammetry to the three-electrode flow-through cell. Figure 7.6 shows the CV of 0.1 M ethanol in 1 M H_2SO_4 at a 0.10 $mL\ min^{-1}$ flow rate. In the forward potential scan, ethanol oxidation commenced at 0.37 V and increased sharply. The current consequently peaked at 0.92 V. The oxide layer is formed on the surface of Pt, and the adsorption of ethanol molecules is suppressed and prevented from forming mass transport limited plateau. In the reverse potential scan, the adsorbed oxide layer on the surface of the electrode is stripped and the ethanol oxidation current is observed on the bare Pt sites. CVs of the 0.1 M ethanol solution at various flow rates are illustrated in Figure 7.7. The flow rate increase resulted in a current increase.

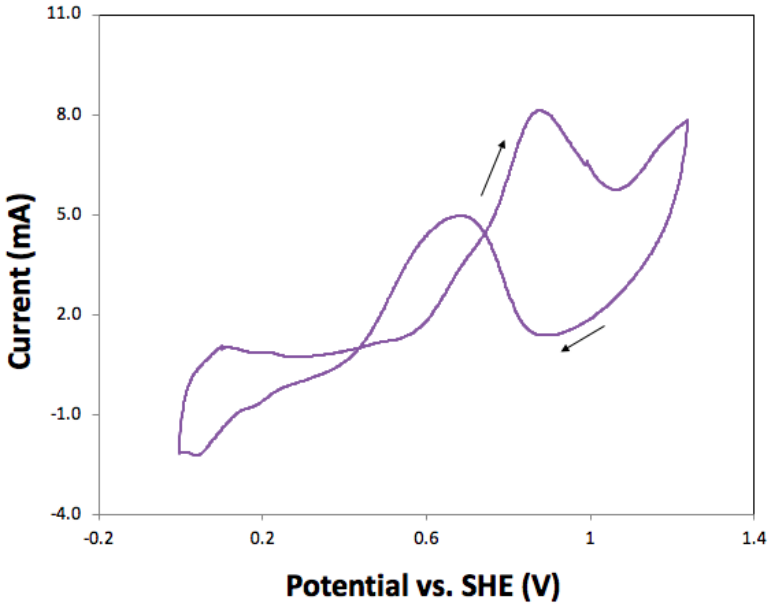

Figure 7.6: Cyclic voltammogram of 0.1 M ethanol in 1 M H_2SO_4(aq) at a 70% Pt (2 $mg\ cm^{-2}$) electrode (10 $mV\ s^{-1}$), flow rate = 0.10 $mL\ min^{-1}$.

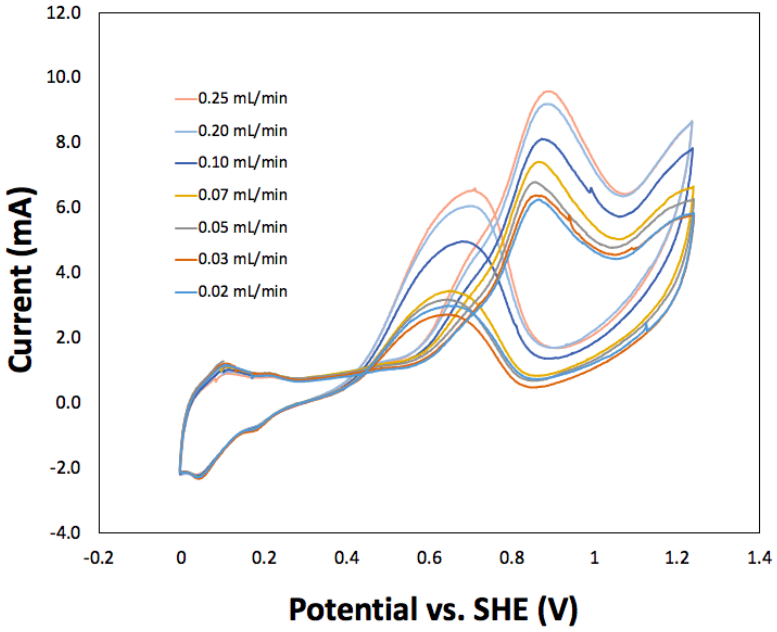

Figure 7.7: Cyclic voltammograms of 0.1 M ethanol in 1 M H_2SO_4(aq) at the 70% Pt (2 $mg\ cm^{-2}$) electrode (10 $mV\ s^{-1}$) and various flow rates.

7.3.1.5 Flow Rate Analysis

The flow rate dependence of the current for formic acid oxidation was examined at a 20% Pt/C electrode (4 $mg\ cm^{-2}$) in a mixed kinetic-mass transport region. In order to decrease background interference, a staircase voltammetry technique was applied to record formic acid oxidation polarization curves at different flow rates.[92] Potential was stepped in 25.0 mV intervals in the range of 0.0 to 0.9 V. Each step was applied for a duration of 10 s (appendix B, Figure B.2). In a step potential technique, after potential application both the faradaic and background currents start to decay while the decay rate for the electrode charging current is higher than the faradaic current.[55] Therefore, by sampling the current at the end of each potential step, one can correct for charging current to a reasonable extent.

Figure 7.8 shows background and resistance corrected of formic acid staircase voltammograms in a mixed kinetic-mass transport region (i.e. 0.425-0.9 V) at the Pt/C electrode and various flow rates. To correct for background interference, the voltammogram of the blank solution was subtracted from all voltammograms and for resistance correction see Section 7.3.1.1. The effect of the flow rate on current increase is evident in the voltammograms. The current peaked from 0.7 to 0.9 V for all the voltammograms. At this potential range, due to formation of an oxide layer on the Pt surface, the mass transport plateau cannot be observed and current was controlled by a mixture of kinetic and mass transport limitations. Therefore, a mathematical treatment is required for determination of kinetic parameters. In our previous study we applied a simplified version of a model reported by Alikire and Gracon[92,206] to study the oxidation of formic acid on Pd/C and Pt black catalyst

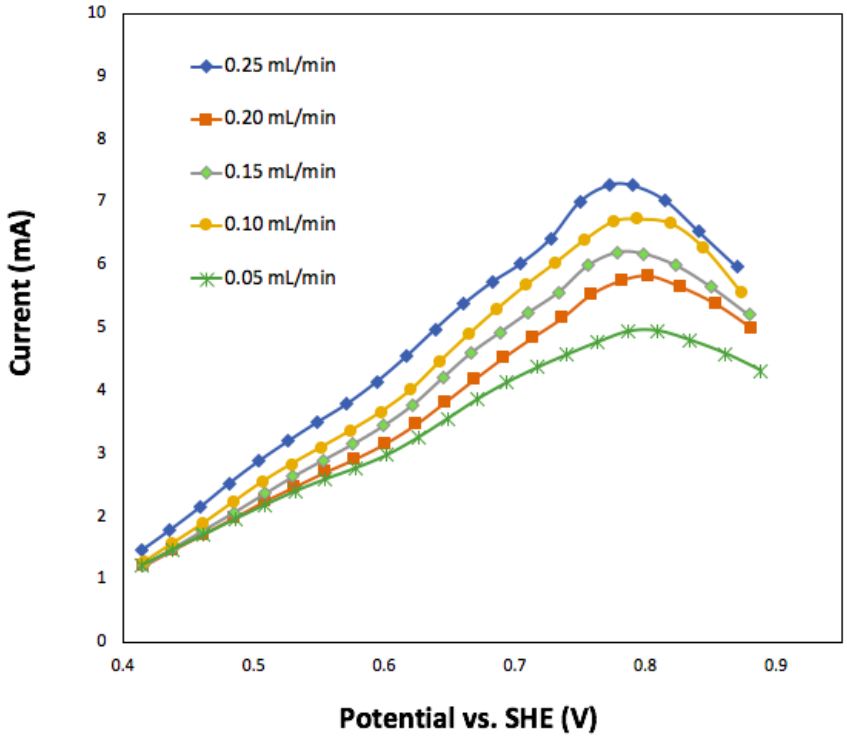

Figure 7.8: Background and resistance corrected staircase voltammograms (mixed kinetic-mass transport region, 0.425-0.9 V) of 0.1 M formic acid in 1 M H_2SO_4(aq) at a 20% Pt/C electrode and various flow rates.

electrodes in a two-electrode flow-through cell.[92] Solution in the flow-through cell passes through the catalyst layer and diffuses in the radial direction within the pores in the catalyst layer. In this model, it was presumed that a linear (steady-state) concentration gradient existed between the surface of the catalyst and the center of each pore (Figure 7.9).

The equations of this model were solved by a finite difference method[55,92] and used here for the flow rate analysis of data from the three-electrode flow-through cell. In the model, catalyst layer is divided to 100 discrete layers (Figure 7.10).[92] Eq. 7.1

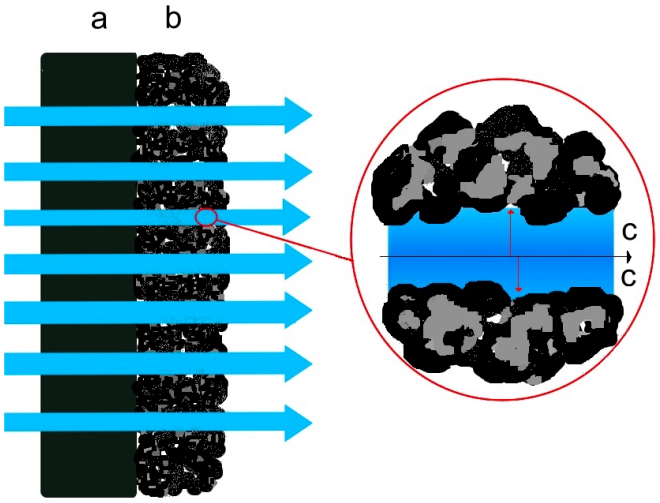

Figure 7.9: Schematic diagram of solution flow through the catalyst in the flow-through cell employed in this work. a is CFP, b is the catalyst layer, and c is the diffusion layer. The black arrow shows the flow direction and red arrows show the diffusion direction.

shows how to determine current at each layer (I_x). Overall current at each flow rate also can be determined by eq. 7.2. Where i_k, (i.e. $nfk(C_{x-1})$) is the kinetic controlled current and i_{lim}, (i.e. $n\lambda u^{\alpha}(C_{x-1})$) is the mass transport limited current in layer x, u is the flow rate in ($cm^3\ s^{-1}$), k is the rate constant in ($cm^3\ s^{-1}$), and α is the mass transport coefficient determined by flow geometry. This parameter was determined to be 0.37 for an electrode with the similar geometry to the Pt/C electrode.[92] When there is no concentration polarization, one can obtain the kinetic current using eq. 7.3.[92] Also, concentration at each segment can be obtained by eq. 7.4.

$$1/100I_x = 1/i_k + 1/i_{lim} = 1/nfk(C_{x-1}) + 1/n\lambda u^{\alpha}(C_{x-1}) \tag{7.1}$$

$$I = \Sigma_{x=1}^{x=100} I_x \tag{7.2}$$

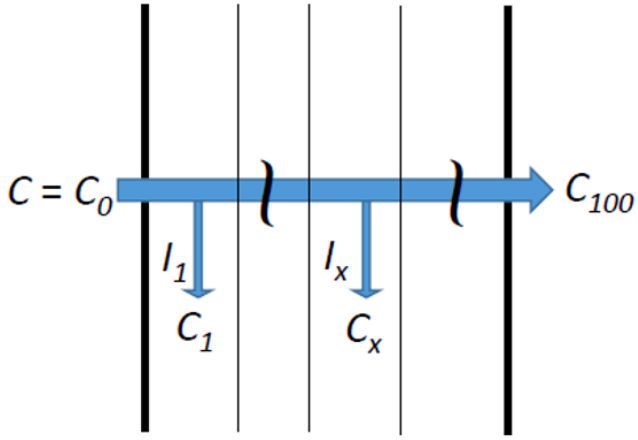

Figure 7.10: Schematic diagram of the finite difference method.[92]

$$i_k = nFkC \tag{7.3}$$

$$\Delta C_x = I_x/(nFu) \tag{7.4}$$

Voltammograms in Figure 7.8 were fitted in a simulation established on the basis of eqs. 7.1 and 7.4 (see appendix B, Section B.2.1). The best fits were obtained by variations of the rate constant (k) and mass transport parameter (λ) while α was assumed to be 0.37 (Figure 7.11).

Table 7.1 shows the kinetic and mass transport parameters obtained from the best fits of data in Figure 7.8 to eq. 7.1 in 25.0 mV intervals (Appendix B, Figures B.3-B.6). The fitting plots were obtained by setting λ at 187 $mA\ s^{\alpha}\ cm^{3(1-\alpha)}\ mol^{-1}$ for all potentials except for 0.700, 0.825, and 0.925 V for which optimization was required to obtain better fit. The steady value of λ emphasizes the fact that the mass transport current is independent of the potential. Figure 7.10 shows log (I) vs. potential plots (Tafel plots) obtained from the best fits. Log (i_k) and log ($I_{measured}$) converge at low potentials which means that effective separation of the kinetic and mass transport components of the current was obtained. At higher potentials (i.e. $> 0.500\ mV$), the

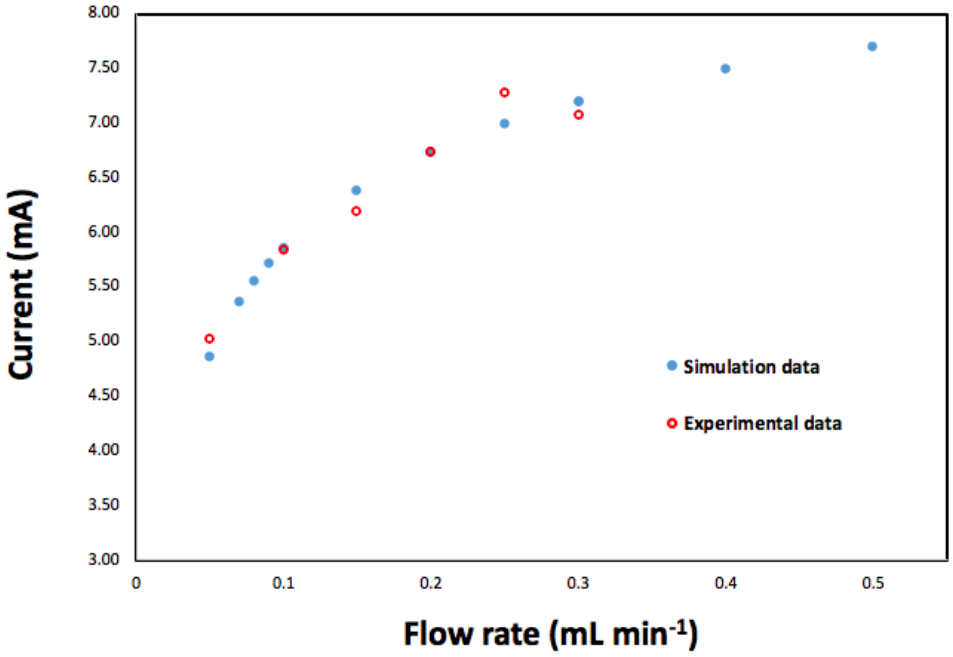

Figure 7.11: Current vs. flow rate for the oxidation of 0.1 M formic acid in 0.1 M H_2SO_4(aq) at the 20% Pt/C electrode and 0.850 V with the best fit theoretical curve from eq. 7.1, $\lambda = 187\ mA\ s^{\alpha}\ cm^{3(1-\alpha)}\ mol^{-1}$ and $\alpha = 0.37$.

i_k Tafel plot showed divergence from the $I_{measured}$ plot representing the involvement of mass transport limitation on overall current. The slope of the kinetic current Tafel plot decreased from 305 to 213 mV with potential increase which means a higher overpotential (92 mV more) was required to increase the kinetic current by tenfold. The Tafel slope for a Pt black catalyst was reported to be 392 mV at 0.4-0.7 V region (using the same model)[92] showing Pt black performed better towards formic acid oxidation at low potential.

The λ parameter is dependent on the diffusion coefficient of the organic fuel (D_o) as it is shown in eq. 7.5,[55] where A is the electrode area, C is the concentration of analyte, F is the Faraday constant, and B is a constant related to the cell geometry.

Table 7.1: Kinetic current (i_k), rate constant (k), and mass transport coefficient (λ) from 0.425 V to 0.925 V vs. SHE for voltammograms in Figure 7.8.

Potential (V)	i_k (mA)	k ($cm^3\ s^{-1}$)	λ ($mA\ s^{\alpha}\ cm^{3(1-\alpha)}\ mol^{-1}$)
0.425	1.37	7.10×10^{-5}	187
0.450	1.70	8.80×10^{-5}	187
0.475	2.05	1.06×10^{-4}	187
0.500	2.51	1.30×10^{-4}	187
0.525	2.87	1.49×10^{-4}	187
0.550	3.28	1.70×10^{-4}	187
0.575	3.65	1.89×10^{-4}	187
0.600	4.01	2.08×10^{-4}	187
0.625	4.44	2.30×10^{-4}	187
0.650	5.10	2.64×10^{-4}	187
0.675	5.87	3.04×10^{-4}	187
0.700	6.56	3.40×10^{-4}	169
0.725	7.47	3.87×10^{-4}	187
0.750	8.24	4.27×10^{-4}	187
0.775	8.92	4.47×10^{-4}	187
0.800	10.4	5.20×10^{-4}	187
0.825	10.92	5.58×10^{-4}	184
0.850	10.8	5.62×10^{-4}	187
0.875	10.5	6.12×10^{-4}	187
0.900	9.64	4.90×10^{-4}	187
0.925	8.19	4.24×10^{-4}	188

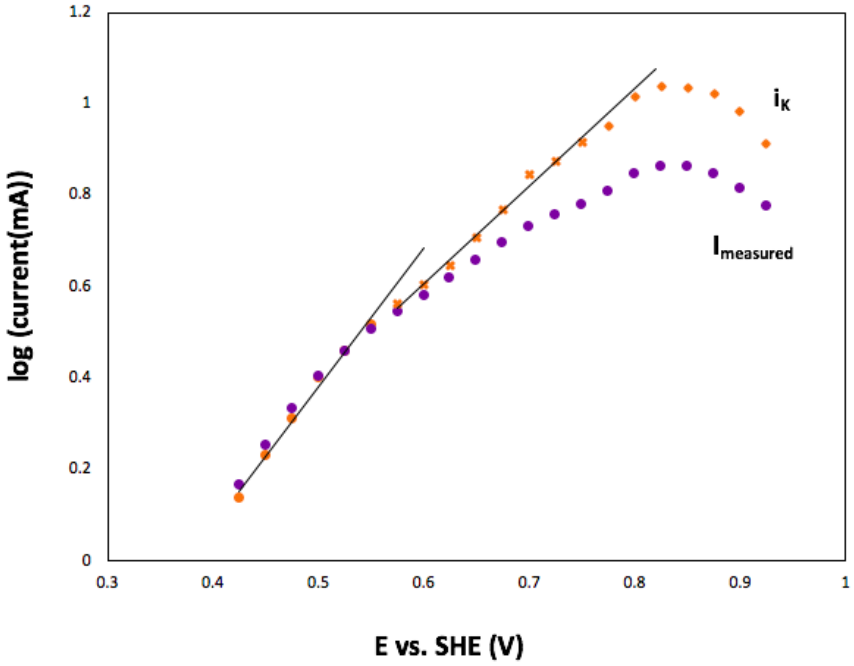

Figure 7.12: Tafel plots of i_k, and the measured current at 0.25 $mL\ min^{-1}$ flow rate for the oxidation of 0.1 M formic acid in 0.1 M H_2SO_4(aq) at the 20% Pt/C electrode.

Therefore, the λ parameter obtained for the formic acid oxidation can be applied to determine an average number of transferred electrons (n_{av}) for more complicated oxidation reactions such as methanol and ethanol oxidation after correction for difference in D value (eq. 7.6). Also, by applying the introduced flow-through cell, a facile and non-expensive assessment of various fuel cell electrodes can be conducted.

$$\lambda_o = FACD_o/B \tag{7.5}$$

$$\lambda_o = D_o \times \lambda_{formic\ acid}/(D_{formic\ acid}) \tag{7.6}$$

7.3.2 Two-Electrode Flow-Through Cell

7.3.2.1 Cell Resistance and Potential of the Cathode

The application of the two-electrode flow-through cell was based on the assumption that the counter electrode potential stays constant during experiments. This assumption has been examined by running electrochemical experiments in order to assess the counter electrode overpotential. A 0.1 M ethanol solution was supplied to the two-electrode flow-through cell and then the solution was kept stationary during all experiments. First, the potential was swept linearly from 0.0 V to 1 V and then back to -0.1 V to produce hydrogen in both electrodes. In the next step, the potential of the working electrode was scanned linearly between -0.02 V to 0.11 V vs. counter electrode at 1 $mV\ s^{-1}$ scan rate. The obtained CV (Figure 7.13) appeared in two overlapping straight lines passing close to zero. This voltammogram shows that the current changed linearly with potential, indicating that it was controlled by the cell resistance. The slope of the lines corresponded to 18 Ω, which was very close to the resistance measured by impedance spectroscopy (i.e. 17 Ω). All of these observations indicate that there is a negligible overpotential for oxidation and reduction of hydrogen and that the counter electrode acts like a dynamic hydrogen electrode (DHE).

7.3.2.2 Product Analysis of Ethanol Oxidation

The two-electrode cell was applied for product analysis purposes of ethanol oxidation in order to assess the n values obtained from the RDV experiments.

***CO_2* Measurements**. For CO_2 measurements, either a constant potential or

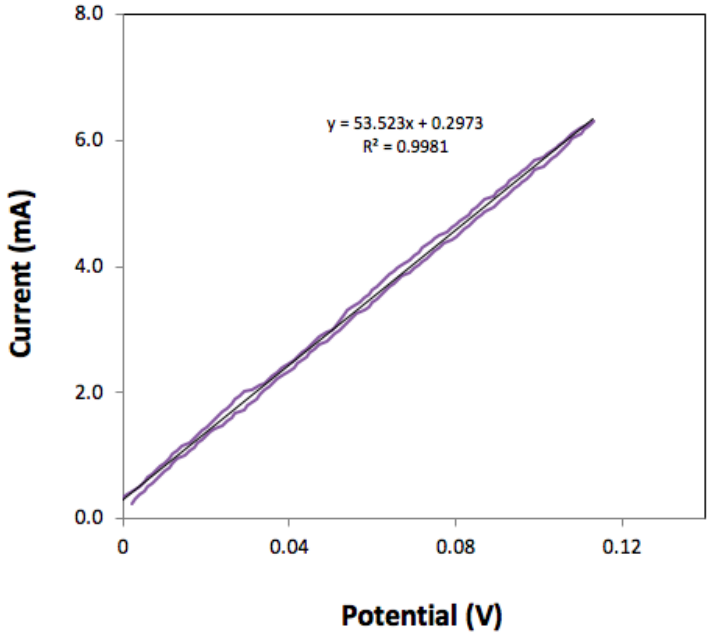

Figure 7.13: Cyclic voltammogram of a stationary 0.1 M ethanol in 0.1 M H_2SO_4(aq) in the two-electrode flow-through cell (1 $mV\ s^{-1}$) and at a 20% Pt/C electrode.

a constant current was applied to the two-electrode flow-through cell using a 20% Pt/C electrode as anode while analyte was supplied to the cell at a certain flow rate. At the same time, the exhausts of the cell were collected in a sealed vial with an inlet for N_2 gas flow into the solution to strip carbon dioxide gas and pass it through the NDIR detector. For faradaic yield measurement, the experimental rate of CO_2 formation was divided by the theoretical rate of CO_2 formation, which are given in equations 7.7 and 7.8, where V_m is the molar volume of any gas (ca. 24.2 $L\ mol^{-1}$), n is the number of electrons transferred to form one molecule of CO_2 (ca. 2 for formic acid oxidation), and $F = 96500\ A\ s\ mol^{-1}$ is the faraday constant. CO_2 (ppm) was obtained by the averaging detector readings over a period of at least 100 s after it became stabilized. I is the current applied to the solution. For the constant potential

experiments, I was obtained by integration of I vs. t plot.

$$\begin{aligned} &Experimental\ rate\ of\ CO_2\ formation \\ &= (CO_2\ (ppm) \times flow\ rate\ of\ N_2\ (L\ min^{-1}))/(60 \times 10^6 \times V_m) \end{aligned} \tag{7.7}$$

$$Theoretical\ rate\ of\ CO_2\ formation = I(A)/(nF) \tag{7.8}$$

To evaluate the cell performance, faradaic yield of CO_2 production for formic acid oxidation was evaluated by constant potential experiments. The experiments resulted in the 96 $\pm$ 1% faradaic yield indicating the appropriate performance of the flow-through cell for CO_2 collection. Figure 7.14 shows CO_2 readings for an example of a constant potential experiment. In this experiment, a potential of 0.11 V was applied to the flow cell for a duration of 2550 s, while 0.1 M formic acid in 1 M sulfuric acid was pumped through the cell at a 0.15 $mL\ min^{-1}$ flow rate. The current vs. time plot is also illustrated in Figure 7.15.

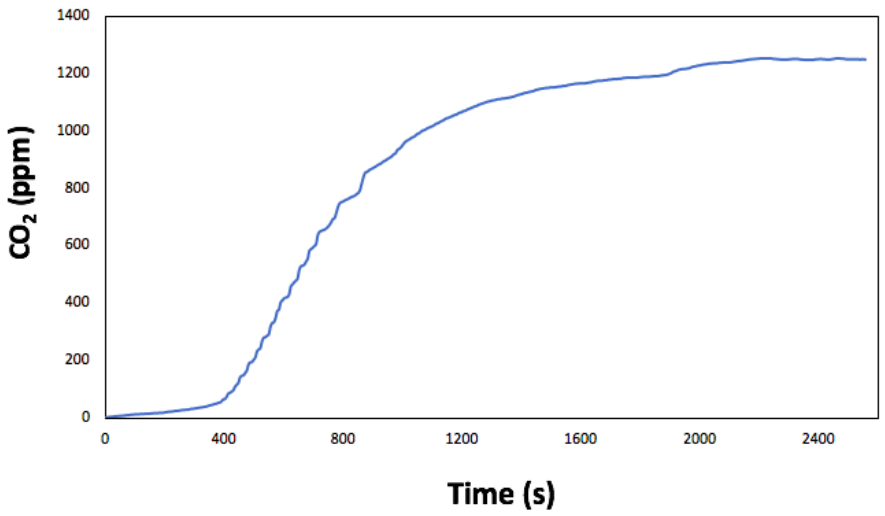

Figure 7.14: CO_2 readings for oxidation of 0.1 M formic acid in 1 M H_2SO_4(aq) at a 20% Pt/C electrode and 0.11 V (flow rate = 0.15 $mL\ min^{-1}$, temperature = 24 $^\circ C$).

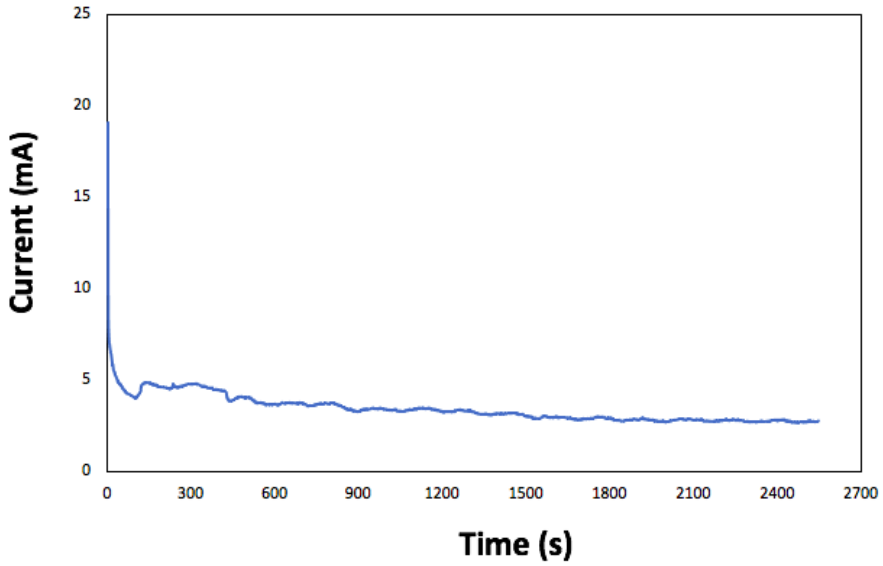

Figure 7.15: Current vs. time plot obtained for oxidation of 0.1 M formic acid in 1 M H_2SO_4(aq) at a 20% Pt/C electrode and 0.11 V (flow rate = 0.15 $mL\ min^{-1}$, temperature = 24 $°C$).

For ethanol solution oxidation, CO_2 measurements were conducted at three different temperatures (i.e. 24, 50 and 80 $°C$). Experimental concentrations of CO_2 in the nitrogen gas stream (ppm) were converted to concentrations in the electrolyte solution (mM) by using eq. 7.9, where u is the flow rate of the ethanol solution.

$$\begin{aligned} &Concentration\ of\ CO_2\ (mM) \\ &= (Experimental\ rate\ of\ CO_2\ formation) \times 60 \times 1000/u\ (L\ min^{-1}) \end{aligned} \tag{7.9}$$

The obtained CO_2 concentrations and CO_2 faradaic yields for the ethanol oxidation in constant current experiments are illustrated in Table 7.2 for all three temperatures. Figure 7.16 shows the potential vs. time plots related to the constant current experiments.

^{1}**H-NMR analysis**. For the analysis of products, intermediates, and non-reacted

Table 7.2: CO_2 concentrations and faradaic yields for oxidation of 0.1 M ethanol in 1 M H_2SO_4(aq) by applying constant current at 24, 50 and 80 $°C$.

Temperature ($°C$)	Current (mA)	CO_2 Concentration (mM)	Faradaic Yield (%)
24	2.5	0.26	5
50	5.2	1.3	12
80	11.1	5.8	24

fuel, a constant potential was applied (i.e., electrolysis cell) while the analyte solution was flowing through a 20% Pt/C anode catalyst in the flow cell. The cell exhausts were collected in a sealed trap cooled by a mixture of ice and dry ice for ^{1}H-NMR measurement purposes. The analyte concentrations including residual ethanol, acetic acid, and acetaldehyde is given by eq. 7.10.

$$Analyte\ concentration = (normalized\ area\ for\ analyte \times standard\ concentration)/(normalized\ area\ for\ standard) \tag{7.10}$$

At 24 $°C$, a constant potential of 0.35 V was applied to the cell while a 104 mM ethanol solution was supplied at a 0.05 $mL\ min^{-1}$ flow rate for a duration of 560 s (Figure 7.17), and the reacted solution was collected in a cooled trap for the measurement purposes. A ^{1}H-NMR spectrum of the cell exhaust is shown in Figure 7.18. The integration of the triplet at 1.10 ppm showed the non-reacted ethanol concentration (i.e. 92.8 mM). A singlet at 2.01 ppm was related to the acetic acid and its integration showed a concentration of 3.6 mM of this compound in the solution. Acetaldehyde's peak appeared as a doublet at 2.15 ppm. Another doublet peak also appeared at 1.24 ppm related to a dimer of acetaldehyde.[202] The

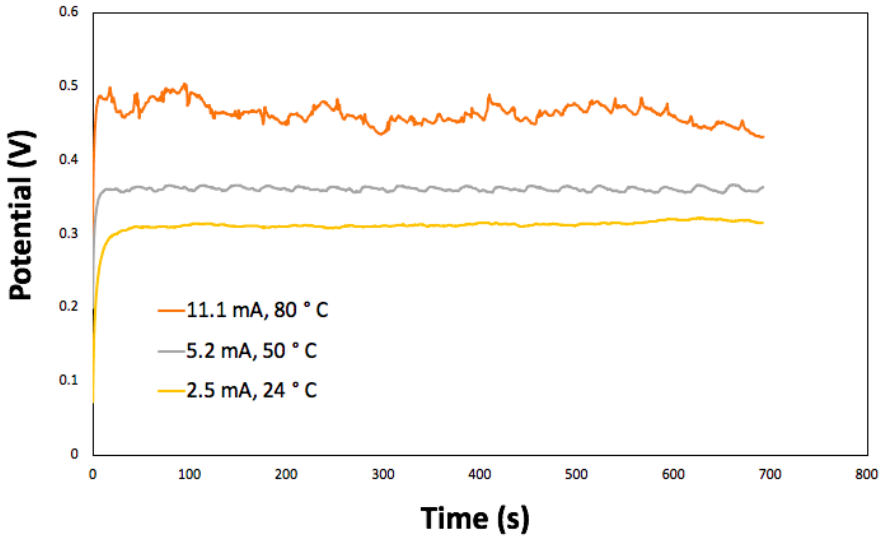

Figure 7.16: Potential vs. time plots obtained for oxidation of 0.1 M ethanol in 1 M H_2SO_4(aq) at a 20% Pt/C electrode, at 3 different constant currents and temperatures.

acetaldehyde concentration of 1.4 mM was obtained by summing up two related peaks integral.

By assumption of no ethanol loss and ethanol quantitative oxidation, a n_{av} value can be calculated using the concentration of ethanol before (C_{in}) and after (C_{out}) its reaction in equation 7.11.[127] u is the flow rate and I is the current obtained from integration of I vs. t plot.

$$n_{av} = I/uF(C_{in} - C_{out}) \tag{7.11}$$

A n_{av} of 2.7 was obtained for an average current of 2.5 mA passed at 24 $^{\circ}C$ for 560 s (Figure 7.14). A n_{av} of 2.7 for 0.01 M ethanol oxidation in H_2SO_4 on a Pt Vulcan reported by applying differential electrochemical mass spectrometry (DEMS) analysis at the room temperature.[38] In another DEMS study, product distribution of

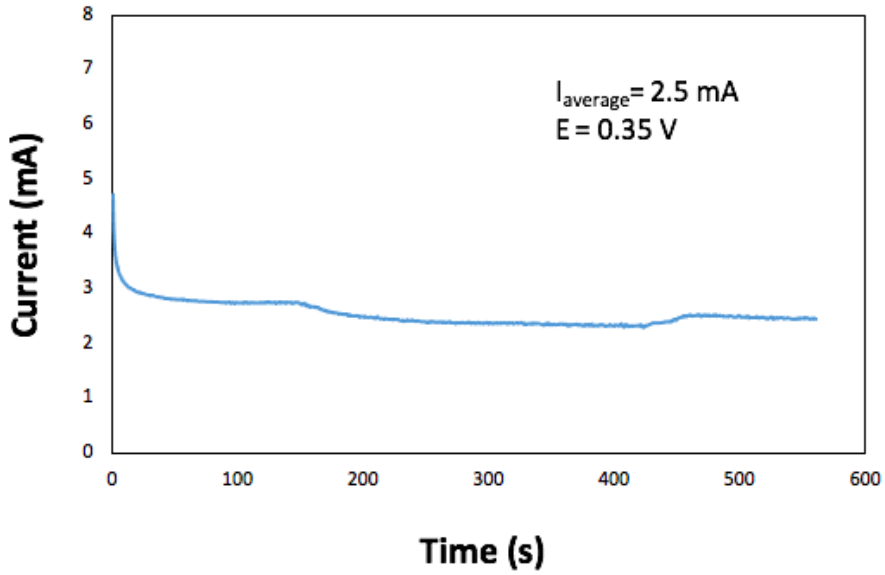

Figure 7.17: Current vs. time plot obtained for oxidation of 0.1 M ethanol in 0.1 M H_2SO_4(aq) at a 20% Pt/C electrode and 0.35 V (temperature = 24 $°C$).

ethanol oxidation at a Pt/C catalyst in H_2SO_4 gives a similar n value at the room temperature.[124]

The cell block was heated by placing two heating cartridge rods into the holes drilled in the cell block until its temperature reached 50 $°C$. A constant potential of 0.35 V was applied to the cell for a duration of 456 s while a 101 mM ethanol solution was supplied to the cell at 0.05 $mL\ min^{-1}$. A n_{av} of 3.1 was obtained at this temperature using eq 7.11. The current vs. time plot for this temperature is illustrated in Figure 7.19. A n_{av} value of 3.4 was reported for ethanol oxidation on the Pt black catalyst at the same temperature and flow rate.[119] The integration of peaks in the ^{1}H-NMR spectrum resulted in 79.9 mM of residual ethanol, 13.7 mM of acetic acid, and 2.9 mM of acetaldehyde.

The same constant potential experiment was conducted on the cell at 80 $°C$

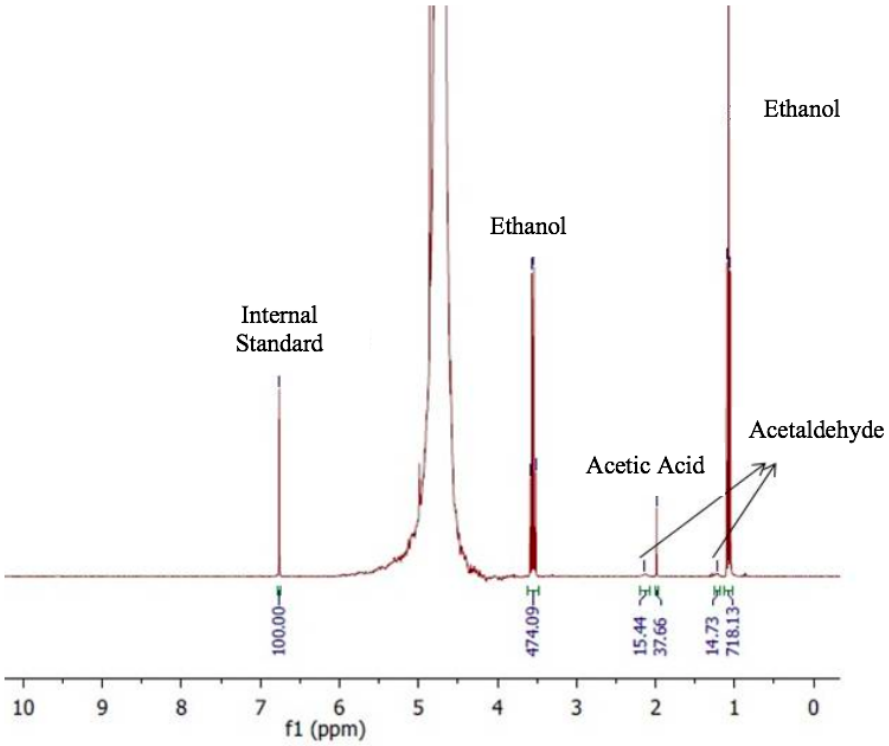

Figure 7.18: ^{1}H-NMR spectrum for the oxidation of 0.1 M ethanol in 0.1 M H_2SO_4 at a 20% Pt/C electrode after running constant potential experiment at 0.35 V for 560 s duration (temperature = 24 $^{\circ}C$).

with initial ethanol concentration of 108 mM for a duration of 470 s (Figure 7.20). Concentrations of 80.6 mM residual ethanol, 10.8 mM of acetic acid and 2.9 mM of acetaldehyde were obtained by the integration of ^{1}H-NMR spectrum peaks. A n_{av} of 5.0 was obtained using eq. 7.11. Similar n_{av} values (i.e. 5.2 and 5.3) were reported for oxidation of ethanol on a Pt black catalyst at 80 $^{\circ}C$ using a proton exchange membrane electrolysis cell.[59] Also, Sun et al. reported n value of 4.83 for ethanol oxidation in sulfuric acid solution on a carbon supported Pt catalyst at 80 $^{\circ}C$.[94]

Chemical yields of ethanol oxidation products were calculated using 7.12, where N_i

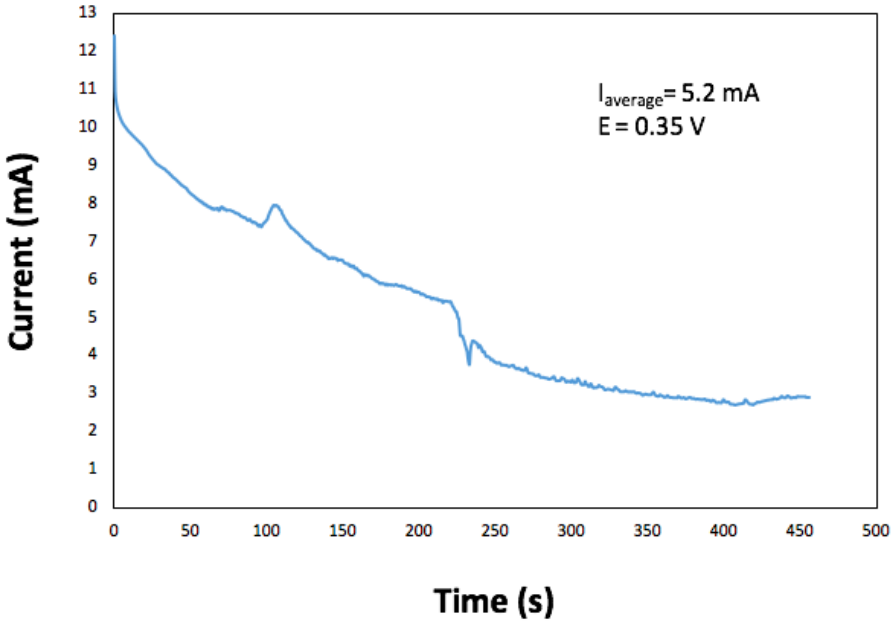

Figure 7.19: Current vs. time plot obtained for oxidation of 0.1 M ethanol in 0.1 M H_2SO_4(aq) at a 20% Pt/C electrode and 0.35 V (temperature = 50 $^{\circ}C$).

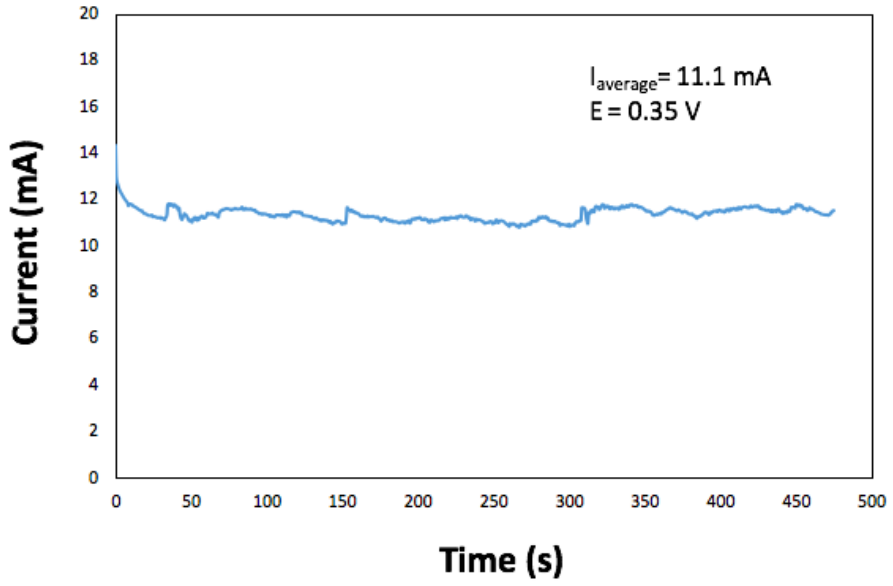

Figure 7.20: Current vs. time plot obtained for oxidation of 0.1 M ethanol in 0.1 M H_2SO_4(aq) at a 20% Pt/C electrode and 0.35 V (temperature = 80 $^{\circ}C$).

is the number of moles of ethanol required for production of i. Due to extremely high volatility of acetaldehyde, there were uncertainties in its concentration. Therefore, acetaldehyde concentration values were estimated using mass balance ($N_{acetaldehyde} = N_{consumed\ ethanol} - (N_{carbon\ dioxide} + N_{acetic\ acid})$).

$$Chemical\ yield\ of\ i = N_i/(N_{carbon\ dioxide} + N_{acetic\ acid} + N_{acetaldehyde}) \qquad (7.12)$$

Table 7.3: Chemical yields of ethanol oxidation products at various temperatures obtained by ^{1}H-NMR and NDIR.

Oxidation Product	24 $°C$	50 $°C$	80 $°C$
% CO_2	1.6	3.1	10.6
% Acetic acid	43.7	64.2	39.5
% Acetaldehyde (Mass Balance)	54.7	32.7	49.9
% Acetaldehyde (NMR)	17.5	13.5	10.5

Comparison of chemical yields of ethanol oxidation products obtained by eq. 7.12 showed that all three products (i.e. acetic acid, acetaldehyde, and CO_2) were produced at 24, 50 and 80 $°C$ to some extent (Table 7.2). By increasing the temperature from 24 to 50 $°C$ and then to 80 $°C$, the chemical yield of CO_2 increased. The chemical yield of acetic acid also increased by the elevation of temperature from 24 to 50 $°C$ but decreased at 80 $°C$. The chemical yield of acetaldehyde decreased by increasing the temperature from 24 to 50 $°C$, while it increased by increasing the temperature from 50 to 80 $°C$. Also, a comparison of n_{av} of this work with n values obtained by RDV[207] (chapter 6, table 6.2) showed similar n values were observed for 24 $°C$ on Pt/C catalyst. However, lower n values were indicated at 50 and 80 $°C$

for RDV experiments compared to flow cell product analysis. This indicates further investigations are required to validate n values at high temperatures.

7.4 Conclusions

The three-electrode flow-through cell with a simple construction facilitates electrochemical studies of organic fuel oxidation. Kinetic and mass transport parameters were obtained by a mathematical model in order to characterize a Pt/C electrode in relation to formic acid oxidation. The application of these parameters can be extended for stoichiometric studies of ethanol and methanol oxidation on a similar Pt/C electrode. The three-electrode flow-through cell emulates the hydrodynamics of an actual fuel cell; therefore, it can provide inexpensive and straightforward evaluation of various catalysts' activity prior to application in a fuel cell. A two-electrode flow-through cell was also applied for product analysis of ethanol oxidation at various temperatures. Results showed that products and unreacted ethanol can be collected and quantified by spectrometric techniques. However, further experiments as well as improvements of the cell in terms of acetaldehyde collection are required to obtain more reliable n_{av} values.

Chapter 8

Summary and Future Work

8.1 Summary

Two different hydrodynamic techniques were applied for kinetic and stoichiometric studies of formic acid, methanol and ethanol oxidation as organic fuels in order to enhance fuel cell technology. By the application of rotating disk voltammetry (RDV) and using thick catalyst layers, it was shown that rotation of the electrode resulted in an increase in the oxidation current of formic acid, methanol and ethanol. However, pure mass transport limited currents were not observed under any of the experiments in any conditions due to oxide layer formation on the catalyst surface at high potentials. The experimental current was separated into its mass transport and kinetic components using the Koutechy- Levich (K-L) equation. Kinetic currents at each potential were obtained from the intercepts of the K-L plots in order to evaluate various catalyst activities in relation to formic acid, methanol and ethanol oxidation. The average number of transferred electrons (n_{av}) for all three organic fuels was extracted from the slopes of the K-L plots. Steady-state experiments were conducted at a range of constant potentials and various rotation rates (i.e., 100, 400, 900, 1600 and 2500 rpm) on Pt/C and $PtRu$ black catalysts. Collected data was used for drawing K-L plots ($1/i$ vs. $\omega^{1/2}$). Linear and parallel K-L plots were obtained for methanol oxidation on a Pt/C and a $PtRu$ black catalyst and complete oxidation of methanol was achieved on the $PtRu$ black catalyst.

Formic acid oxidation on Pt/C also was studied by RDV and K-L plots were extracted from the steady-state experiments. By means of chronoamperometric studies on formic acid oxidation, it was shown that rate of electrode poisoning by CO adsorption depended on rotation rate and resulted in nonlinear K-L plots. In

these cases, i_k should be obtained at each individual rotation rate by using the mass transport limited current (Section 5.1, eq. 5.3). Linear and nonlinear K-L plots were obtained for ethanol oxidation on $PtRu$ black and Pt/C catalysts respectively. Also, investigation of the ethanol oxidation current dependence on Pt/C catalyst loading showed a linear increase behavior of the current with catalyst loading increase. The electrochemical oxidation of ethanol on Pt/C and $PtRu/C$ was investigated and compared at three different temperatures (ca. 24, 50, and 80 $^{\circ}C$). The K-L plots were extracted from steady-state experiments to determine i_k and n_{av}. Both linear and nonlinear K-L plots were observed for these experiments.

New methodologies were required in order to validate RDV K-L plots data. Therefore, we designed two-electrode and three-electrode flow-through cells as the second approach for electrochemical hydrodynamic studies. The resistance of the cell was probed and corrected for prior to each experiment. The oxidation current showed an increase with flow rate for all three organic fuels. The three-electrode flow-through cell was applied for the investigation of the flow rate dependence of the formic acid oxidation current. The mass transport and kinetic parameters of the Pt/C electrode were determined using mathematical treatments which can be further extended to methanol and ethanol to determine n_{av} values. A two-electrode flow through cell was applied in stoichiometric studies of formic acid as a model and then for ethanol oxidation at three different temperatures (ca. 24, 50, and 80 $^{\circ}C$). Real time measurements of CO_2 were conducted by an infrared nondispersive CO_2 detector (NDIR). Other products of ethanol oxidation, including acetic acid, acetaldehyde and residual ethanol were collected from the cell exhaust in a cooled trap and probed by NMR spectrometry. n_{av} values of ethanol oxidation on Pt/C

were determined at all three temperatures.

8.2 Future Work

There are some aspects of this project that can be further explored. The development of new mathematical model and/or the modification of the K-L equation model can be considered for validating obtained parameters and interpretations of experimental data that resulted in non-linear K-L plots. The three-electrode flow-through cell application can be extended to the investigation of more varieties of fuel cell catalysts and fuels at various temperatures. Mass transport and kinetic parameters can be obtained by mathematical treatments for ethanol and methanol oxidation on a variety of Pt-based catalysts at elevated temperatures using the flow-through cell.

Modification of flow cell to achieve more convenient and efficient product analysis can result in obtaining more accurate and reliable n_{av} values for SOM electrochemical oxidation. It would be more beneficial if studies get further extended at simulated actual conditions of DOFC operation such as potential and fuel flow rate. Also, some minor difficulties associated with experiments should be eliminated. One of the concerns during real time CO_2 measurements was prevention of solution penetration into the CO_2 detector. This problem should be eliminated by modification of the flow-through cell and/or the detector in the future. Acetaldehyde is an extremely volatile product of ethanol oxidation and so modification of the flow-through cell should be investigated in order to achieve an efficient real time measurement of it. One way can be using online differential electrochemical mass spectrometry (DEMS). Also, in situ infrared spectroscopy techniques can be considered as other ways of acetaldehyde

quantification as well as other soluble products and intermediates.

Complementary spectroscopic studies can be conducted on catalyst layer structure and porosity to probe their effect on the diffusion of organic fuels into the pores of the deposited catalyst layer. Transmission electron microscopy (TEM) and scanning electron microscopy (SEM) can be considered for these study purposes for instance. The deposition of thick catalyst on the carbon fiber paper in a way that prevented catalyst detachment at high flow rates was complex and time consuming. New approaches of catalyst ink dispersion on the carbon fiber paper (CFP) should be explored in order to prevent the resulting consequences. Modifications of electrode alignments in the cell or the overall configuration of the flow cell can be considered to facilitate removal of CO_2 gas bubbles which can become trapped inside of the cell and produce noise during current recording.

Bibliography

[1] Torrero, J.; Pérez-Alonso, F. J.; Peña, M. A.; Domínguez, C.; Al-Youbi, A. O.; Al-Thabaiti, S. A.; Basahel, S. N.; Alshehri, A. A.; Rojas, S. In situ infrared study of the electrooxidation of ethanol and acetaldehyde in acid electrolyte. *ChemElectroChem* **2016**, *3*, 1072–1083.

[2] Soloveichik, G. L. Liquid fuel cells. *Beilstein J. Nanotechnol.* **2014**, *5*, 1399–1418.

[3] Srinivasan, S. *Fuel cells: from fundamentals to applications*; Springer Science & Business media, 2006.

[4] Wang, Y.; Chen, K. S.; Mishler, J.; Cho, S. C.; Adroher, X. C. A review of polymer electrolyte membrane fuel cells: technology, applications, and needs on fundamental research. *Appl. Energy* **2011**, *88*, 981–1007.

[5] O'hayre, R.; Cha, S.; Colella, W.; Prinz, F. B. *Fuel cell fundamentals*; John Wiley & Sons, 2016.

[6] Puthiyapura, V. K.; Lin, W. F.; Russell, A. E.; Brett, D. J.; Hardacre, C. Effect of mass transport on the electrochemical oxidation of alcohols over

electrodeposited film and carbon-supported Pt electrodes. *Top Catal* **2018**, *61*, 240–253.

[7] Sharaf, O. Z.; Orhan, M. F. An overview of fuel cell technology: fundamentals and applications. *Renew. Sust. Energ. Rev.* **2014**, *32*, 810–853.

[8] Rosli, R.; Sulong, A. B.; Daud, W. R. W.; Zulkifley, M. A.; Husaini, T.; Rosli, M. I.; Majlan, E.; Haque, M. A review of high-temperature proton exchange membrane fuel cell (HT-PEMFC) system. *Int. J. Hydrog. Energy* **2017**, *42*, 9293–9314.

[9] Daud, W. R. W.; Rosli, R.; Majlan, E.; Hamid, S.; Mohamed, R.; Husaini, T. PEM fuel cell system control: a review. *J. Renew. Energy* **2017**, *113*, 620–638.

[10] Chandan, A.; Hattenberger, M.; El-Kharouf, A.; Du, S.; Dhir, A.; Self, V.; Pollet, B. G.; Ingram, A.; Bujalski, W. High temperature (HT) polymer electrolyte membrane fuel cells (PEMFC): A review. *J. Power Sources* **2013**, *231*, 264–278.

[11] Bi, W.; Gray, G. E.; Fuller, T. F. PEM fuel cell Pt/ C dissolution and deposition in nafion electrolyte. *Electrochem. Solid-State Lett.* **2007**, *10*, B101–B104.

[12] Tiwari, R.; Garcia, E. The state of understanding of ionic polymer metal composite architecture: a review. *Smart Mater Struct* **2011**, *20*, 083001.

[13] Paddison, S. The modeling of molecular structure and ion transport in sulfonic acid based ionomer membranes. *J. New Mater. Electrochem. Syst.* **2001**, *4*, 197–208.

[14] Kirubakaran, A.; Jain, S.; Nema, R. A review on fuel cell technologies and power electronic interface. *Renew. Sust. Energ. Rev.* **2009**, *13*, 2430–2440.

[15] Braunchweig, B.; Hibbitts, D.; Neurock, M.; Wieckowski, A. Electrocatalysis: a direct alcohol fuel cell and Surface Science perspective. *Catal. Today* **2013**, *202*, 197–209.

[16] Jeon, H.; Jeong, B.; Joo, J.; Lee, J. Electrocatalytic oxidation of formic acid: closing the gap between fundamental study and technical applications. *Electrocatalysis* **2015**, *6*, 20–32.

[17] Nacef, M.; Affoune, A. Comparison between direct small molecular weight alcohols fuel cells' and hydrogen fuel cell's parameters at low and high temperature. Thermodynamic study. *Int. J. Hydrog. Energy* **2011**, *36*, 4208–4219.

[18] Spiegel, C. *Designing and building fuel cells*; Citeseer, 2007; Vol. 87.

[19] Kamarudin, S. K.; Achmad, F.; Daud, W. R. W. Overview on the application of direct methanol fuel cell (DMFC) for portable electronic devices. *Int. J. Hydrog. Energy* **2009**, *34*, 6902–6916.

[20] Demirci, U. B. Direct liquid-feed fuel cells: thermodynamic and environmental concerns. *J. Power Sources* **2007**, *169*, 239–246.

[21] Lamy, C.; Lima, A.; LeRhun, V.; Delime, F.; Coutanceau, C.; Léger, J. M. Recent advances in the development of direct alcohol fuel cells (DAFC). *J. Power Sources* **2002**, *105*, 283–296.

[22] Carrette, L.; Friedrich, K.; Stimming, U. Fuel cells–fundamentals and applications. *Fuel cells* **2001**, *1*, 5–39.

[23] McNicol, B.; Rand, D.; Williams, K. Direct methanol–air fuel cells for road transportation. *J. Power Sources* **1999**, *83*, 15–31.

[24] Hassan, K.; Hathoot, A.; Maher, R.; Azzem, M. A. Electrocatalytic oxidation of ethanol at Pd, Pt, Pd/Pt and Pt/Pd nano particles supported on poly 1, 8-diaminonaphthalene film in alkaline medium. *RSC Adv.* **2018**, *8*, 15417–15426.

[25] Roth, C.; Papworth, A.; Hussain, I.; Nichols, R.; Schiffrin, D. A Pt/Ru nanoparticulate system to study the bifunctional mechanism of electrocatalysis. *J. Electroanal. Chem.* **2005**, *581*, 79–85.

[26] Breiter, M. Role of adsorbed species for the anodic methanol oxidation on platinum in acidic electrolytes. *Discuss. Faraday Soc.* **1968**, *45*, 79–86.

[27] Yang, M. L.; Zhu, Y. A.; Fan, C.; Sui, Z. J.; Chen, D.; Zhou, X. G. DFT study of propane dehydrogenation on Pt catalyst: effects of step sites. *Phys. Chem. Chem. Phys.* **2011**, *13*, 3257–3267.

[28] Kariya, N.; Fukuoka, A.; Utagawa, T.; Sakuramoto, M.; Goto, Y.; Ichikawa, M. Efficient hydrogen production using cyclohexane and decalin by pulse-spray mode reactor with Pt catalysts. *Appl Catal A Gen* **2003**, *247*, 247–259.

[29] Cohen, J. L.; Volpe, D. J.; Abruna, H. D. Electrochemical determination of activation energies for methanol oxidation on polycrystalline platinum in acidic and alkaline electrolytes. *Phys. Chem. Chem. Phys.* **2007**, *9*, 49–77.

[30] Wasmus, S.; Küver, A. Methanol oxidation and direct methanol fuel cells: a selective review. *J. Electroanal. Chem.* **1999**, *461*, 14–31.

[31] Jiang, J.; Kucernak, A. Solid polymer electrolyte membrane composite microelectrode investigations of fuel cell reactions. II: voltammetric study of methanol oxidation at the nanostructured platinum microelectrode, Nafion® membrane interface. *J. Electroanal. Chem.* **2005**, *576*, 223–236.

[32] Vielstich, W.; Lamm, A.; Gasteiger, H. A. *Handbook of fuel cells: fundamentals technology and applications*; Wiley New York, 2003; Vol. 2.

[33] Yu, X.; Pickup, P. G. Recent advances in direct formic acid fuel cells (DFAFC). *J. Power Sources* **2008**, *182*, 124–132.

[34] Briega-Martos, V.; Solla-Gullón, J.; Koper, M. T.; Herrero, E.; Feliu, J. M. Electrocatalytic enhancement of formic acid oxidation reaction by acetonitrile on well-defined platinum surfaces. *Electrochim. Acta* **2019**, *295*, 835–845.

[35] Conway, B.; Bai, L. Determination of adsorption of OPD H species in the cathodic hydrogen evolution reaction at Pt in relation to electrocatalysis. *J. Electroanal. Chem. Interf. Electrochem.* **1986**, *198*, 149–175.

[36] Friedl, J.; Stimming, U. Model catalyst studies on hydrogen and ethanol oxidation for fuel cells. *Electrochim. Acta* **2013**, *101*, 41–58.

[37] Vigier, F.; Coutanceau, C.; Hahn, F.; Belgsir, E.; Lamy, C. On the mechanism of ethanol electro-oxidation on Pt and PtSn catalysts: electrochemical and in situ IR reflectance spectroscopy studies. *J. Electroanal. Chem.* **2004**, *563*, 81–89.

[38] Wang, H.; Jusys, Z.; Behm, R. Ethanol and acetaldehyde adsorption on a carbon-supported Pt catalyst: a comparative DEMS study. *Fuel Cells* **2004**, *4*, 113–125.

[39] Kutz, R. B.; Braunschweig, B.; Mukherjee, P.; Behrens, R. L.; Dlott, D. D.; Wieckowski, A. Reaction pathways of ethanol electrooxidation on polycrystalline platinum catalysts in acidic electrolytes. *J. Catal.* **2011**, *278*, 181–188.

[40] Zhang, J. *PEM fuel cell electrocatalysts and catalyst layers: fundamentals and applications*; Springer Science & Business Media, 2008.

[41] Nørskov, J. K.; Rossmeisl, J.; Logadottir, A.; Lindqvist, L.; Kitchin, J. R.; Bligaard, T.; Jonsson, H. Origin of the overpotential for oxygen reduction at a fuel cell cathode. *J. Phys. Chem. B* **2004**, *108*, 17886–17892.

[42] Elnabawy, A. O.; Herron, J. A.; Scaranto, J.; Mavrikakis, M. Structure sensitivity of formic acid electrooxidation on transition metal surfaces: a first-principles study. *J. Electrochem. Soc.* **2018**, *165*, J3109–J3121.

[43] Al-Akraa, I. M.; Asal, Y. M.; Darwish, S. A. A simple and effective way to overcome carbon monoxide poisoning of platinum surfaces in direct formic acid fuel cells. *Int. J. Electrochem. Sci* **2019**, *14*, 8267–8275.

[44] Samjeské, G.; Miki, A.; Ye, S.; Osawa, M. Mechanistic study of electrocatalytic oxidation of formic acid at platinum in acidic solution by time-resolved surface-enhanced infrared absorption spectroscopy. *J. Phys. Chem. B* **2006**, *110*, 16559–16566.

[45] Grozovski, V.; Solla-Gullón, J.; Climent, V.; Herrero, E.; Feliu, J. M. Formic acid oxidation on shape-controlled Pt nanoparticles studied by pulsed voltammetry. *J. Phys. Chem. C* **2010**, *114*, 13802–13812.

[46] Joshi, V. S.; Poudyal, D. C.; Satpati, A. K.; Patil, K. R.; Haram, S. K. Methanol oxidation reaction on Pt based electrocatalysts modified ultramicroelectrode (UME): novel electrochemical method for monitoring rate of CO adsorption. *Electrochim. Acta* **2018**, *286*, 287–295.

[47] Prabhuram, J.; Manoharan, R. Investigation of methanol oxidation on unsupported platinum electrodes in strong alkali and strong acid. *J. Power Sources* **1998**, *74*, 54–61.

[48] Zhao, Y.; Li, X.; Schechter, J. M.; Yang, Y. Revisiting the oxidation peak in the cathodic scan of the cyclic voltammogram of alcohol oxidation on noble metal electrodes. *RSC Adv.* **2016**, *6*, 5384–5390.

[49] Kamarudin, M.; Kamarudin, S. K.; Masdar, M.; Daud, W. R. W. Direct ethanol fuel cells. *Int. J. Hydrog. Energy* **2013**, *38*, 9438–9453.

[50] Schmidt, V. M.; Ianniello, R.; Pastor, E.; González, S. Electrochemical reactivity of ethanol on porous Pt and PtRu: oxidation/reduction reactions in 1 M $HClO_4$. *J. Phys. Chem. B* **1996**, *100*, 17901–17908.

[51] Gootzen, J.; Visscher, W.; Van Veen, J. Characterization of ethanol and 1, 2-ethanediol adsorbates on platinized platinum with fourier transform infrared spectroscopy and differential electrochemical mass spectrometry. *Langmuir* **1996**, *12*, 5076–5082.

[52] Wang, Q.; Sun, G.; Jiang, L.; Xin, Q.; Sun, S.; Jiang, Y.; Chen, S.; Jusys, Z.; Behm, R. Adsorption and oxidation of ethanol on colloid-based Pt/C, PtRu/C and Pt_3Sn/C catalysts: In situ FTIR spectroscopy and on-line DEMS studies. *Phys. Chem. Chem. Phys.* **2007**, *9*, 2686–2696.

[53] Shao, M.; Adzic, R. Electrooxidation of ethanol on a Pt electrode in acid solutions: in situ ATR-SEIRAS study. *Electrochim. Acta* **2005**, *50*, 2415–2422.

[54] Flórez-Montaño, J.; García, G.; Guillén-Villafuerte, O.; Rodríguez, J. L.; Planes, G. A.; Pastor, E. Mechanism of ethanol electrooxidation on mesoporous Pt electrode in acidic medium studied by a novel electrochemical mass spectrometry set-up. *Electrochim. Acta* **2016**, *209*, 121–131.

[55] Bard, A. J.; Faulkner, L. R., et al. *Fundamentals and applications*; 2nd ed., Wiley New York, 2001.

[56] Guy, O. J.; Walker, K. A. D. *Silicon Carbide Biotechnology*; Elsevier, 2016; pp 85–141.

[57] Liu, L.; Corma, A. Metal catalysts for heterogeneous catalysis: from single atoms to nanoclusters and nanoparticles. *Chem. Rev.* **2018**, *118*, 4981–5079.

[58] Nakagawa, N.; Kaneda, Y. Product distribution and the reaction kinetics at the anode of direct ethanol fuel cell with Pt/C, PtRu/C and PtRuRh/C. *J. Power Sources* **2012**, *199*, 103–109.

[59] Altarawneh, R. M.; Majidi, P.; Pickup, P. G. Determination of the efficiency

of ethanol oxidation in a proton exchange membrane electrolysis cell. *J. Power Sources* **2017**, *351*, 106–114.

[60] Altarawneh, R. M.; Pickup, P. G. Product distributions and efficiencies for ethanol oxidation in a proton exchange membrane electrolysis cell. *J. Electrochem. Soc.* **2017**, *164*, F861–F865.

[61] Antolini, E. Catalysts for direct ethanol fuel cells. *J. Power Sources* **2007**, *170*, 1–12.

[62] Jerkiewicz, G. Electrochemical hydrogen adsorption and absorption. Part 1: under-potential deposition of hydrogen. *Electrocatalysis* **2010**, *1*, 179–199.

[63] Łosiewicz, B.; Jurczakowski, R.; Lasia, A. Kinetics of hydrogen underpotential deposition at polycrystalline rhodium in acidic solutions. *Electrochim. Acta* **2011**, *56*, 5746–5753.

[64] Siwek, H.; Łukaszewski, M.; Czerwiński, A. Electrochemical study on the adsorption of carbon oxides and oxidation of their adsorption products on platinum group metals and alloys. *Phys. Chem. Chem. Phys.* **2008**, *10*, 3752–3765.

[65] Stacy, J.; Regmi, Y. N.; Leonard, B.; Fan, M. The recent progress and future of oxygen reduction reaction catalysis: a review. *Renew. Sust. Energ. Rev.* **2017**, *69*, 401–414.

[66] Lankiang, S.; Chiwata, M.; Baranton, S.; Uchida, H.; Coutanceau, C. Oxygen

reduction reaction at binary and ternary nanocatalysts based on Pt, Pd and Au. *Electrochim. Acta* **2015**, *182*, 131–142.

[67] Lankiang, S. D.; Baranton, S.; Coutanceau, C. Electrocatalytic behaviour towards oxygen reduction reaction of carbon-supported $Pt_xM_yAu_z$ (M = Ni, Cu, Co) binary and ternary catalysts. *Electrochim. Acta* **2017**, *242*, 287–299.

[68] Wang, J. *Analytical electrochemistry*; 3rd ed., John Wiley & Sons, 2006.

[69] Zhao, M.; Rice, C.; Masel, R. I.; Waszczuk, P.; Wieckowski, A. Kinetic study of electro-oxidation of formic acid on spontaneously-deposited Pt/Pd nanoparticles: CO tolerant fuel cell chemistry. *J. Electrochem. Soc.* **2003**, *151*, A131–A136.

[70] Liu, Z.; Hong, L.; Tham, M. P.; Lim, T. H.; Jiang, H. Nanostructured Pt/C and Pd/C catalysts for direct formic acid fuel cells. *J. Power Sources* **2006**, *161*, 831–835.

[71] Grozovski, V.; Climent, V.; Herrero, E.; Feliu, J. M. Intrinsic activity and poisoning rate for HCOOH oxidation on platinum stepped surfaces. *Phys. Chem. Chem. Phys.* **2010**, *12*, 8822–8831.

[72] Arico, A.; Cretı, P.; Antonucci, P.; Antonucci, V. Comparison of ethanol and methanol oxidation in a liquid-feed solid polymer electrolyte fuel cell at high temperature. *Electrochem. Solid-State Lett.* **1998**, *1*, 66–68.

[73] Garsany, Y.; Baturina, O. A.; Swider-Lyons, K. E.; Kocha, S. S. Experimental

methods for quantifying the activity of platinum electrocatalysts for the oxygen reduction reaction. *Anal. Chem.* **2010**, *82*, 6321–6328.

[74] Ruvinskiy, P. S.; Bonnefont, A.; Pham-Huu, C.; Savinova, E. R. Using ordered carbon nanomaterials for shedding light on the mechanism of the cathodic oxygen reduction reaction. *Langmuir* **2011**, *27*, 9018–9027.

[75] Zhou, R.; Zheng, Y.; Jaroniec, M.; Qiao, S. Z. Determination of the electron transfer number for the oxygen reduction reaction: from theory to experiment. *ACS Catalysis* **2016**, *6*, 4720–4728.

[76] Mohan, N.; Cindrella, L. Template-free synthesis of Pt-MOx (M = Ni, Co & Ce) supported on cubic zeolite-A and their catalytic role in methanol oxidation and oxygen reduction reactions characterized by the hydrodynamic study. *Int. J. Hydrog. Energy* **2017**, *42*, 21719–21731.

[77] Pavese, A.; Solis, V. Comparative investigation of formic acid and formaldehyde oxidation on palladium by a rotating ring-disc electrode and on-line mass spectroscopy in acidic solutions. *J. Electroanal. Chem. Interf. Electrochem.* **1991**, *301*, 117–127.

[78] Seland, F.; Tunold, R.; Harrington, D. A. Activating and deactivating mass transport effects in methanol and formic acid oxidation on platinum electrodes. *Electrochim. Acta* **2010**, *55*, 3384–3391.

[79] Matsumoto, F.; Roychowdhury, C.; DiSalvo, F. J.; Abruña, H. D. Electrocatalytic activity of ordered intermetallic PtPb nanoparticles prepared

by borohydride reduction toward formic acid oxidation. *J. Electrochem. Soc.* **2008**, *155*, B148–B154.

[80] Casado-Rivera, E.; Gal, Z.; Angelo, A.; Lind, C.; DiSalvo, F. J.; Abruna, H. D. Electrocatalytic oxidation of formic acid at an ordered intermetallic PtBi surface. *ChemPhysChem* **2003**, *4*, 193–199.

[81] Tian, Q.; Zhu, Z.; Fu, B.; Li, Y. Kinetic study of formic acid electrochemical oxidation on supported Pd based electrocatalysts. *J. Electrochem. Soc.* **2018**, *165*, F1075–F1083.

[82] Gojković, S. L. Mass transfer effect in electrochemical oxidation of methanol at platinum electrocatalysts. *J. Electroanal. Chem.* **2004**, *573*, 271–276.

[83] Gojković, S. L. Electrochemical oxidation of methanol on Pt_3Co bulk alloy. *J. Serb. Chem. Soc.* **2003**, *68*, 859–870.

[84] Velázquez-Palenzuela, A.; Centellas, F.; Garrido, J. A.; Arias, C.; Rodríguez, R. M.; Brillas, E.; Cabot, P. L. Kinetic analysis of carbon monoxide and methanol oxidation on high performance carbon-supported Pt-Ru electrocatalyst for direct methanol fuel cells. *J. Power Sources* **2011**, *196*, 3503–3512.

[85] Zheng, L.; Xiong, L.; Liu, Q.; Han, K.; Liu, W.; Li, Y.; Tao, K.; Niu, L.; Yang, S.; Xia, J. Enhanced electrocatalytic activity for the oxidation of liquid fuels on PtSn nanoparticles. *Electrochim. Acta* **2011**, *56*, 9860–9867.

[86] Hou, G.; Parrondo, J.; Ramani, V.; Prakash, J. Kinetic and mechanistic

investigation of methanol oxidation on a smooth polycrystalline Pt surface. *J. Electrochem. Soc.* **2014**, *161*, F252–F258.

[87] Xu, J.; Wang, P.; Yu, R.; Zheng, Z.; Shah, S. S. A.; Chen, C. A new insight into the effect of scan rate and mass transport from Pt rotating disk electrode on the electrochemical oxidation process of methanol. *Mater. Lett.* **2020**, *260*, 126950.

[88] Shieh, D. T.; Hwang, B. J. Kinetics for electro-oxidation of ethanol on thermally prepared ruthenium oxide in alkaline solution. *J. Electrochem. Soc.* **1995**, *142*, 816–823.

[89] Seland, F.; Foss, C. E. L.; Tunold, R.; Harrington, D. Increasing and decreasing mass transport effects in the oxidation of small organic molecules. *ECS Trans* **2010**, *28*, 203–210.

[90] McClure, J. P.; Boltersdorf, J.; Baker, D. R.; Farinha, T. G.; Dzuricky, N.; Villegas, C. E.; Rocha, A. R.; Leite, M. S. Structure-property-performance relationship of ultrathin Pd–Au alloy catalyst layers for low-temperature ethanol oxidation in alkaline media. *ACS Appl. Mater. Interfaces* **2019**, *11*, 24919–24932.

[91] Pushkarev, A. S.; Pushkareva, I. V.; Ivanova, N. A.; du Preez, S. P.; Bessarabov, D.; Chumakov, R. G.; Stankevich, V. G.; Fateev, V. N.; Evdokimov, A. A.; Grigoriev, S. A. Pt/C and Pt/SnO_x/C catalysts for ethanol electrooxidation: rotating disk electrode study. *Catalysts* **2019**, *9*, 271–286.

[92] Zhang, Q.; Sayadi, A.; Pickup, P. G. Separation of kinetic and mass transport effects in the electrolysis of formic acid in a flow-through cell. *Electrochim. Acta* **2019**, *294*, 110–116.

[93] Martins, C. A.; Ibrahim, O. A.; Pei, P.; Kjeang, E. In situ decoration of metallic catalysts in flow-through electrodes: application of Fe/Pt/C for glycerol oxidation in a microfluidic fuel cell. *Electrochim. Acta* **2019**, *305*, 47–55.

[94] Sun, S.; Halseid, M. C.; Heinen, M.; Jusys, Z.; Behm, R. Ethanol electrooxidation on a carbon-supported Pt catalyst at elevated temperature and pressure: A high-temperature/high-pressure DEMS study. *J. Power Sources* **2009**, *190*, 2–13.

[95] Temmel, S.; Tschupp, S.; Schmidt, T. J. A highly flexible electrochemical flow cell designed for the use of model electrode materials on non-conventional substrates. *Rev. Sci. Instrum.* **2016**, *87*, 045115.

[96] Bondue, C. J.; Königshoven, P.; Baltruschat, H. A new 2-compartment flow through cell for the simultaneous detection of electrochemical reaction products by a detection electrode and mass spectroscopy. *Electrochim. Acta* **2016**, *214*, 241–252.

[97] Luque, G. C.; de Chialvo, M. R. G.; Chialvo, A. C. Kinetic study of the formic acid oxidation on steady state using a flow cell. *J. Electrochem. Soc.* **2017**, *164*, H748–H754.

[98] Cychy, S.; Hiltrop, D.; Andronescu, C.; Muhler, M.; Schuhmann, W. Operando thin-layer ATR-FTIR spectroelectrochemical radial flow cell with tilt correction and borehole electrode. *Anal. Chem.* **2019**, *91*, 14323–14331.

[99] Gibson, D.; MacGregor, C. A novel solid state non-dispersive infrared CO_2 gas sensor compatible with wireless and portable deployment. *Sensors* **2013**, *13*, 7079–7103.

[100] Iwasita, T. Electrocatalysis of methanol oxidation. *Electrochim. Acta* **2002**, *47*, 3663–3674.

[101] Spendelow, J. S.; Wieckowski, A. Electrocatalysis of oxygen reduction and small alcohol oxidation in alkaline media. *Phys. Chem. Chem. Phys.* **2007**, *9*, 2654–2675.

[102] Koper, M. T.; Lai, S. C.; Herrero, E. *Mechanisms of the oxidation of carbon monoxide and small organic molecules at metal electrodes*; John Wiley & Sons Inc, 2009; pp 159–207.

[103] Dillon, R.; Srinivasan, S.; Arico, A.; Antonucci, V. International activities in DMFC R&D: status of technologies and potential applications. *J. Power Sources* **2004**, *127*, 112–126.

[104] Song, S.; Maragou, V.; Tsiakaras, P. How far are direct alcohol fuel cells from our energy future? *J. Fuel Cell Sci. Technol.* **2007**, *4*, 203–209.

[105] Kumar, P.; Dutta, K.; Das, S.; Kundu, P. P. An overview of unsolved deficiencies

of direct methanol fuel cell technology: factors and parameters affecting its widespread use. *Int. J. Energy Res.* **2014**, *38*, 1367–1390.

[106] Li, X.; Faghri, A. Review and advances of direct methanol fuel cells (DMFCs) part I: design, fabrication, and testing with high concentration methanol solutions. *J. Power Sources* **2013**, *226*, 223–240.

[107] Kakati, N.; Maiti, J.; Lee, S. H.; Jee, S. H.; Viswanathan, B.; Yoon, Y. S. Anode catalysts for direct methanol fuel cells in acidic media: do we have any alternative for Pt or Pt–Ru? *Chem. Rev.* **2014**, *114*, 12397–12429.

[108] Hernandez-Fernandez, P.; Lund, P. B.; Kallesøe, C.; Clausen, H. F.; Christensen, L. H. Supported Pt-based nanoparticulate catalysts for the electro-oxidation of methanol: an experimental protocol for quantifying its activity. *Int. J. Hydrog. Energy* **2015**, *40*, 284–291.

[109] Schmidt, T.; Gasteiger, H.; Stäb, G.; Urban, P.; Kolb, D.; Behm, R. Characterization of high-surface-area electrocatalysts using a rotating disk electrode configuration. *J. Electrochem. Soc.* **1998**, *145*, 2354–2358.

[110] Mayrhofer, K.; Strmcnik, D.; Blizanac, B.; Stamenkovic, V.; Arenz, M.; Markovic, N. Measurement of oxygen reduction activities via the rotating disc electrode method: from Pt model surfaces to carbon-supported high surface area catalysts. *Electrochim. Acta* **2008**, *53*, 3181–3188.

[111] Childers, C. L.; Huang, H.; Korzeniewski, C. Formaldehyde yields from methanol electrochemical oxidation on carbon-supported platinum catalysts. *Langmuir* **1999**, *15*, 786–789.

[112] Wang, H.; Wingender, C.; Baltruschat, H.; Lopez, M.; Reetz, M. Methanol oxidation on Pt, PtRu, and colloidal Pt electrocatalysts: a DEMS study of product formation. *J. Electroanal. Chem.* **2001**, *509*, 163–169.

[113] Jusys, Z.; Kaiser, J.; Behm, R. Methanol electrooxidation over Pt/C fuel cell catalysts: dependence of product yields on catalyst loading. *Langmuir* **2003**, *19*, 6759–6769.

[114] Van Loon, L. L.; Allen, H. C.; Wyslouzil, B. E. Effective diffusion coefficients for methanol in sulfuric acid solutions measured by Raman spectroscopy. *J. Phys. Chem. A* **2008**, *112*, 10758–10763.

[115] Seidel, Y.; Schneider, A.; Jusys, Z.; Wickman, B.; Kasemo, B.; Behm, R. Transport effects in the electrooxidation of methanol studied on nanostructured Pt/glassy carbon electrodes. *Langmuir* **2010**, *26*, 3569–3578.

[116] Vigier, F.; Rousseau, S.; Coutanceau, C.; Leger, J. M.; Lamy, C. Electrocatalysis for the direct alcohol fuel cell. *Top Catal* **2006**, *40*, 111–121.

[117] Reichert, R.; Schnaidt, J.; Jusys, Z.; Behm, R. J. The influence of reactive side products on the electrooxidation of methanol, a combined in situ infrared spectroscopy and online mass spectrometry study. *Phys. Chem. Chem. Phys.* **2014**, *16*, 13780–13799.

[118] Abdelkareem, M. A.; Masdar, M. S.; Tsujiguchi, T.; Nakagawa, N.; Sayed, E. T.; Barakat, N. A. Elimination of toxic products formation in vapor-feed passive DMFC operated by absolute methanol using air cathode filter. *Chem. Eng. J.* **2014**, *240*, 38–44.

[119] Majidi, P.; Pickup, P. G. Determination of the average number of electrons released during the oxidation of ethanol in a direct ethanol fuel cell. *Electrochim. Acta* **2015**, *182*, 856–860.

[120] Wang, H.; Löffler, T.; Baltruschat, H. Formation of intermediates during methanol oxidation: a quantitative DEMS study. *J. Appl. Electrochem.* **2001**, *31*, 759–765.

[121] Jusys, Z.; Behm, R. Methanol oxidation on a carbon-supported Pt fuel cell catalyst a kinetic and mechanistic study by differential electrochemical mass spectrometry. *J. Phys. Chem. B* **2001**, *105*, 10874–10883.

[122] Gojković, S. L.; Vidaković, T. Methanol oxidation on an ink type electrode using Pt supported on high area carbons. *Electrochim. Acta* **2001**, *47*, 633–642.

[123] Rosenthal, N. S.; Vilekar, S. A.; Datta, R. A comprehensive yet comprehensible analytical model for the direct methanol fuel cell. *J. Power Sources* **2012**, *206*, 129–143.

[124] Wang, H.; Baltruschat, H. DEMS study on methanol oxidation at poly and monocrystalline platinum electrodes: the effect of anion, temperature, surface structure, Ru adatom, and potential. *J. Phys. Chem. C* **2007**, *111*, 7038–7048.

[125] Jusys, Z.; Kaiser, J.; Behm, R. J. Composition and activity of high surface area PtRu catalysts towards adsorbed CO and methanol electrooxidation: a DEMS study. *Electrochim. Acta* **2002**, *47*, 3693–3706.

[126] Treimer, S.; Tang, A.; Johnson, D. C. A Consideration of the application

of Koutecký-Levich plots in the diagnoses of charge-transfer mechanisms at rotated disk electrodes. *Electroanalysis* **2002**, *14*, 165–171.

[127] Badwal, S.; Giddey, S.; Kulkarni, A.; Goel, J.; Basu, S. Direct ethanol fuel cells for transport and stationary applications, A comprehensive review. *Appl. Energy* **2015**, *145*, 80–103.

[128] Ramachandran, S.; Stimming, U. Well to wheel analysis of low carbon alternatives for road traffic. *Energy Environ. Sci.* **2015**, *8*, 3313–3324.

[129] Wang, Y.; Zou, S.; Cai, W. B. Recent advances on electro-oxidation of ethanol on Pt-and Pd-based catalysts: from reaction mechanisms to catalytic materials. *Catalysts* **2015**, *5*, 1507–1534.

[130] Wang, H. F.; Liu, Z.-P. Comprehensive mechanism and structure-sensitivity of ethanol oxidation on platinum: new transition-state searching method for resolving the complex reaction network. *J. Am. Chem. Soc.* **2008**, *130*, 10996–11004.

[131] Wang, Y.; Mi, Y.; Redmon, N.; Holiday, J. Understanding electrocatalytic activity enhancement of bimetallic particles to ethanol electro-oxidation. 1. Water adsorption and decomposition on Pt_nM (n= 2, 3, and 9; M = Pt, Ru, and Sn). *J. Phys. Chem. C* **2010**, *114*, 317–326.

[132] Kavanagh, R.; Cao, X. M.; Lin, W. F.; Hardacre, C.; Hu, P. Origin of low CO_2 selectivity on platinum in the direct ethanol fuel cell. *Angew. Chem. Int. Ed.* **2012**, *51*, 1572–1575.

[133] Kavanagh, R.; Cao, X. M.; Lin, W.; Hardacre, C.; Hu, P. Acetaldehyde production in the direct ethanol fuel cell: mechanistic elucidation by density functional theory. *J. Phys. Chem. C* **2012**, *116*, 7185–7188.

[134] Jin, J. M.; Sheng, T.; Lin, X.; Kavanagh, R.; Hamer, P.; Hu, P.; Hardacre, C.; Martinez-Bonastre, A.; Sharman, J.; Thompsett, D., et al. The origin of high activity but low CO_2 selectivity on binary PtSn in the direct ethanol fuel cell. *Phys. Chem. Chem. Phys.* **2014**, *16*, 9432–9440.

[135] Sheng, T.; Lin, W. F.; Hardacre, C.; Hu, P. Significance of β-dehydrogenation in ethanol electro-oxidation on platinum doped with Ru, Rh, Pd, Os and Ir. *Phys. Chem. Chem. Phys.* **2014**, *16*, 13248–13254.

[136] Asiri, H. A.; Anderson, A. B. Mechanisms for ethanol electrooxidation on Pt (111) and adsorption bond strengths defining an ideal catalyst. *J. Electrochem. Soc.* **2015**, *162*, F115–F122.

[137] Beden, B.; Morin, M. C.; Hahn, F.; Lamy, C. "In situ" analysis by infrared reflectance spectroscopy of the adsorbed species resulting from the electrosorption of ethanol on platinum in acid medium. *J. Electroanal. Chem. Interf. Electrochem.* **1987**, *229*, 353–366.

[138] Iwasita, T.; Vielstich, W. The electrochemical oxidation of ethanol on platinum: a SNIFTIRS study. *J. Electroanal. Chem. Interf. Electrochem.* **1988**, *257*, 319–324.

[139] Hitmi, H.; Belgsir, E.; Léger, J. M.; Lamy, C.; Lezna, R. A kinetic analysis

of the electro-oxidation of ethanol at a platinum electrode in acid medium. *Electrochim. Acta* **1994**, *39*, 407–415.

[140] Simões, F.; Dos Anjos, D.; Vigier, F.; Léger, J. M.; Hahn, F.; Coutanceau, C.; Gonzalez, E. R.; Tremiliosi-Filho, G.; De Andrade, A.; Olivi, P., et al. Electroactivity of tin modified platinum electrodes for ethanol electrooxidation. *J. Power Sources* **2007**, *167*, 1–10.

[141] Dos Anjos, D.; Hahn, F.; Léger, J. M.; Kokoh, K. B.; Tremiliosi-Filho, G. In situ FTIRS studies of the electrocatalytic oxidation of ethanol on Pt alloy electrodes. *J. Solid State Electrochem.* **2007**, *11*, 1567–1573.

[142] Colmati, F.; Tremiliosi-Filho, G.; Gonzalez, E. R.; Berná, A.; Herrero, E.; Feliu, J. M. The role of the steps in the cleavage of the C–C bond during ethanol oxidation on platinum electrodes. *Phys. Chem. Chem. Phys.* **2009**, *11*, 9114–9123.

[143] Heinen, M.; Jusys, Z.; Behm, R. Ethanol, acetaldehyde and acetic acid adsorption/electrooxidation on a Pt thin film electrode under continuous electrolyte flow: an in situ ATR-FTIRS flow cell study. *J. Phys. Chem.C* **2010**, *114*, 9850–9864.

[144] Gomes, J. F.; Bergamaski, K.; Pinto, M. F.; Miranda, P. B. Reaction intermediates of ethanol electro-oxidation on platinum investigated by SFG spectroscopy. *J. Catal.* **2013**, *302*, 67–82.

[145] Erini, N.; Loukrakpam, R.; Petkov, V.; Baranova, E. A.; Yang, R.; Teschner, D.; Huang, Y.; Brankovic, S. R.; Strasser, P. Ethanol electro-oxidation on ternary

platinum–rhodium–tin nanocatalysts: insights in the atomic 3D structure of the active catalytic phase. *ACS Catal.* **2014**, *4*, 1859–1867.

[146] Busó-Rogero, C.; Brimaud, S.; Solla-Gullon, J.; Vidal-Iglesias, F. J.; Herrero, E.; Behm, R. J.; Feliu, J. M. Ethanol oxidation on shape-controlled platinum nanoparticles at different pHs: a combined in situ IR spectroscopy and online mass spectrometry study. *J. Electroanal. Chem.* **2016**, *763*, 116–124.

[147] Delpeuch, A. B.; Maillard, F.; Chatenet, M.; Soudant, P.; Cremers, C. Ethanol oxidation reaction (EOR) investigation on Pt/C, Rh/C, and Pt-based bi-and tri-metallic electrocatalysts: a DEMS and in situ FTIR study. *Appl. Catal. B* **2016**, *181*, 672–680.

[148] Pereira, M. G.; Jiménez, M. D.; Elizalde, M.; Manzo-Robledo, A.; Alonso-Vante, N. Study of the electrooxidation of ethanol on hydrophobic electrodes by DEMS and HPLC. *Electrochim. Acta* **2004**, *49*, 3917–3925.

[149] Wang, J.; Wasmus, S.; Savinell, R. Evaluation of ethanol, 1-propanol, and 2-propanol in a direct oxidation polymer-electrolyte fuel cell a real-time mass spectrometry study. *J. Electrochem. Soc.* **1995**, *142*, 4218–4224.

[150] Delpeuch, A. B.; Chatenet, M.; Cremers, C.; Tübke, T. Mass spectrometric investigation of ethanol and acetaldehyde adsorbates electrooxidation on Pt electrocatalyst. *Electrochim. Acta* **2014**, *141*, 102–112.

[151] Guillén-Villafuerte, O.; García, G.; Arévalo, M. C.; Rodríguez, J. L.; Pastor, E. New insights on the electrochemical oxidation of ethanol on carbon-supported

Pt electrode by a novel electrochemical mass spectrometry configuration. *Electrochem. Commun.* **2016**, *63*, 48–51.

[152] Fujiwara, N.; Friedrich, K.; Stimming, U. Ethanol oxidation on PtRu electrodes studied by differential electrochemical mass spectrometry. *J. Electroanal. Chem.* **1999**, *472*, 120–125.

[153] Neto, A. O.; Giz, M. J. d.; Perez, J.; Ticianelli, E. A.; Gonzalez, E. R. The electro-oxidation of ethanol on Pt-Ru and Pt-Mo particles supported on high-surface-area carbon. *J. Electrochem. Soc.* **2002**, *149*, A272–A279.

[154] Profeti, D.; Servat, K.; Hahn, F.; Kokoh, K.; Olivi, P. Electrocatalytic oxidation of ethanol on $Sn_{(1-x)}Ir_xO_2$ electrodes in acid medium. *J. Appl. Electrochem.* **2008**, *38*, 837–843.

[155] Purgato, F.; Olivi, P.; Léger, J. M.; De Andrade, A.; Tremiliosi-Filho, G.; Gonzalez, E.; Lamy, C.; Kokoh, K. Activity of platinum–tin catalysts prepared by the Pechini–Adams method for the electrooxidation of ethanol. *J. Electroanal. Chem.* **2009**, *628*, 81–89.

[156] Zhu, M.; Sun, G.; Xin, Q. Effect of alloying degree in PtSn catalyst on the catalytic behavior for ethanol electro-oxidation. *Electrochim. Acta* **2009**, *54*, 1511–1518.

[157] Nakagawa, N.; Kaneda, Y.; Wagatsuma, M.; Tsujiguchi, T. Product distribution and the reaction kinetics at the anode of direct ethanol fuel cell with Pt/C, PtRu/C and PtRuRh/C. *J. Power Sources* **2012**, *199*, 103–109.

[158] Seweryn, J.; Lewera, A. High selectivity of ethanol electrooxidation to carbon dioxide on platinum nanoparticles in low temperature polymer electrolyte membrane direct ethanol fuel cell. *Appl. Catal. B* **2014**, *144*, 129–134.

[159] Rousseau, S.; Coutanceau, C.; Lamy, C.; Léger, J. M. Direct ethanol fuel cell (DEFC): electrical performances and reaction products distribution under operating conditions with different platinum-based anodes. *J. Power Sources* **2006**, *158*, 18–24.

[160] Vigier, F.; Coutanceau, C.; Perrard, A.; Belgsir, E.; Lamy, C. Development of anode catalysts for a direct ethanol fuel cell. *J. Appl. Electrochem.* **2004**, *34*, 439–446.

[161] James, D. D.; Pickup, P. G. Measurement of carbon dioxide yields for ethanol oxidation by operation of a direct ethanol fuel cell in crossover mode. *Electrochim. Acta* **2012**, *78*, 274–278.

[162] Shinozaki, K.; Zack, J. W.; Richards, R. M.; Pivovar, B. S.; Kocha, S. S. Oxygen reduction reaction measurements on platinum electrocatalysts utilizing rotating disk electrode technique I. Impact of impurities, measurement protocols and applied corrections. *J. Electrochem. Soc.* **2015**, *162*, F1144–F1158.

[163] Barbosa, A.; Oliveira, V.; Van Drunen, J.; Tremiliosi-Filho, G. Ethanol electro-oxidation reaction using a polycrystalline nickel electrode in alkaline media: temperature influence and reaction mechanism. *J. Electroanal. Chem.* **2015**, *746*, 31–38.

[164] Figueiredo, M. C.; Arán-Ais, R. M.; Climent, V.; Kallio, T.; Feliu, J. M. Evidence of local pH changes during ethanol oxidation at Pt electrodes in alkaline media. *J. Chem. ElectroChem.* **2015**, *2*, 1254–1258.

[165] Sayadi, A.; Pickup, P. G. Evaluation of methanol oxidation catalysts by rotating disc voltammetry. *Electrochim. Acta* **2016**, *199*, 12–17.

[166] Freitas, K. S.; Concha, B. M.; Ticianelli, E. A.; Chatenet, M. Mass transport effects in the borohydride oxidation reaction—Influence of the residence time on the reaction onset and faradaic efficiency. *Catal. Today* **2011**, *170*, 110–119.

[167] Harris, K. R.; Newitt, P. J.; Derlacki, Z. Alcohol tracer diffusion, density, NMR and FTIR studies of aqueous ethanol and 2, 2, 2-trifluoroethanol solutions at 25 $^{\circ}C$. *J. Chem. Soc. Faraday Trans.* **1998**, *94*, 1963–1970.

[168] Colmenares, L.; Wang, H.; Jusys, Z.; Jiang, L.; Yan, S.; Sun, G.; Behm, R. Ethanol oxidation on novel, carbon supported Pt alloy catalysts—model studies under defined diffusion conditions. *Electrochim. Acta* **2006**, *52*, 221–233.

[169] Schneider, A.; Colmenares, L.; Seidel, Y.; Jusys, Z.; Wickman, B.; Kasemo, B.; Behm, R. Transport effects in the oxygen reduction reaction on nanostructured, planar glassy carbon supported Pt/GC model electrodes. *Phys. Chem. Chem. Phys.* **2008**, *10*, 1931–1943.

[170] Katikawong, P.; Ratana, T.; Veerasai, W. Temperature dependence studies on the electro-oxidation of aliphatic alcohols with modified platinum electrodes. *J. Chem. Sci.* **2009**, *121*, 329–337.

[171] Velázquez-Palenzuela, A.; Brillas, E.; Arias, C.; Centellas, F.; Garrido, J. A.; Rodríguez, R. M.; Cabot, P.-L. Carbon monoxide, methanol and ethanol electro-oxidation on Ru-decorated carbon-supported Pt nanoparticles prepared by spontaneous deposition. *J. Power Sources* **2013**, *225*, 163–171.

[172] Jiang, L.; Hsu, A.; Chu, D.; Chen, R. Ethanol electro-oxidation on Pt/C and PtSn/C catalysts in alkaline and acid solutions. *Int. J. Hydrog. Energy* **2010**, *35*, 365–372.

[173] Bach Delpeuch, A.; Asset, T.; Chatenet, M.; Cremers, C. Influence of the temperature for the ethanol oxidation reaction (EOR) on Pt/C, Pt-Rh/C and Pt-Rh-SnO_2/C. *Fuel Cells* **2015**, *15*, 352–360.

[174] Fang, Y. H.; Liu, Z. P. First principles Tafel kinetics of methanol oxidation on Pt (111). *Surf. Sci.* **2015**, *631*, 42–47.

[175] Habibi, E.; Razmi, H. Kinetics of direct ethanol fuel cell based on Pt-PoPd nano particle anode catalyst. *Int. J. Hydrog. Energy* **2013**, *38*, 5442–5448.

[176] Antoniassi, R.; Neto, A. O.; Linardi, M.; Spinacé, E. The effect of acetaldehyde and acetic acid on the direct ethanol fuel cell performance using PtSnO_2/C electrocatalysts. *Int. J. Hydrog. Energy* **2013**, *38*, 12069–12077.

[177] Amarasinghe, S.; Ta-Yung, C.; Moberg, P.; Paul, H. J.; Tinoco, F.; Zook, L. A.; Leddy, J. Models for mediated reactions at film modified electrodes: controlled electrode potential. *Anal. Chim. Acta* **1995**, *307*, 227–244.

[178] Gloaguen, F.; Andolfatto, F.; Durand, R.; Ozil, P. Kinetic study of

electrochemical reactions at catalyst-recast ionomer interfaces from thin active layer modelling. *J. Appl. Electrochem.* **1994**, *24*, 863–869.

[179] Ruvinskiy, P.; Bonnefont, A.; Houllé, M.; Pham-Huu, C.; Savinova, E. Preparation, testing and modeling of three-dimensionally ordered catalytic layers for electrocatalysis of fuel cell reactions. *Electrochim. Acta* **2010**, *55*, 3245–3256.

[180] Ruvinskiy, P. S.; Bonnefont, A.; Bayati, M.; Savinova, E. R. Mass transport effects in CO bulk electrooxidation on Pt nanoparticles supported on vertically aligned carbon nanofilaments. *Phys. Chem. Chem. Phys.* **2010**, *12*, 15207–15216.

[181] Rees, N. V.; Compton, R. G. Sustainable energy: a review of formic acid electrochemical fuel cells. *J. Solid State Electrochem.* **2011**, *15*, 2095–2100.

[182] Mallick, R. K.; Thombre, S. B.; Shrivastava, N. K. Vapor feed direct methanol fuel cells (DMFCs): a review. *Renew. Sust. Energ. Rev.* **2016**, *56*, 51–74.

[183] Boronat-González, A.; Herrero, E.; Feliu, J. M. Fundamental aspects of HCOOH oxidation at platinum single crystal surfaces with basal orientations and modified by irreversibly adsorbed adatoms. *J. Solid State Electrochem.* **2014**, *18*, 1181–1193.

[184] Jiang, K.; Zhang, H. X.; Zou, S.; Cai, W. B. Electrocatalysis of formic acid on palladium and platinum surfaces: from fundamental mechanisms to fuel cell applications. *Phys. Chem. Chem. Phys.* **2014**, *16*, 20360–20376.

[185] Frumkin, A. N.; Tedoradze, G. A. The ionization kinetics of molecular chlorine. *Dokl. Akad. Nauk SSSR* **1958**, *118*, 530–533.

[186] Frumkin, A. N.; Aikazyan, E. A. Kinetics of molecular hydrogen ionization on a platinum electrode and the role of anions. *Dokl. Akad. Nauk SSSR* **1955**, *100*, 20360–20376.

[187] Koutetskii, Y.; Levich, V. G. The use of a rotating disc electrode for studying kinetic and catalytic processes in electrochemistry. *Dokl. Akad. Nauk SSSR* **1957**, *117*, 441–444.

[188] Albery, W.; Greenwood, A.; Kibble, R. Diffusion coefficients of carboxylic acids. *J. Chem. Soc. Faraday Trans.* **1967**, *63*, 360–368.

[189] Shin, D.; Kim, Y. R.; Choi, M.; Rhee, C. K. Formic Acid Oxidation Depending on Rotating Speed of Smooth Pt Disk Electrode. *J. Electrochem. Sci. Technol.* **2014**, *5*, 82–86.

[190] Tripković, A. V.; Popović, K. D.; Stevanović, R.; Socha, R.; Kowal, A. Activity of a PtBi alloy in the electrochemical oxidation of formic acid. *Electrochem. Commun.* **2006**, *8*, 1492–1498.

[191] Ghosh, T.; Zhou, Q.; Gregoire, J. M.; van Dover, R. B.; DiSalvo, F. J. Pt-Cd and Pt- Hg phases as high activity catalysts for methanol and formic acid oxidation. *J. Phys. Chem. C* **2010**, *114*, 12545–12553.

[192] Lović, J.; Tripković, D.; Popović, K.; Jovanović, V.; Tripković, A. V.

Electrocatalytic properties of Pt-Bi electrodes towards the electro-oxidation of formic acid. *J. Serb. Chem. Soc.* **2013**, *78*, 1189–1202.

[193] Bauskar, A. S.; Rice, C. A. Spontaneously Bi decorated carbon supported Pd nanoparticles for formic acid electro-oxidation. *Electrochim. Acta* **2013**, *107*, 562–568.

[194] Brimaud, S.; Solla-Gullón, J.; Weber, I.; Feliu, J. M.; Behm, R. J. Formic acid electrooxidation on noble-metal electrodes: role and mechanistic implications of pH, surface structure, and anion adsorption. *ChemElectroChem* **2014**, *1*, 1075–1083.

[195] Garsany, Y.; Singer, I. L.; Swider-Lyons, K. E. Impact of film drying procedures on RDE characterization of Pt/VC electrocatalysts. *J. Electroanal. Chem.* **2011**, *662*, 396–406.

[196] Lović, J.; Tripković, A. V.; Gojković, S. L.; Popović, K. D.; Tripković, D.; Olszewski, P.; Kowal, A. Kinetic study of formic acid oxidation on carbon-supported platinum electrocatalyst. *J. Electroanal. Chem.* **2005**, *581*, 294–302.

[197] Corti, H. R.; Gonzalez, E. R. *Direct alcohol fuel cells*; Springer, 2014; Vol. 1.

[198] Lima, F.; Gonzalez, E. Ethanol electro-oxidation on carbon-supported Pt–Ru, Pt–Rh and Pt–Ru–Rh nanoparticles. *Electrochim. Acta* **2008**, *53*, 2963–2971.

[199] Oelkers, E. H. Calculation of diffusion coefficients for aqueous organic species at temperatures from 0 to 350 °C. *Geochim. Cosmochim. Acta* **1991**, *55*, 3515–3529.

[200] Delpeuch, A. B.; Jacquot, M.; Chatenet, M.; Cremers, C. The influence of mass-transport conditions on the ethanol oxidation reaction (EOR) mechanism of Pt/C electrocatalysts. *Phys. Chem. Chem. Phys.* **2016**, *18*, 25169–25175.

[201] Olah, G. A.; Goeppert, A.; Prakash, G. S. *Beyond oil and gas: the methanol economy*; John Wiley & Sons, 2018.

[202] Suib, S. L. *New and future developments in catalysis: batteries, hydrogen storage and fuel cells*; Newnes, 2013.

[203] Rao, L.; Jiang, Y.; Zhang, B.; You, L.; Li, Z.; Sun, S. Electrocatalytic oxidation of ethanol. *Prog. Chem.* **2014**, *26*, 727–736.

[204] Sayadi, A.; Pickup, P. G. Evaluation of ethanol oxidation catalysts by rotating disc voltammetry. *Electrochim. Acta* **2016**, *215*, 84–92.

[205] Sayadi, A.; Pickup, P. G. Electrochemical oxidation of formic acid at carbon supported Pt coated rotating disk electrodes. *Russ. J. Electrochem.* **2017**, *53*, 1054–1060.

[206] Alkire, R.; Gracon, B. Flow-through porous electrodes. *J. Electrochem. Soc.* **1975**, *122*, 1594–1601.

[207] Sayadi, A.; Pickup, P. G. Hydrodynamic studies of ethanol oxidation at Pt and PtRu catalysts at elevated temperatures. *ECS Trans* **2020**, *97*, 869–875.

[208] Harris, D. C. Nonlinear least-squares curve fitting with Microsoft Excel Solver. *J. Chem. Educ.* **1998**, *75*, 119–121.

Appendix A

K-L plots of Pt/C and PtRu/C electrodes at various temperatures

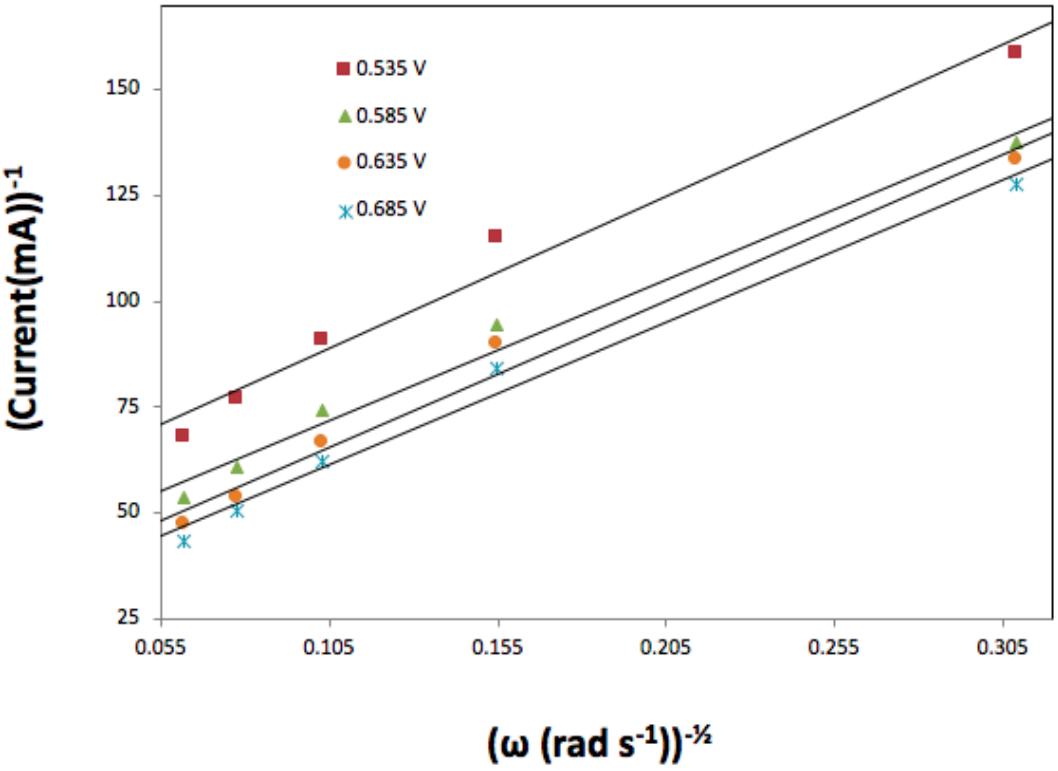

Figure A.1: Steady-state Koutecky-Levich plots (i^{-1} vs. $\omega^{-1/2}$) for oxidation of 0.1 M ethanol in 1 M H_2SO_4(aq) at a 75% $PtRu/C$ (7 $mg\ cm^{-2}$) electrode (temperature = 24 $^{\circ}C$).

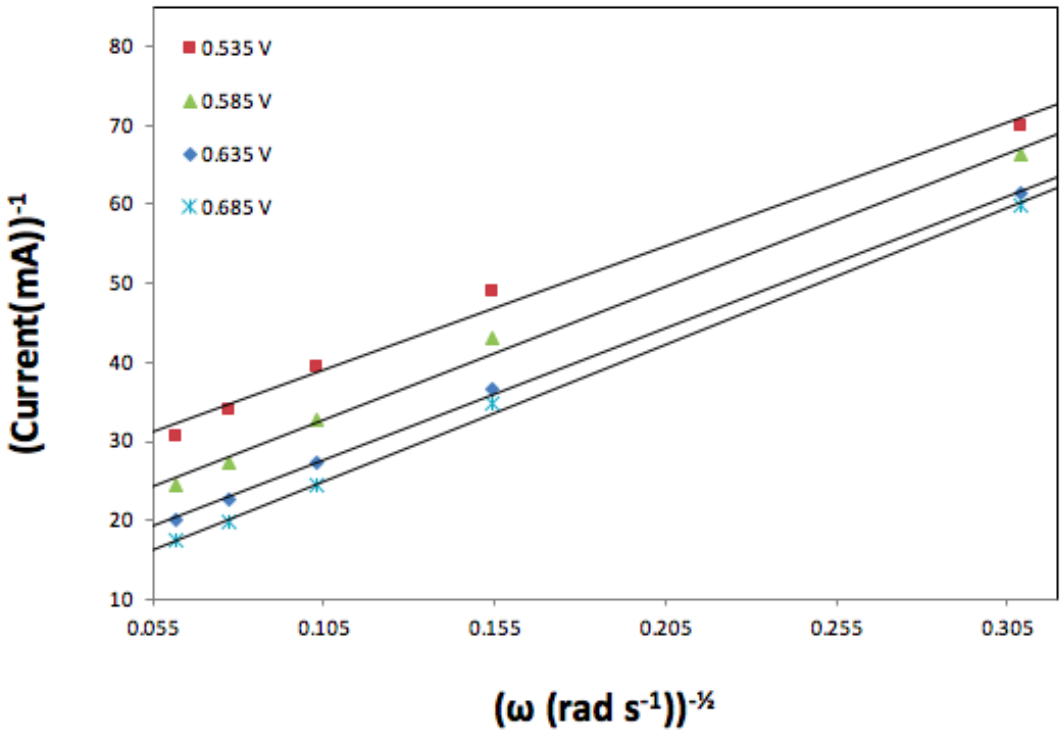

Figure A.2: Steady-state Koutecky-Levich plots (i^{-1} vs. $\omega^{-1/2}$) for oxidation of 0.1 M ethanol in 1 M H_2SO_4(aq) at a 75% $PtRu/C$ (7 $mg\ cm^{-2}$) electrode (temperature = 50 $^{\circ}C$).

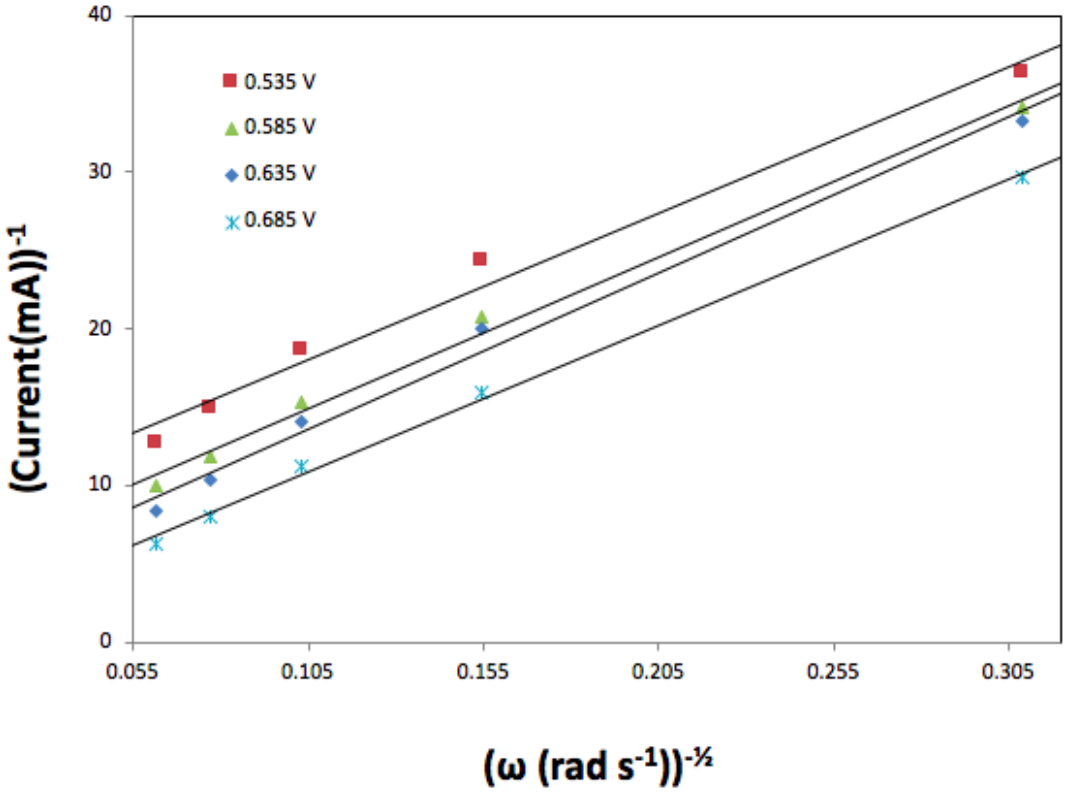

Figure A.3: Steady-state Koutecky-Levich plots (i^{-1} vs. $\omega^{-1/2}$) for oxidation of 0.1 M ethanol in 1 M H_2SO_4(aq) at a 75% $PtRu/C$ (7 $mg\ cm^{-2}$) electrode (temperature = 80 $^{\circ}C$).

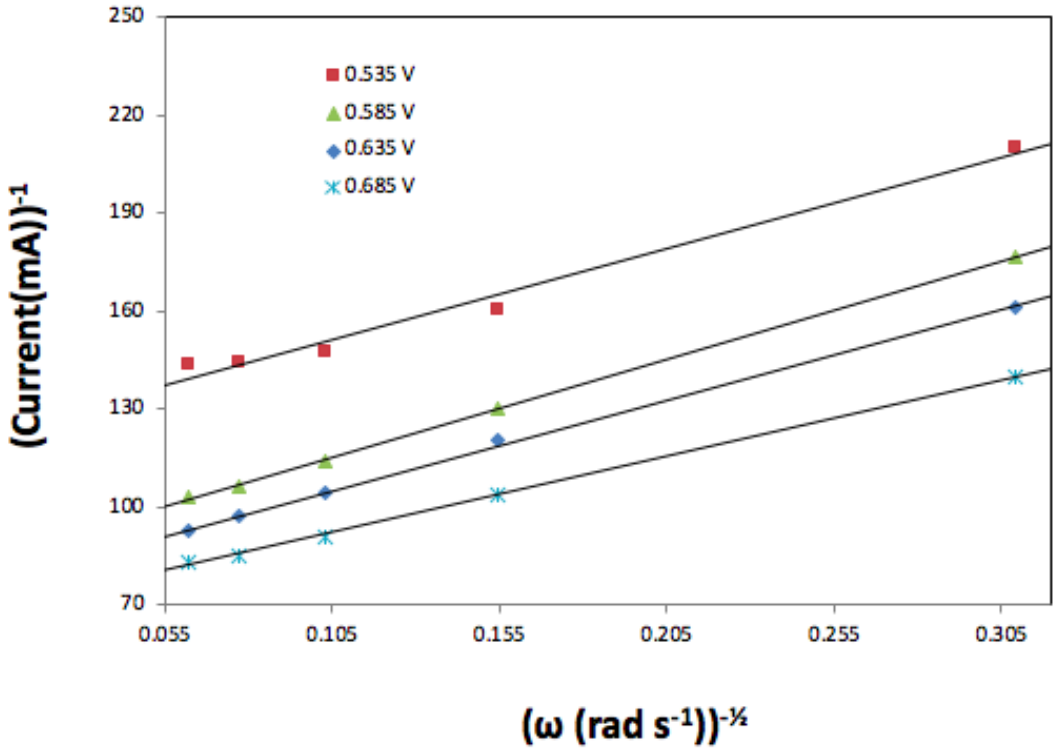

Figure A.4: Steady-state Koutecky-Levich plots (i^{-1} vs. $\omega^{-1/2}$) for oxidation of 0.1 M ethanol in 1 M H_2SO_4(aq) at a 70% Pt/C (7 $mg\ cm^{-2}$) electrode (temperature = 24 $^{\circ}C$).

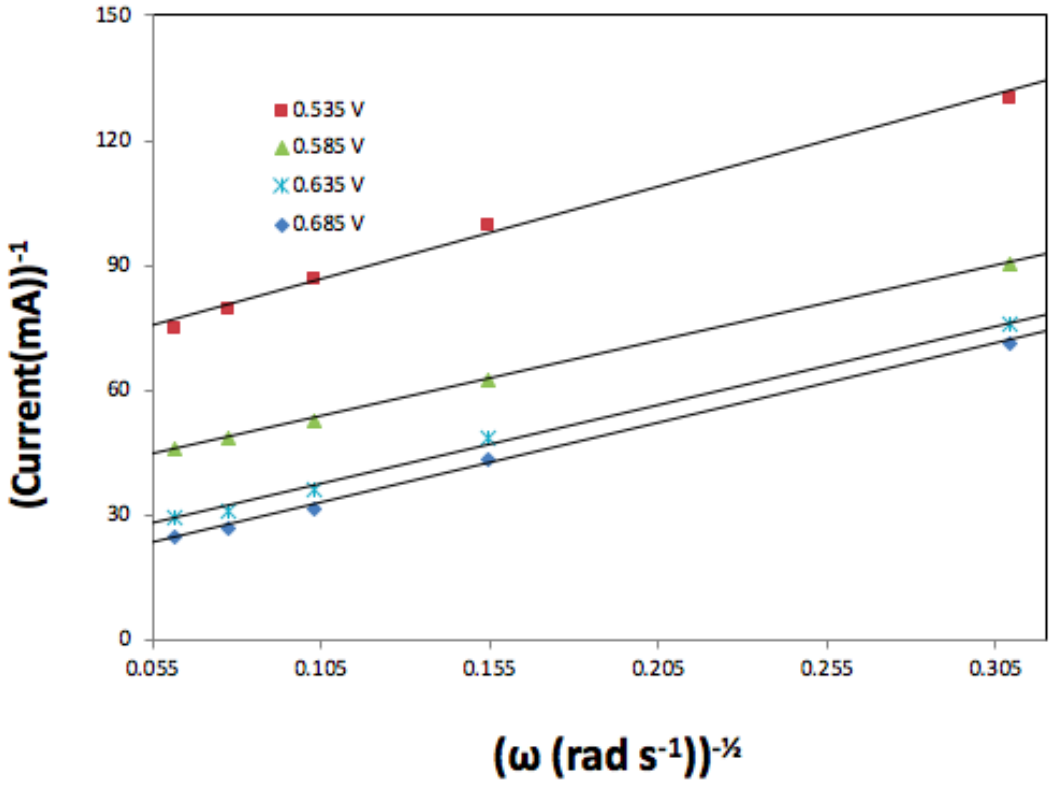

Figure A.5: Steady-state Koutecky-Levich plots (i^{-1} vs. $\omega^{-1/2}$) for oxidation of 0.1 M ethanol in 1 M H_2SO_4(aq) at a 70% Pt/C (7 $mg\ cm^{-2}$) electrode (temperature = 50 $^{\circ}C$).

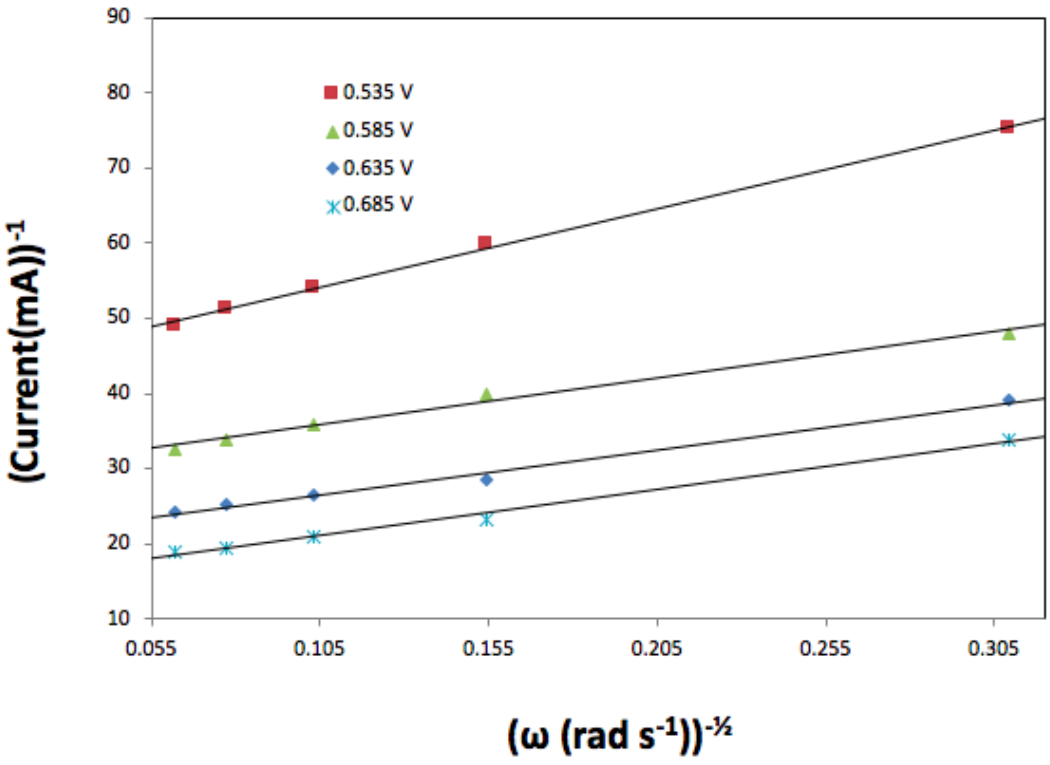

Figure A.6: Steady-state Koutecky-Levich plots (i^{-1} vs. $\omega^{-1/2}$) for oxidation of 0.1 M ethanol in 1 M H_2SO_4(aq) at a 70% Pt/C (7 $mg\ cm^{-2}$) electrode (temperature = 80 $^{\circ}C$).

Appendix B

Raw data and graphs for chapter 7

B.1 Flow-Through Cell Resistance

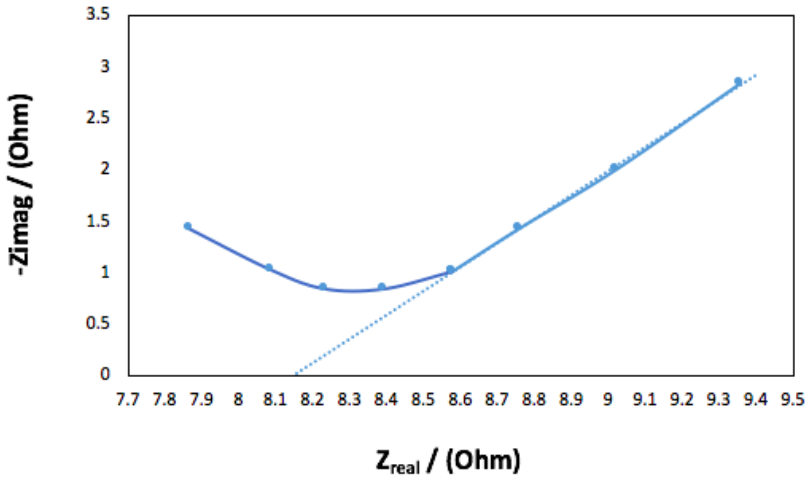

Figure B.1: Nyquist plot example for three-electrode flow-through cell recorded prior to experiments.

B.2 Flow Rate Analysis

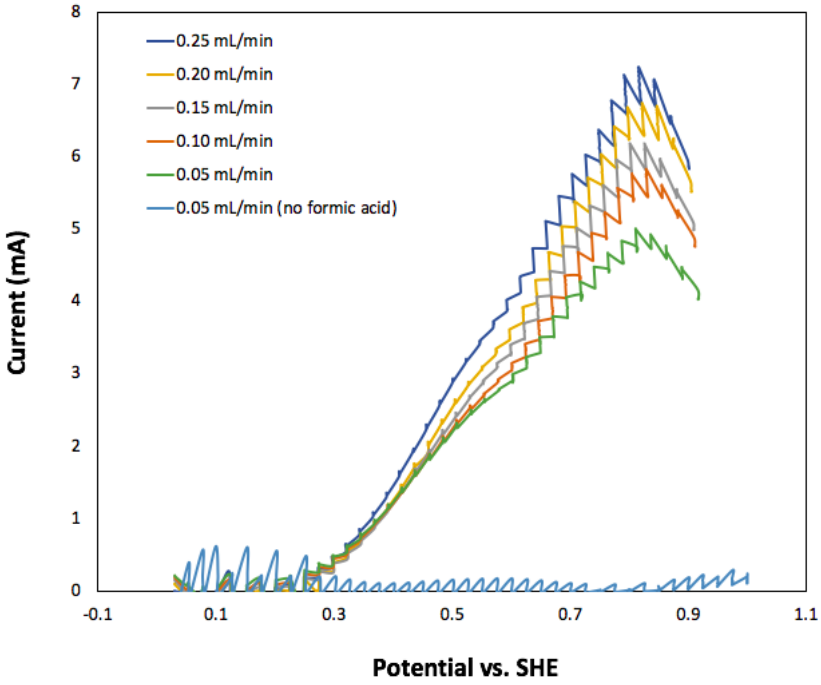

Figure B.2: Staircase voltammograms of 0.1 M formic acid solution in 1 M H_2SO_4 at various flow rates at a 20% Pt/C electrode.

B.2.1 Simulations

In the model that we applied for our flow rate dependence studies, the catalyst layer was divided into 100 discrete layers. The current at each segment of the catalyst layer (I_x) was simulated using eqs. B.1 and B.2 for a range of flow rates (i.e. 0.05, 0.07, 0.08, 0.09, 0.10, 0.15, 0.2, 0.25, 0.3, 0.4, 0.5 $mL\ min^{-1}$) at each potential. n is the number of electrons transferred, u is the flow rate, α is the mass transport coefficient, and F is the faraday constant. C_x is the concentration of formic acid at

segment x which was also simulated for 100 discrete layers. k (rate constant) and λ (mass transport parameter) are two parameters whose variations were the basis of our simulations.[92,206]

$$I_x = 1/(1/n\lambda C_x u^{\alpha} + 1/nC_x Fk)/100 \tag{B.1}$$

$$C_x = C - I_x/nFu(mL\ s^{-1}) \tag{B.2}$$

Simulated overall currents related to each flow rate were also calculated using eq. B.3.[92,206]

$$I = \Sigma_{x=1}^{x=100} I_x \tag{B.3}$$

The calculations related to each potential were conducted on a single excel spreadsheet via non-linear least square method. First, the λ and k variables were adjusted manually to obtain a proper fit of the experimental and simulated curves. Then the sum of the squares of residuals (i.e., experimental data minus simulated data) was calculated. In the next step, a solver operation was applied to find values of λ and k that minimized the sum of the squares of the residuals. In other words, the basis of solver operation basis was to minimize the vertical deviations of the simulated and experimental points. The initial values of λ and k, which were entered manually, play an important role in the solver operation output. Inappropriate guesses of initial values could affect the accuracy of the solver operation, and as a result refinements were required. Therefore, each time after running the solver, either one or both of the variables were adjusted to run the solver again and obtain a lower sum of the squares of the residuals. The cycle of solver operation and adjustments were repeated until the sum of the squares of the residuals became optimized.[208] λ is independent of the potential and it should be constant over a range of potentials. Therefore,

first it was adjusted by its variation and simulation for the first few points (i.e. $\lambda = 187\ mA\ s^{\alpha}\ cm^{3(1-\alpha)}\ mol^{-1}$). Then the same value was set for the rest of the calculations and k was the only parameter to be varied to obtain best fits. However, for 0.700, 0.825, and 0.925 V it was needed to optimize λ value with minor variations (Table 7.1).

B.2.2 Simulations Graphs

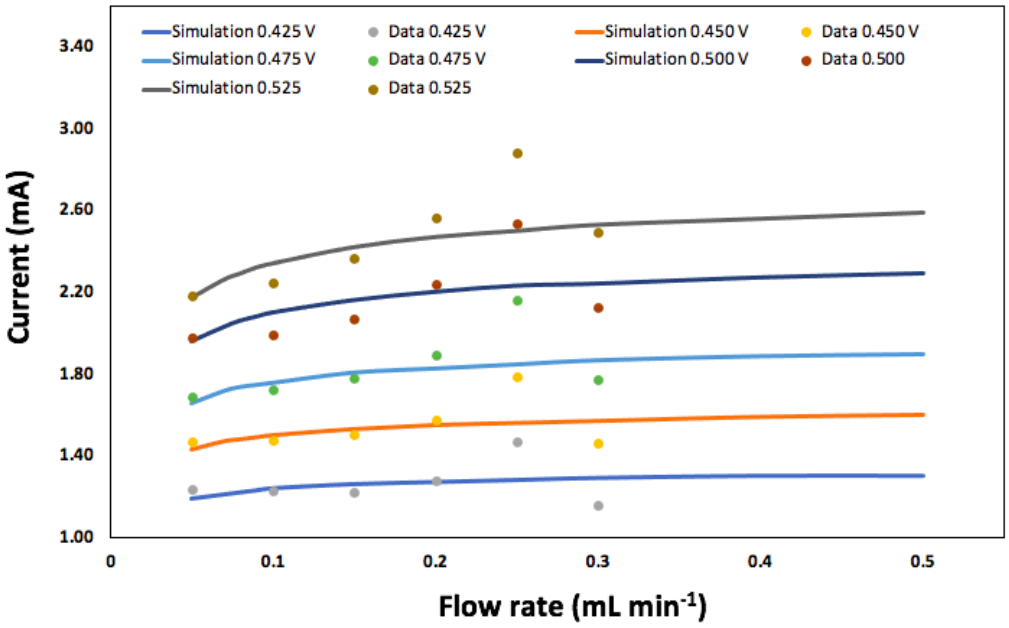

Figure B.3: Current vs. flow rate plots for the oxidation of 0.1 M formic acid in 1 M H_2SO_4(aq) at a 20% Pt/C electrode and 0.425-0.525 V (dots), with best fit theoretical curves from eq. 7.1 (lines), with $\lambda = 187\ mA\ s^{\alpha}\ cm^{3(1-\alpha)}\ mol^{-1}$ and $\alpha = 0.37$.

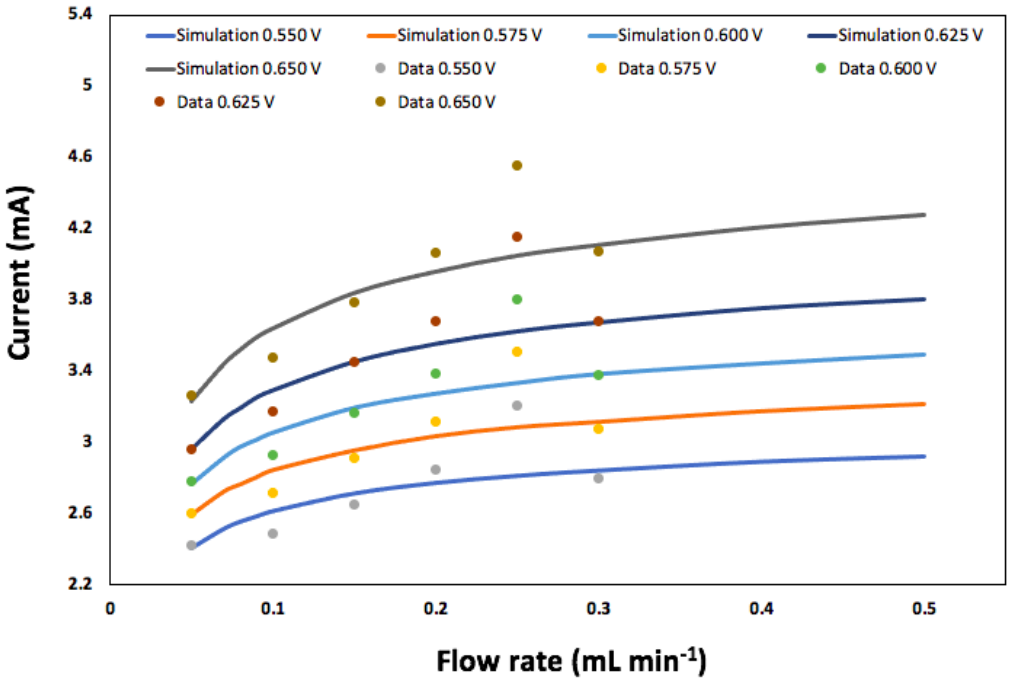

Figure B.4: Current vs. flow rate plots for the oxidation of 0.1 M formic acid in 1 M H_2SO_4(aq) at a 20% Pt/C electrode and 0.550-0.650 V (dots), with best fit theoretical curves from eq. 7.1 (lines), with $\lambda = 187\ mA\ s^{\alpha}\ cm^{3(1-\alpha)}\ mol^{-1}$ and $\alpha = 0.37$.

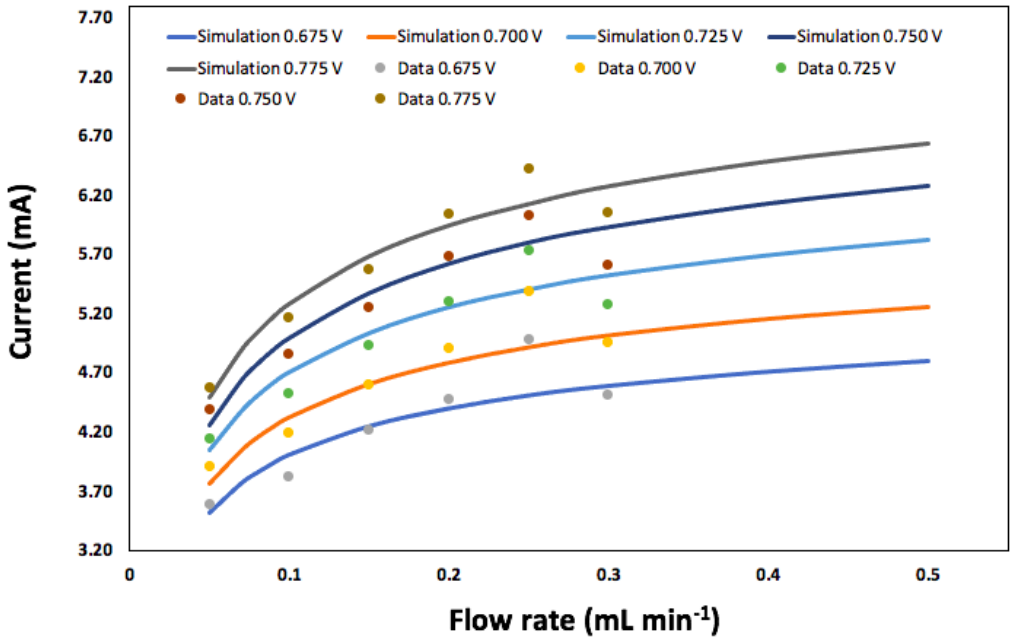

Figure B.5: Current vs. flow rate plots for the oxidation of 0.1 M formic acid in 1 M H_2SO_4(aq) at a 20% Pt/C electrode and 0.675-0.725 V (dots), with best fit theoretical curves from eq. 7.1 (lines), with $\lambda = 187\ mA\ s^{\alpha}\ cm^{3(1-\alpha)}\ mol^{-1}$ and $\alpha = 0.37$.

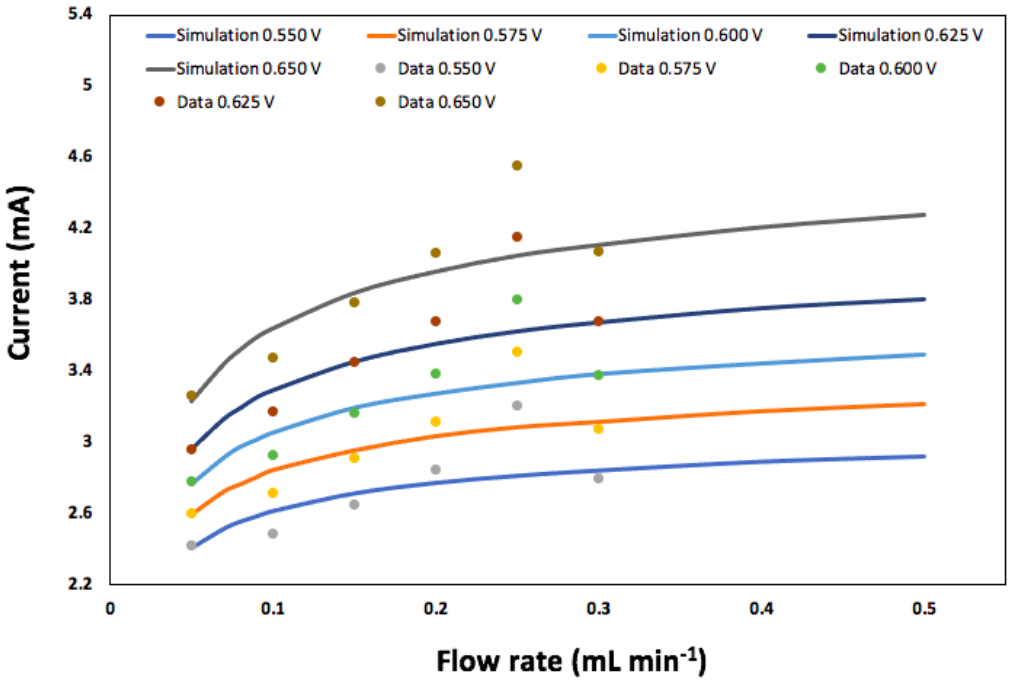

Figure B.6: Current vs. flow rate plots for the oxidation of 0.1 M formic acid in 1 M H_2SO_4(aq) at a 20% Pt/C electrode and 0.750-0.925 V (dots), with best fit theoretical curves from eq. 7.1 (lines), with $\lambda = 187\ mA\ s^{\alpha}\ cm^{3(1-\alpha)}\ mol^{-1}$ and $\alpha = 0.37$.